AD-A034 674 PHYSICAL SCIENCES INC WOBURN MASS F/G 20/5
ANALYTIC MODELING OF ELECTRICALLY EXCITED D2/HCL AND HCL LASER --ETC(U)
JUL 76 R TAYLOR, G CALEDONIA, P LEWIS, P WU N00014-75-C-0035
UNCLASSIFIED PSI-TR-58 NL

1 OF 2
AD
A034674

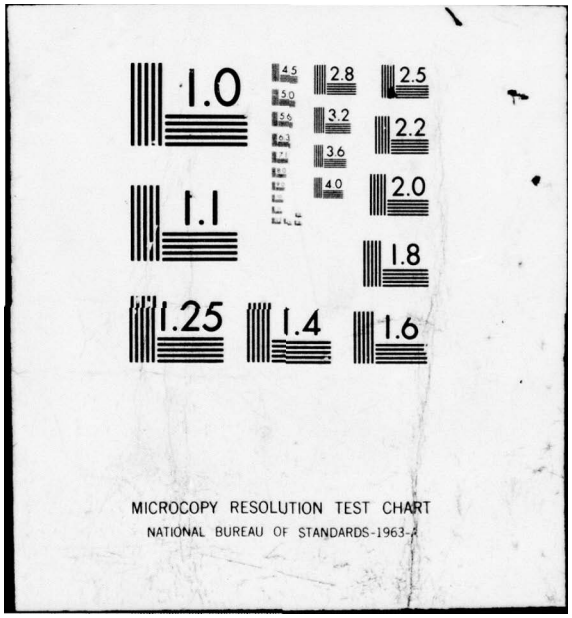
1.0
1.1
1.25
1.4
1.6
1.8
2.0
2.2
2.5
2.8
3.2
3.6
4.0
4.5
5.0
5.6
MICROCOPY RESOLUTION TEST CHART
NATIONAL BUREAU OF STANDARDS-1963-A

PSI TR-58

ANALYTIC MODELING OF ELECTRICALLY EXCITED D_2/HCl AND HCl LASER EXPERIMENTS

FINAL REPORT

JULY 1976

by

R. TAYLOR, G. CALEDONIA, P. LEWIS, P. WU,
J. D. TEARE AND J. CRONIN

Sponsored by

OFFICE OF NAVAL RESEARCH
Department of the Navy
Arlington, Virginia 22217

Contract No. N00014-75-C-0035
NRL Req. 173-75-RQ-06009

PSI TR-58

ANALYTIC MODELING OF ELECTRICALLY EXCITED D_2/HCl AND HCl LASER EXPERIMENTS

FINAL REPORT

by

R. Taylor, G. Caledonia, P. Lewis, P. Wu,
J. D. Teare* and J. Cronin

July 1976

Sponsored by

OFFICE OF NAVAL RESEARCH
Department of the Navy
Arlington, Virginia 22217

Contract No. N00014-75-C-0035

NRL Req. 173-75-RQ-06009

PHYSICAL SCIENCES INC.
30 Commerce Way
Woburn, Mass. 01801

---

*Present address: W. J. Schafer Associates, Inc., Wakefield, MA 01880

ABSTRACT

An analytic capability has been developed to model two type of laser experiments: (i) a D_2/HCl EDL and (ii) an e-beam sustainer discharge HCl laser.

For the former device, a discharge in D_2/inert gas mixtures provides excitation of the vibrational mode of D_2. This gas is then supersonically expanded and HCl injected. The gases mix and flow into a cavity where vibrational energy transfer pumps the HCl. Complete modeling of this sequence of steps has been achieved. The relevant electron impact rate constants for D_2 (and H_2) as well as the vibrational energy transfer rate constants for the D_2/HCl molecular system were selected from available data and theory. Comparison of the results of this model with data from the NRL EDL experiment were in qualitative agreement, although more definitive comparison was precluded by experimental difficulties. A conceptual design of a next generation experiment was performed and indicates the requirement for an e-beam sustainer discharge operating at about one atmosphere plenum pressure. Under these conditions laser demonstration of a D_2/HCl EDL is predicted to be feasible.

In the second experiment, HCl/inert gas mixtures are directly excited by a pulsed, high current e-beam sustainer discharge. The discharge conditions were modeled by developing a set of electron impact cross sections for HCl by a critical review of existing data. The results of model calculations indicate that for the conditions of the NRL experiment, sufficient atoms may be generated in the discharge to prevent attainment of high gain. Definitive modeling of the atom generation is not possible at present due to lack of kinetic information. A significant range of experimental variation could not be achieved due to device limitations. Additional, controlled experiments are suggested to assess the critical technical questions concerning an HCl discharge laser.

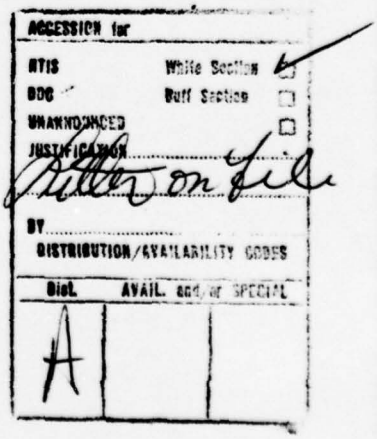

TABLE OF CONTENTS

TABLE OF CONTENTS (Cont'd)

LIST OF ILLUSTRATIONS

LIST OF ILLUSTRATIONS (Cont'd)

LIST OF ILLUSTRATIONS (Cont'd)

LIST OF ILLUSTRATIONS (Cont'd)

LIST OF ILLUSTRATIONS (Cont'd)

LIST OF TABLES

I. D_2/HCl EDL MODEL

A. INTRODUCTION

This Section of the report describes analytical modeling of the D_2/HCl electric discharge gas dynamic laser (EDGDL) under investigation at NRL. The concept of this device is as follows: D_2/diluent mixtures are passed through a low to medium pressure D.C. glow discharge. In principle, a high, i.e., atmospheric pressure sustained discharge could also be employed. It is expected that at the proper value of E/N, a substantial fraction of the discharge energy will be dissipated in exciting the vibrational mode of the D_2. The vibrationally excited D_2 is then expanded through a supersonic nozzle and mixed with HCl. Further downstream in the cavity, the D_2 transfers its vibrational energy to the HCL via a V→V process:

$$D_2\ (v = 1) + HCl\ (v = 0) \rightarrow D_2\ (v = 0) + HCl\ (v = 1) \qquad (I\text{-}1)$$

In addition, rapid intramode V→V pumping occurs among the vibrationally excited HCl molecules:

$$HCl\ (v = n) + HCl\ (v = 1) \rightarrow HCl\ (v = n + 1) + HCl\ (0) \qquad (I\text{-}2)$$

The occurrence of processes (I-1) and (I-2) under conditions of high vibrational and low translational temperatures is an example of Teare-Trainor pumping and, in principle, can produce a partial inversion on the HCl upper vibrational levels.

A schematic of the NRL experimental apparatus* is shown in Fig. I-1. The discharge is struck between a set of ballasted pins and the

---

* Further details concerning the NRL EDGDL and the results of the experiments performed on this apparatus may be found in the following series of reports: ARPA-NRL Laser Program Semi-Annual Technical Reports: 1 July 1973-31 Dec. 1973 NRL Memorandum Report 2846, July 1974 p. 19; 1 Jan. 1974-30 June 1974, NRL Memorandum Report 3005, April 1975, pp. 52-56; 1 July 1974-31 Dec. 1974, NRL Memorandum Report 3084, July 1975, pp. 18-27; 1 Jan. 1975-30 June 1975, NRL Memorandum Report 3217, Feb. 1973, pp. 13-21.

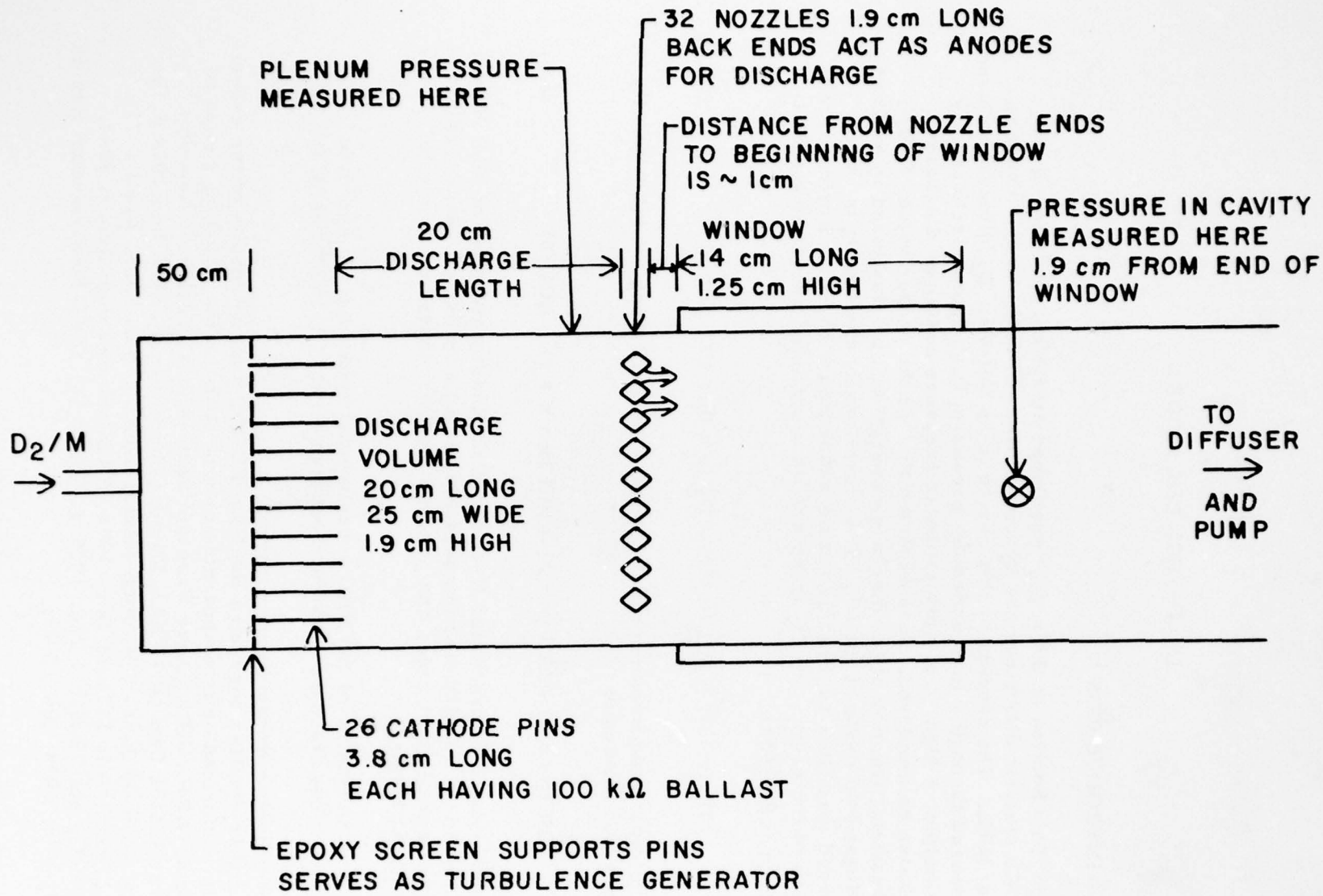

Fig. I-1 Schematic Top View of NRL Electric Discharge Laser Device

end of the nozzle blades. The discharge length is about 20 cm. Typical plenum conditions are 100 - 150 torr of 30% D_2 - 70% He mixture.* The discharged D_2 is expanded to approximately Mach 2 and mixed with a small amount of HCl. Final gas mixture composition in the cavity is typically 0.3% HCl/30% D_2/70% He at a pressure of ~6 torr. Observation windows extend from about the end of the nozzles to 15 cm downstream. An additional 14 cm of downstream observation is available by repositioning the windows. The transverse cavity dimension is 25 cm.

The primary diagnostics consist of the discharge parameters, gas flow rates and pressures, and HCl infrared fluorescence. This latter measurement is made via an optical system which translates parallel to the cavity during a run. Data of HCl fluorescence intensity versus downstream distance are obtained.

In the following sections of this report we will discuss the analytical modeling of this experiment, comparisons with data, and preliminary concepts for an improved device. Because of the geometry of the experiment, the modeling naturally divides into major tasks: (i) the discharge or plenum region and (ii) the cavity region. A major portion of the first effort was devoted to the development of a state-of-art electron impact cross section data package for D_2 over the electron energy range of interest in this study. Because of the existing limited data base for D_2, cross sections were first developed for H_2, and theoretical arguments used to extrapolate the H_2 data to D_2. Under the cavity modeling, we will discuss the vibrational energy transfer rate constants for the D_2/HCl molecular system, approximate mixing models, and calculations of fluorescence and small signal gain under typical experimental conditions. Finally, some limited comparison with data are discussed. It is shown that fluid mechanical problems associated with the device during much of the program preclude a detailed comparison. Suggestions are developed to construct a second generation experiment by which to provide laser device verification.

---

* More specific experimental conditions are presented later in this report.

B. DISCHARGE MODELING IN H_2/D_2

1. Boltzmann Code

The purpose of this task was to determine the electron energy distribution and molecular excitation rates arising from electric discharges in the gases H_2 and D_2 with the ultimate goal of providing laser performances predictions. The phenomena modeled involve: (i) the application of an electric field across a partially ionized gas which causes the electron acceleration; (ii) the various inelastic collisions of electrons with the gas molecules; (iii) the resulting electron energy distribution caused by the combination of these inelastic collisions with the electric field strength; and (iv) the excitation rate constants determined by integrating the relevant excitation cross sections over the resulting electron velocity distribution.

The electron energy distributions in discharges are generally non-Maxwellian and must be determined by a solution of the Boltzmann transport equation. Fortunately, much effort has been directed toward the solution of this problem. The computer code used in the present analysis was originally developed by Carleton and McGill[1] and has since been updated by Lenander[2] among others. The inelastic processes considered and included in the code are: (a) momentum transfer, (b) rotational excitation, (c) vibrational excitation, (d) dissociative attachment, (e) molecular dissociation, (f) electron excitation, and (g) ionization. The main thrust of the present effort was to develop a cross section data package for the H_2/D_2 molecular system to be used with the existing computer code.

The derivation of the Boltzmann equation is discussed in detail in Carleton and McGill.[1] The specific solution starts with the Boltzmann equation for a spatially uniform electron distribution $f(\underline{v},t)$:

$$\frac{df}{dt} + \underline{a} \cdot (\underline{\nabla}_v f) = \left(\frac{df}{dt}\right)_c \qquad \text{(I-3)}$$

where a is the acceleration due to the driving force, $\underline{\nabla}_v$ is the gradient in velocity ($\underline{v}$) space, and t is time. A solution is assumed of the form:

$$f(\underline{v}) = f_o(\underline{v}) + \underline{E} \cdot \underline{v}\, f_1(\underline{v}) + (\underline{B} \times \underline{E}) \cdot \underline{v}\, f_2(\underline{v}) \qquad \text{(I-4)}$$

where $\underline{E}$ and $\underline{B}$ are the electric and magnetic fields, respectively.

An expansion of $f(\underline{v})$ in spherical harmonics in $\underline{v}$ space results in the following

$$\frac{dg}{du} = -\sum_i \frac{M^2 N_i}{(eE)^2 \alpha(u) k} \left\{ \frac{3}{2} \frac{m}{M_i} \sqrt{\frac{u}{k}} \sigma_{ic}(u)\, g(u) + \frac{12k\, W_i\, \sigma_{ir}(u)}{m\sqrt{u}} g(u) \right.$$

$$\left. + \frac{0.75}{\sqrt{ku}} \sum_j \int_o^u \left[(u + u_{ij})\, \sigma_{ij}(u + u_{ij})\, g(u + u_{ij}) - u\sigma_{ij}(u)\, g(u) \right] du \right\} \tag{I-5}$$

E is the rms amplitude of the electric field with angular frequency ω; $g(u) = f_o(u)$; $u(eV) = kv^2$ where k is a unit conversion factor; e/m is the electron charge to mass ratio; N_i is the density of species i with mass M_i which has elastic cross section $\sigma_{ic}(u)$, an average rotational cross section σ_{ir}, and inelastic cross section σ_{ij} for inelastic process j with threshold energy u_{ij} (eV). W_i is the average energy loss in a rotational collision with species i.

In Eq. (I-5) it can be seen that the first term represents the momentum transfer, the second term the rotational excitation collisions, and the third term includes all other inelastic processes such as vibrational excitation, ionization, dissociation, electronic excitation, and dissociative attachment. In our calculations the rotational cross section, σ_{ir}, is set to zero and rotation is treated as another group of inelastic processes.

The expression for $f_1(u)$ and $f_2(u)$ are given in terms of g (u) as:

$$f_1(u) + - \frac{2ke}{m} \alpha(u) \frac{dg}{du} \tag{I-6}$$

$$f_2(u) = \frac{\Omega}{\nu(u)} f_1(u) \tag{I-7}$$

where $\Omega = (e\,B/m)$ and

$$\alpha(u) = \frac{\nu(u)\left[\omega^2 + \Omega^2 + \nu^2(u)\right]}{(\omega^2 - \Omega^2) + \nu^4(u) + 2\nu^2(u)\left[\omega^2 + \Omega^2\right]} \qquad \text{(I-8)}$$

$$\nu(u) = \sum_i N_i \sqrt{\frac{u}{k}} \left[\sigma_{ic}(u) + \sigma_{ir}(u) + \sum_j \sigma_{ij}(u)\right] \qquad \text{(I-9)}$$

The small perturbation solution as described above is valid for a periodically fluctuating electric field $\underline{E}$, with frequency ω, and magnetic field $\underline{B}$. It is of questionable accuracy at high field strengths and/or low frequencies; however it is valid for $\omega = 0$. For the current application considerable simplification exists because the electric field is constant, therefore $\omega = 0$, and there is no magnetic field. Hence, Eq. (I-8) becomes $\alpha(u) = 1/\nu$, $f_2(u) = 0$ and further simplification of the other relations are obvious. Further discussion of the limits of validity of the theory may be found in Ref. 2.

2. *Data Base*

The only comparison between predicted (i.e. solutions developed from Eq. (I-3)) and measured electron transport properties in H_2/D_2 discharges, which has been performed for a wide range of the Townsend parameter E/N, is the study of Englehardt and Phelps.[3] At the time of this latter study the available cross section data base for elastic and inelastic collisions between electrons and H_2/D_2 was very limited and many of the cross sections were deduced by Englehardt and Phelps through a technique involving trial and error comparisons between predicted and measured transport properties. (In this analysis theoretical and experimental guidelines were used wherever possible in specifying the cross sections.) Since the time of this analysis a considerable amount of new data concerning the collision processes in the $e/H_2/D_2$ system have been amassed, and it has become evident that the Englehardt and Phelps cross section base requires substantial revision.

This re-interpretation is due, in part, to the fact that the measured transport properties of H_2/D_2 are now more accurately defined. In particular, it has been found that the transport data used in Ref. 3 for H_2

at large E/N, $\geq 6 \times 10^{-16}$ V/cm^2, were erroneous. This led to an incorrect definition of the momentum transfer and electronic state excitation cross sections at high electron energies, i.e., $\geq$ 10 eV. More important, from the viewpoint of laser performance predictions, is the fact that the theoretical treatment applied by Englehardt and Phelps[3] to specify the cross sections for rotational excitation has since been found to be inadequate, and therefore, both the rotational and vibrational cross sections presented in Ref. 3 are invalid. In the present analysis the cross section data base has been updated. The goal of this update was not to provide the most "exact" comparison with the available transport data, but rather to ensure that the comparison between predicted and measured transport properties was sufficiently good so that laser performance predictions could be developed with a reasonable degree of confidence.

Much of the relevant cross section data base for H_2 molecules may be found in the recent data compilation by Kieffer;[4] however, no recommended cross sections nor comparison with theoretical predictions are included in this compilation. Therefore, a search of the recent literature was performed, the available experimental data and theoretical predictions for each process were reviewed, and a "best" cross section representation chosen. These selected cross sections represent the authors' personal judgement (and perhaps biases) concerning the relative merits of the various measurements and theoretical calculations. In most cases the high energy (> 10 eV) portion of the cross sections had to be extrapolated as no theoretical predictions or measurements are available.

The most studied inelastic process for H_2 is the cross section for the $v = 0 \rightarrow 1$ vibrational excitation. The data base[3, 5-11] for this process is shown in Fig. I-2. The larger cross sections were deduced from drift tube results, while the remainder of the data were determined by electron beam experiments. The latter measurements are preferred, since the data analysis for a beam experiment is more straightforward than for the drift tube. The cross section selected to be used for the present calculations was essentially that of Ehrhardt et al[10] extrapolated into the higher energy data of Trajmar et al.[9] The data for excitation into higher vibrational levels of H_2 is more sparse, and the choice of these cross sections is, therefore, considerably more subjective. As an example, the data base for vibrational excitation to $v = 2$ is shown in Fig. I-3. Again the cross section selected was that of Ehrhardt et al[10] extrapolated into the high energy data of Trajmar et al.[9] Fortunately, the larger excitation cross section is to the first vibrational level.

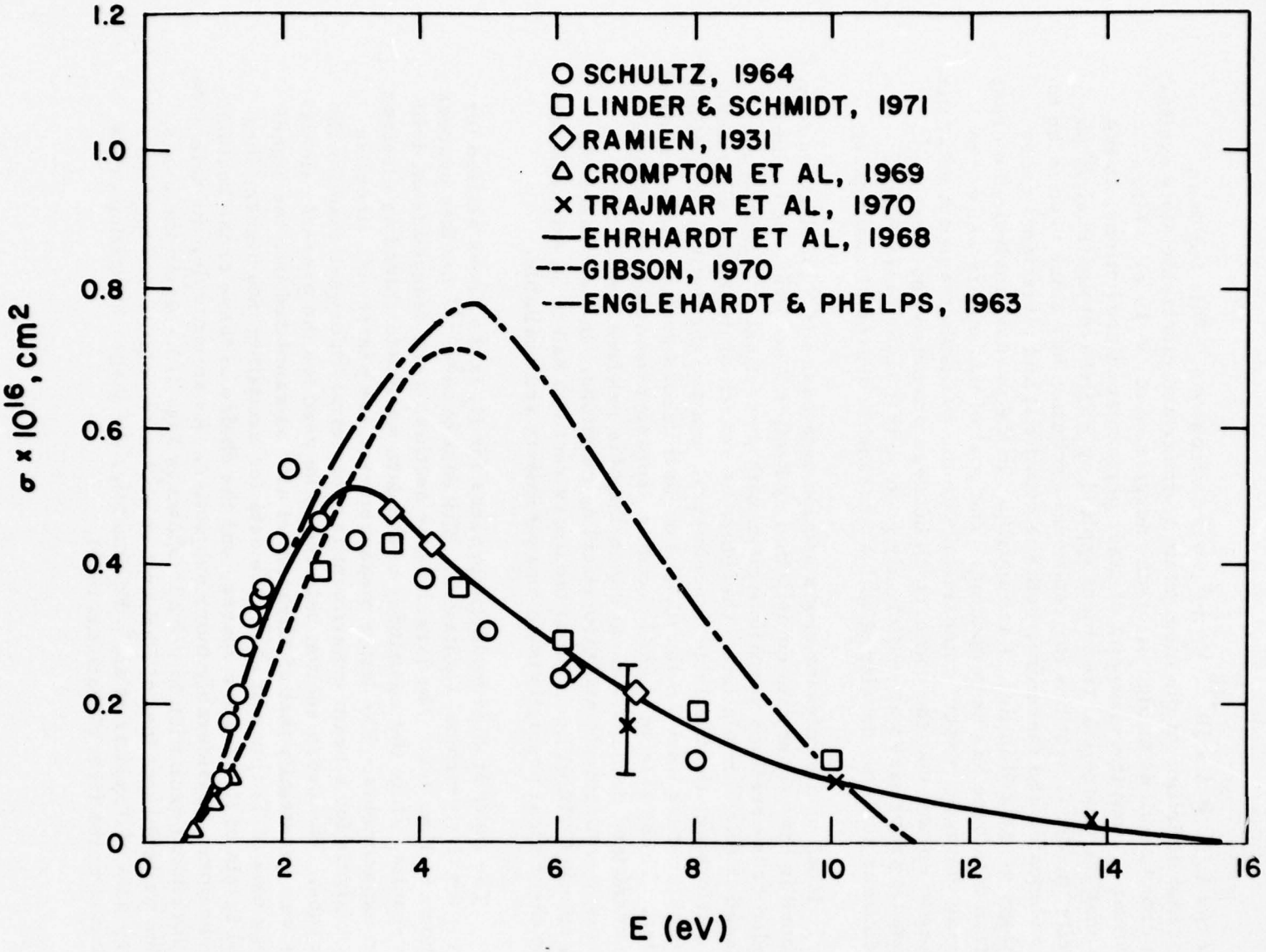

Fig. I-2 Experimental Electron Excitation Cross Section for the $v = 0 \rightarrow 1$ Vibrational Transition of H_2 versus Electron Energy. The Threshold Energy for the $v = 0 \rightarrow 1$ Transition is $E_o = 0.516$ eV.

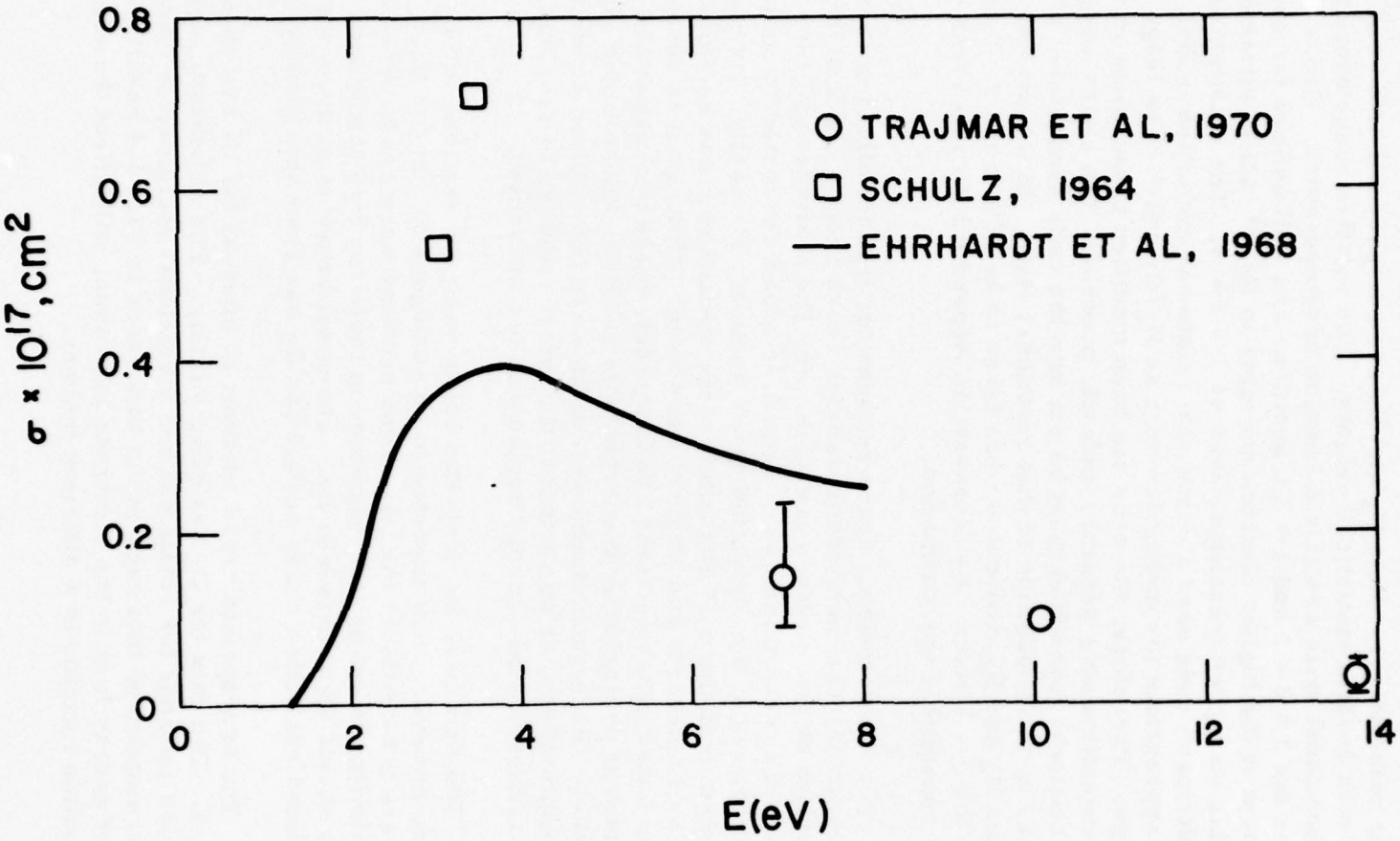

Fig. I-3 Experimental Electron Excitation Cross Section for the $v = 0 \rightarrow 2$ Vibrational Transition of H_2 versus Electron Energy.

Rotational excitation was handled in an approximate manner in the present calculations. Both H_2 and D_2 are composed of ortho and para states with certain statistical weights. The relative concentrations of each rotational state are also a function of temperature. Cross section data for the $J = 0 \rightarrow 2$ and $1 \rightarrow 3$ transitions are well defined for both H_2 and D_2 except at the higher electron energies in D_2.[11] Little information is available on higher transitions such as $J = 2 \rightarrow 4$. The existing version of the Boltzmann code uses a continuum rotational excitation model, but this is not appropriate for molecules such as H_2/D_2 which have large rotational spacings. Therefore, the code has been modified to calculate each rotational transition as a separate inelastic process. The cross section for each rotational transition must be put into the code separately, properly weighted by the population of that rotational state. In the present predictions the H_2 and D_2 molecules were taken to be 50% in the $J = 0$ state and 50% in the $J = 1$ state. As discussed in Appendix I-A, this turns out to be a very reasonable approximation.

For the remaining cross sections for H_2 the following correlations were used: (a) The momentum transfer cross section deduced by Gibson[11] was applied at low electron energies. (b) The dissociation cross section used was that determined by Corrigan,[12] albeit corrected by more recent measurements of the ionization cross section. (3) Lastly, the high energy momentum transfer and electronic state excitation cross sections determined by Englehardt and Phelps[3] were used. Although it is recognized that the latter cross sections are incorrect, these processes are only important at characteristic energies beyond those for optimum vibrational excitation. Since such discharge regimes are not of interest for the present laser applications, it was felt that the effort required to develop accurate cross sections in this energy region was not warranted.

The data base for inelastic collision cross sections for D_2 is very limited, however, it is expected to be analogous to that for H_2.[3] Where data were not available for D_2, cross sections were constructed which were similar in shape and magnitude to those for H_2 but adjusted to have energy onsets appropriate to D_2. The onset behavior of the $v = 0 \rightarrow 1$ vibrational excitation cross section for D_2 has been specified by Gibson.[11]

The appropriate cross sections of interest for H_2 are shown in Fig. I-4. The data for D_2 are quite similar. For simplicity, only one of the cross sections for rotational and vibrational excitation is shown. It is to be remembered that each of the processes in Fig. I-4 results in a distinct energy loss to the electrons and, thus, will affect the electron distribution function in a different manner.

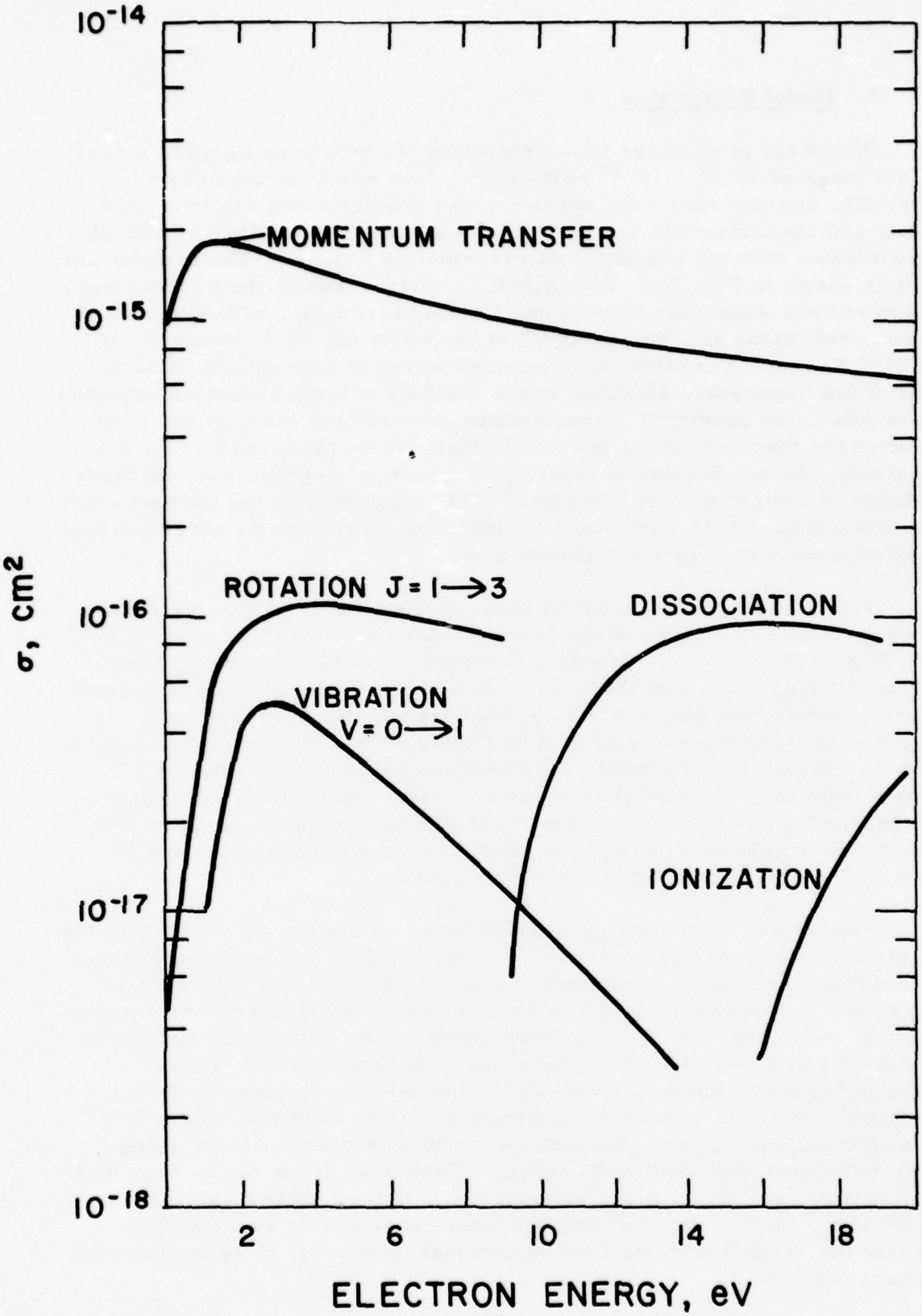

Fig. I-4 Inelastic Cross Section Data for H_2 used in Boltzmann Transport Code.

3. Model Predictions

Discharge predictions have been made for both pure H_2 and D_2 over the E/N range of 10^{-16} - 10^{-15} volts-cm^2. As a check on the validity of the results, comparisons were made between the predicted electron drift velocity and characteristic electron energy and the best available drift tube measurements of these quantities as presented in Ref. 13. The comparison for H_2 is shown in Fig. I-5. Although it is obvious that further refinements could have been made, the agreement is quite reasonable, with differences between predictions and data being 7% at the worst for E/N between 1 and 6×10^{-16} V-cm^2. The difference becomes worse at increased E/N as a result of the improperly specified cross sections at higher electron energies. In particular, the predicted characteristic energies are too high and drift velocities too low, continuing the trend which can be observed in Fig. I-5. Conversely, the predictions at higher E/N are in fair agreement with those developed by Enhglehardt and Phelps.[3] This suggests that the changes made in the low energy cross sections, i.e. rotation, vibration, do not affect the predicted transport properties at high E/N.

Such a comparison cannot be made in the case of D_2 inasmuch as there are no measurements of the room temperature transport properties[13] for E/N $\geq 10^{-16}$ V-cm^2. Gibson[11] has shown that the low energy cross sections for D_2, which are essentially identical to those used in the present analysis, provide good agreement ($\leq$ 1%) with the observed transport properties of D_2 in the range of E/N of 1 to 10×10^{-17} V-cm^2. Nonetheless, he points out that the rotational cross sections cannot be determined uniquely from the available electron swarm data. Inasmuch as the conjecture that the H_2 and D_2 cross sections are similar cannot be confirmed at present, the predictions for D_2 presented in the following pages must be considered as qualitative rather than quantitative.

Predictions of the energy deposition and excitation rate constants for pure H_2 are shown in Figs. I-6 and I-7 respectively. While the excitation rate constants are required to perform kinetic calculations, the relative energy distribution can be used to determine optimum discharge parameters. As can be seen from Fig. I-6, optimum pumping into the vibrational mode of H_2 occurs at E/N $\sim 3 \times 10^{-16}$ volts-cm^2. At lower E/N rotational excitation begins to dominate, while at higher E/N dissociation becomes important. Note that even at the optimum operating condition only $\sim$ 70% of the electron energy loss goes into vibration with the remainder going into translational and rotational heating. From Fig. I-7 it can be seen that the vibrational excitation rate constants are also near their maximum at an E/N of 3×10^{-16} volts-cm^2 and decrease considerably at lower E/N. Note that the excitation of the first vibrational level of H_2 is by far the dominant process.

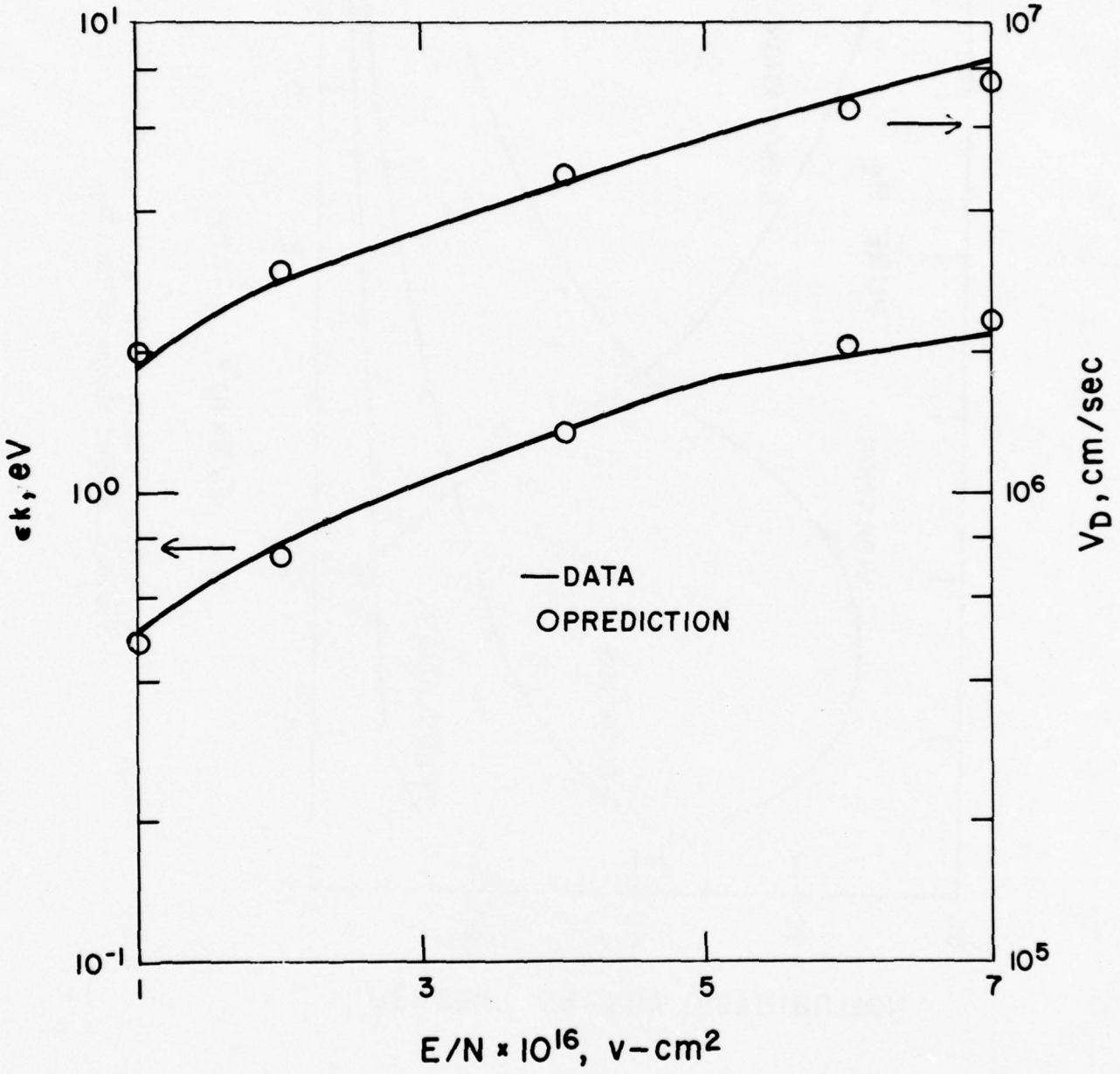

Fig. I-5 Comparison Between Predicted and Measured Discharge Properties of Pure H_2 at T = 293°K.

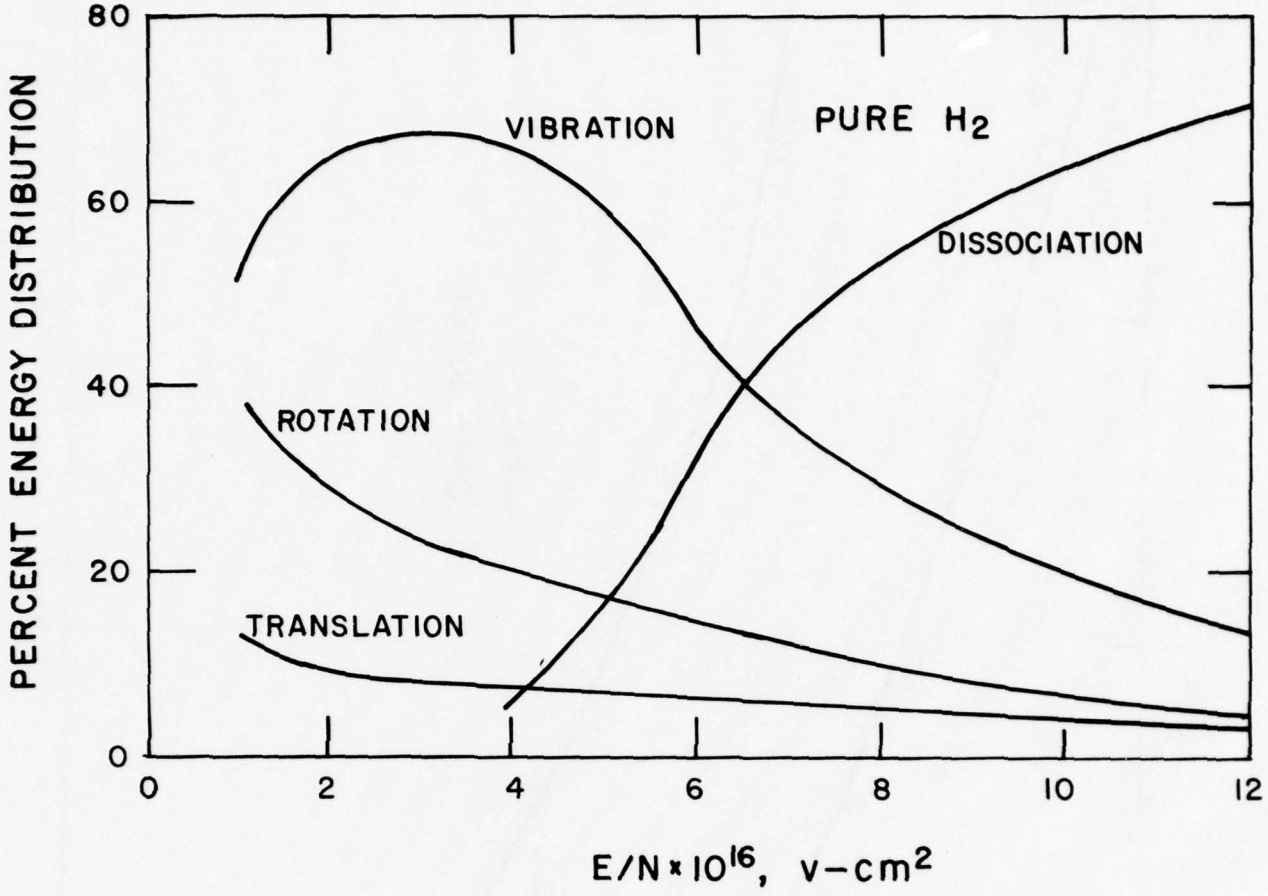

Fig. I-6 Calculated Percent Discharge Energy Deposition into Various Internal Modes of Pure H_2.

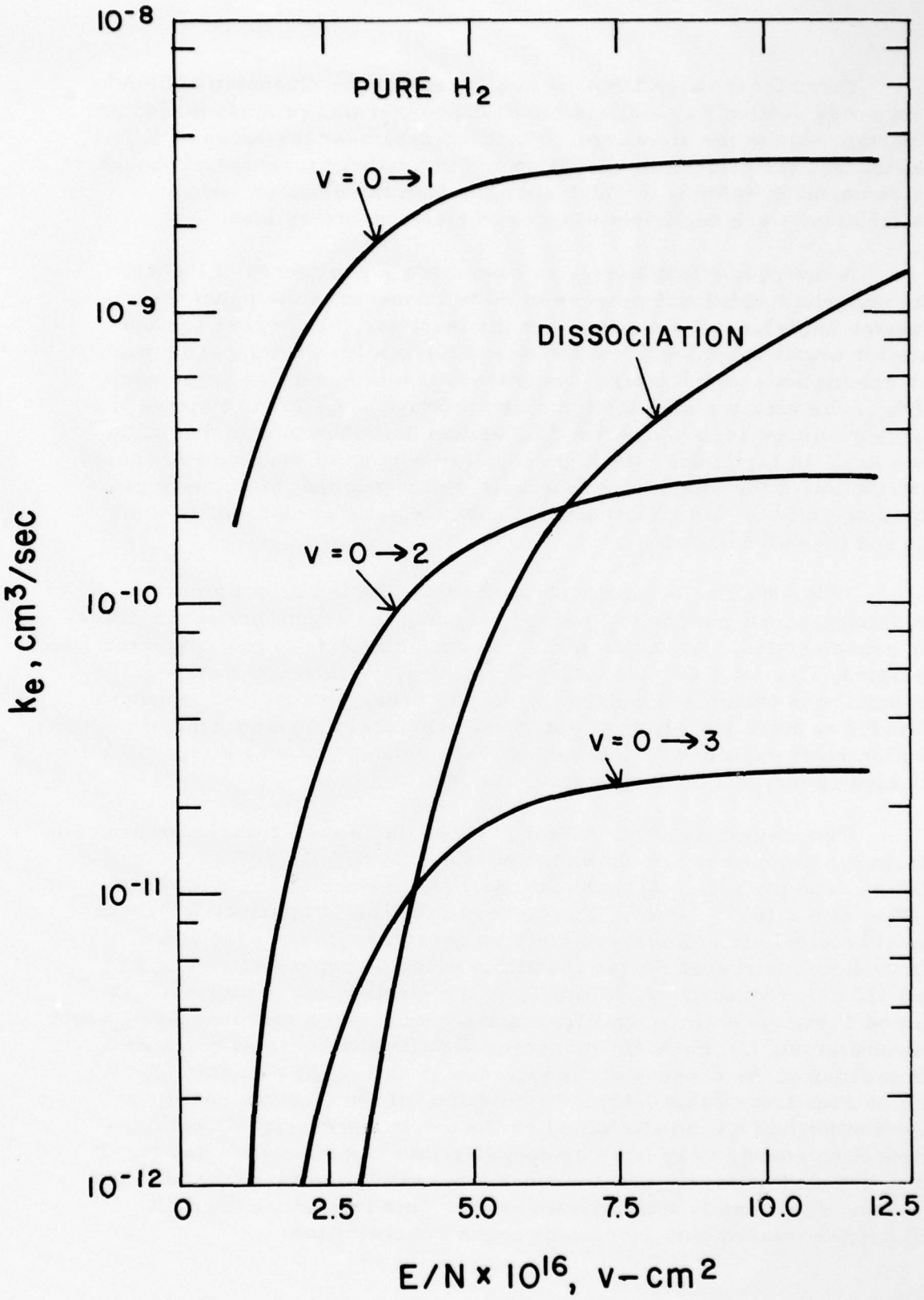

Fig. I-7 Predicted Excitation Rate Constants for a Pure H_2 Discharge at 300°K versus E/N.

From these calculations it was found that the dissociative attachment cross section was sufficiently small so that this process played no important role in the discharge. Furthermore, over the range of E/N considered, the electronic excitation and ionization processes, although instrumental in defining the high energy tail of the electron energy distribution, were negligible sources of electron energy loss.

A few predictions have also been made for mixtures of H_2/Ar. The important additional process in these mixtures is the momentum transfer collisions of electrons with the inert gas. The cross section data for argon was taken from Frost and Phelps.[14] On comparing pure gas calculations with mixture predictions, it was found that at the same E/N_{H_2}, the electron distribution of the mixture has a lower average electron energy and a more non-Maxwellian distribution than that of the pure gas. In particular, the higher energy portion of the electron energy distribution of the mixture is decreased relative to that of the pure gas. The magnitude of this effect depends upon the ratio of diatomic to inert gas and the value of E/N_{H_2}.

This behavior is intimately connected with the deep Ramsauer minimum occuring in the low energy region of the argon momentum transfer cross section. At values of E/N_{H_2} corresponding to low characteristic energies, i.e., < 1 eV, the effect of argon on the mixture transport properties is minimized because of the low cross section for momentum transfer at these low electron energies. This Ar momentum transfer cross section rises rapidly with increasing electron energy, and, thus, will effect the high energy tail of the electron distribution.

The magnitude of this effect is shown in Table I-1 where predicted discharge properties are shown for mixtures of 50% H_2/50% Ar, 15% H_2/85% Ar, and pure H_2. All calculations were performed for a constant E/N_{H_2} of 8×10^{-16} v-cm^2. The most interesting comparison is between the characteristic and average electron energies. In the case of a Maxwellian distribution these quantities would be representative of kT_e and $3/2\ kT_e$ respectively, where T_e is the electron temperature[2]. As can be seen, these two quantities approach each other with increasing argon concentration, i.e. the electron energy distribution becomes more non-Maxwellian at the expense of the high energy tail of the distribution. As can be seen from Table I-1 this "truncation" of the electron energy distribution has a dramatic effect on the discharge energy allocation, channeling energy away from dissociation into vibrational excitation. It is to be noted however, that the vibrational excitation rate constant does not vary significantly with mixture ratio. This is because the drift velocity decreases with increasing argon concentration.

TABLE I-1

EFFECT OF Ar ON TRANSPORT PROPERTIES OF H_2

(all calculations performed for $E/N_{H_2} = 8 \times 10^{-16}$ v-cm^2)

GAS MIX	100% H_2	50% H_2 50% Ar	15% H_2 85% Ar
Characteristic Energy, eV	2.63	2.56	2.1
Average Energy, eV	3.83	3.45	2.4
Drift Velocity, cm/sec	8.5×10^6	5.3×10^6	3.2×10^6
Fractional Discharge Energy Lost to Vibrational Excitation	0.29	0.46	0.68
Fractional Discharge Energy Lost to Dissociation	0.55	0.32	0.02
Vibrational Excitation Rate Constant $v = 0 \rightarrow 1$, cm^3/sec	3.3×10^{-9}	3.3×10^{-9}	3×10^{-9}

As alluded to earlier, this effect of Ar becomes less pronounced with decreasing E/N_{H_2}, because the fraction of electrons which would fall into the higher energy region dominated by the argon momentum transfer cross section decreases with decreasing characteristic electron energy. The importance of the argon Ramsauer minimum in the transport behavior of H_2/Ar discharges had previously been discussed by Englehardt and Phelps.[15] Although the H_2 cross sections employed in the present analysis are different than those used in Ref. 15, the phenomenology is the same.

Predictions of the energy deposition and excitation rate constants for pure D_2 are shown as a function of E/N in Figs. I-8 and I-9. The results are quite analogous to those for H_2, except that the optimum discharge conditions for vibrational excitation are at slightly lower E/N and the maximum amount of energy transferred to vibration is slightly higher. No predictions have been provided for D_2/Ar mixtures; however, it is expected that the mixture behavior would be similar to that observed for H_2/Ar.

Discharge calculations have been performed for D_2/He mixtures.* A composite of the momentum transfer cross sections for He determined by Frost and Phelps[14] and Crompton et al,[16] was employed in these calculations. The predicted characteristic energy and drift velocity for mixtures of 100% D_2, 40% D_2/60% He, and 20% D_2/80% He are shown in Fig. I-10 as a function of E/N_{D_2}. As can be seen, both characteristic energy and drift velocity decrease monotonically with increasing helium concentration. Unlike argon, helium exhibits a relatively smooth momentum transfer cross section with no Ramsauer minimum, thus the electron energy distribution is not truncated. Indeed, the ratio of average to characteristic electron energy approaches 1.5, the Maxwellian distribution value, with increasing He concentration.

The predicted discharge energy deposition and excitation rate constants for D_2/He mixtures of 20, 30 and 40% D_2 are shown in Figs. I-11 and I-12. These latter two figures are plotted vs E/N_T (N_T = total gas density) rather than E/N_{D_2}. As can be seen, the peak efficiency for vibrational excitation is essentially the same for all mixtures. Thus, the addition of helium would not be kinetically detrimental to laser performance as far as the discharge excitation is concerned.

---

*(At the time of this analysis it was thought that He would be the carrier gas in the D_2/HCl EDL experiment. As is discussed in the following sections it has since been found that Ar would be more appropriate because of fluid dynamic mixing considerations.)

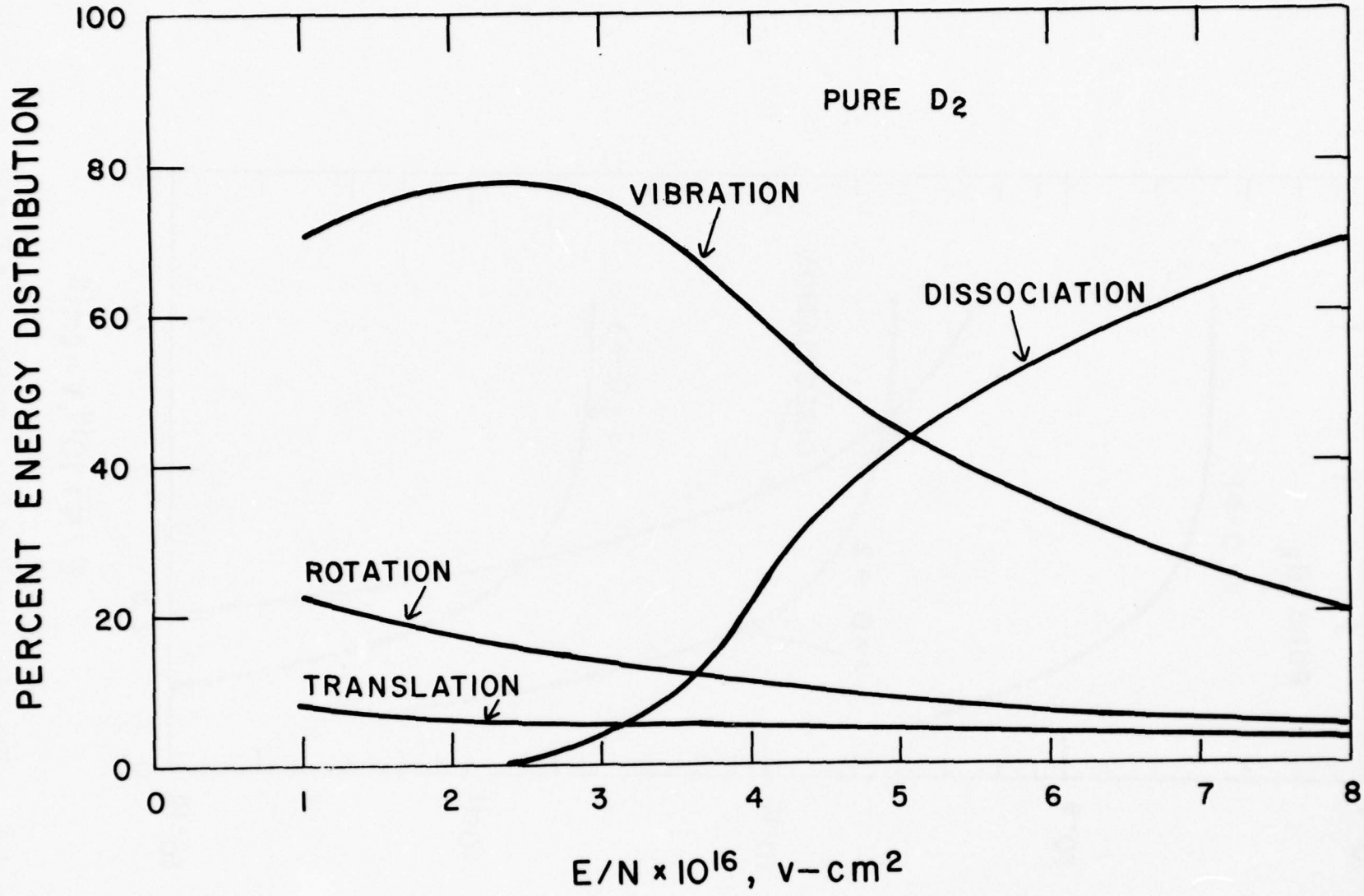

Fig. I-8 Calculated Percent Discharge Energy Deposition into Various Internal Modes of Pure D_2

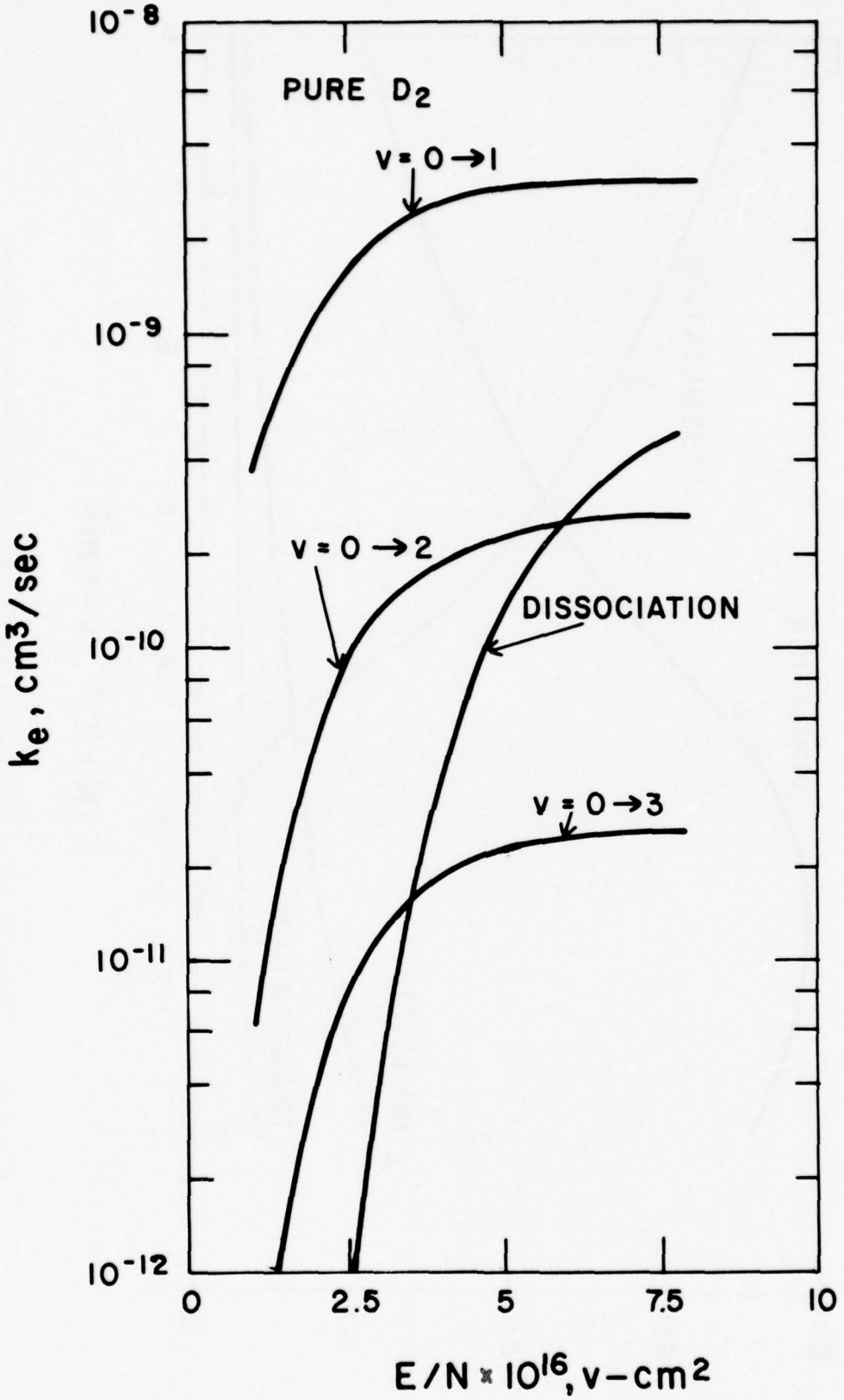

Fig. I-9 Predicted Excitation Rate Constants for a Pure D_2 Discharge at 300°K versus E/N.

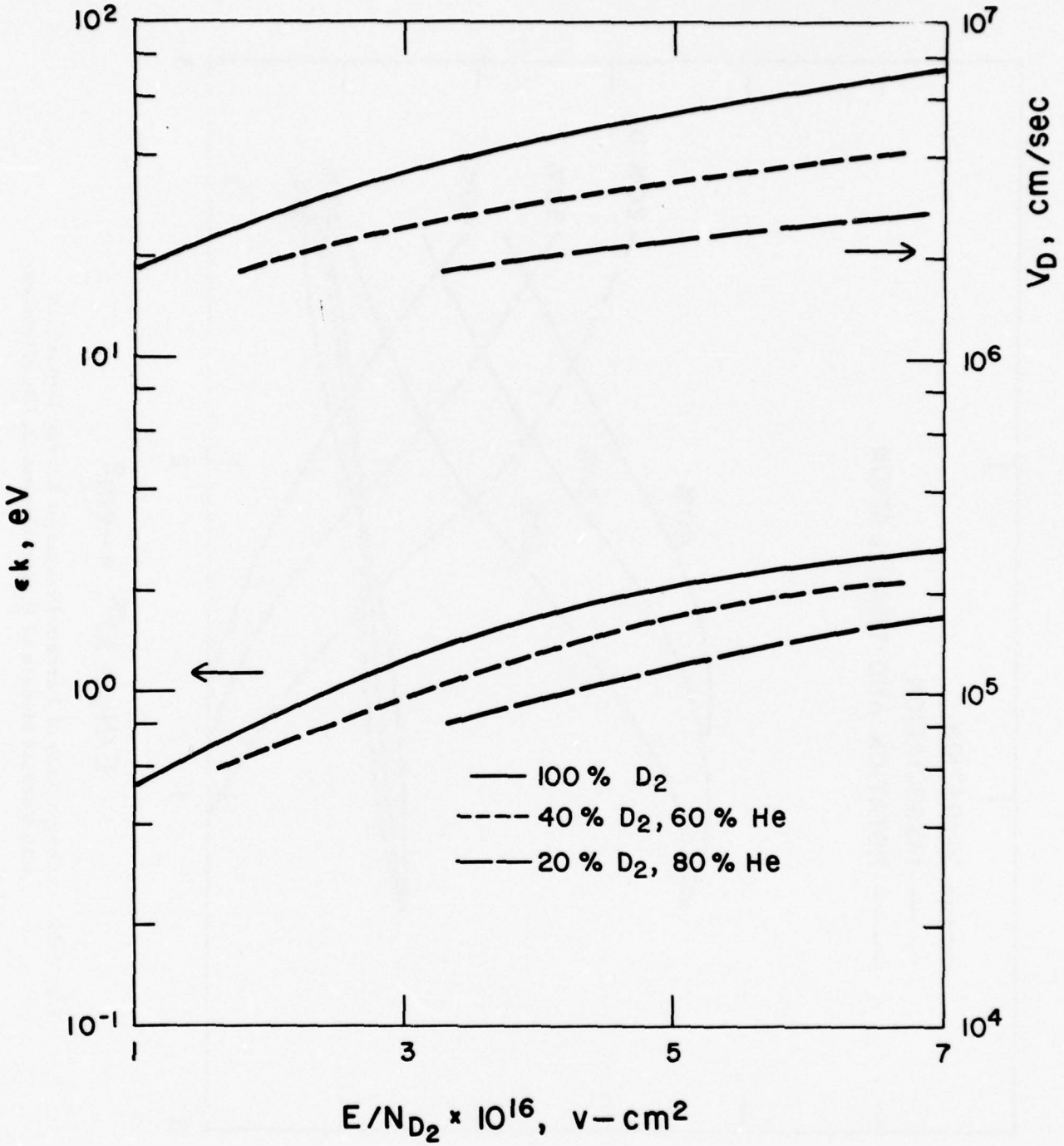

Fig. I-10 Comparison of Predicted Discharge Properties of Pure D_2 with D_2/He Mixtures.

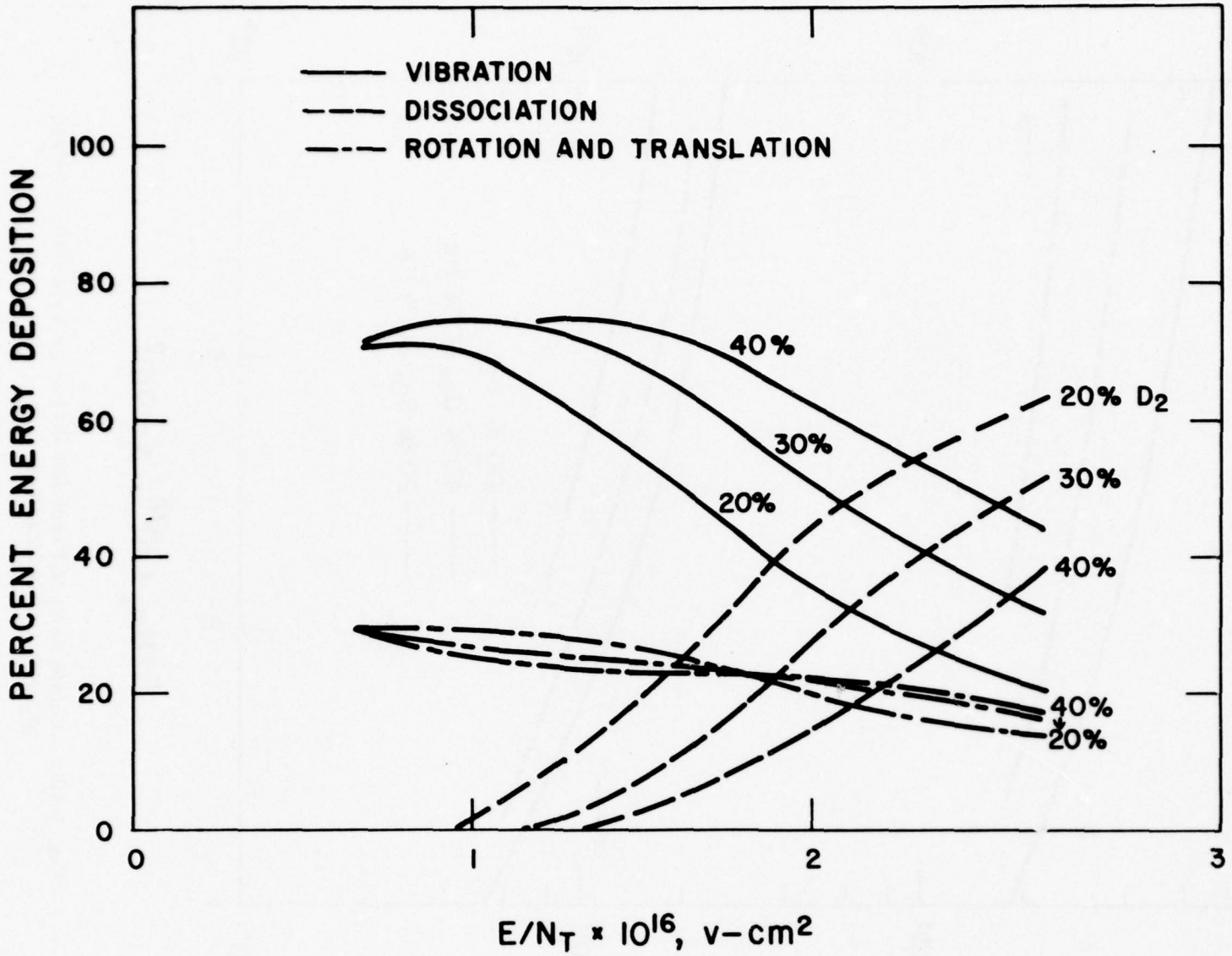

Fig. I-11 Comparison of Percent Discharge Energy Deposition into Internal Models of D_2 for Various D_2/He Mixtures.

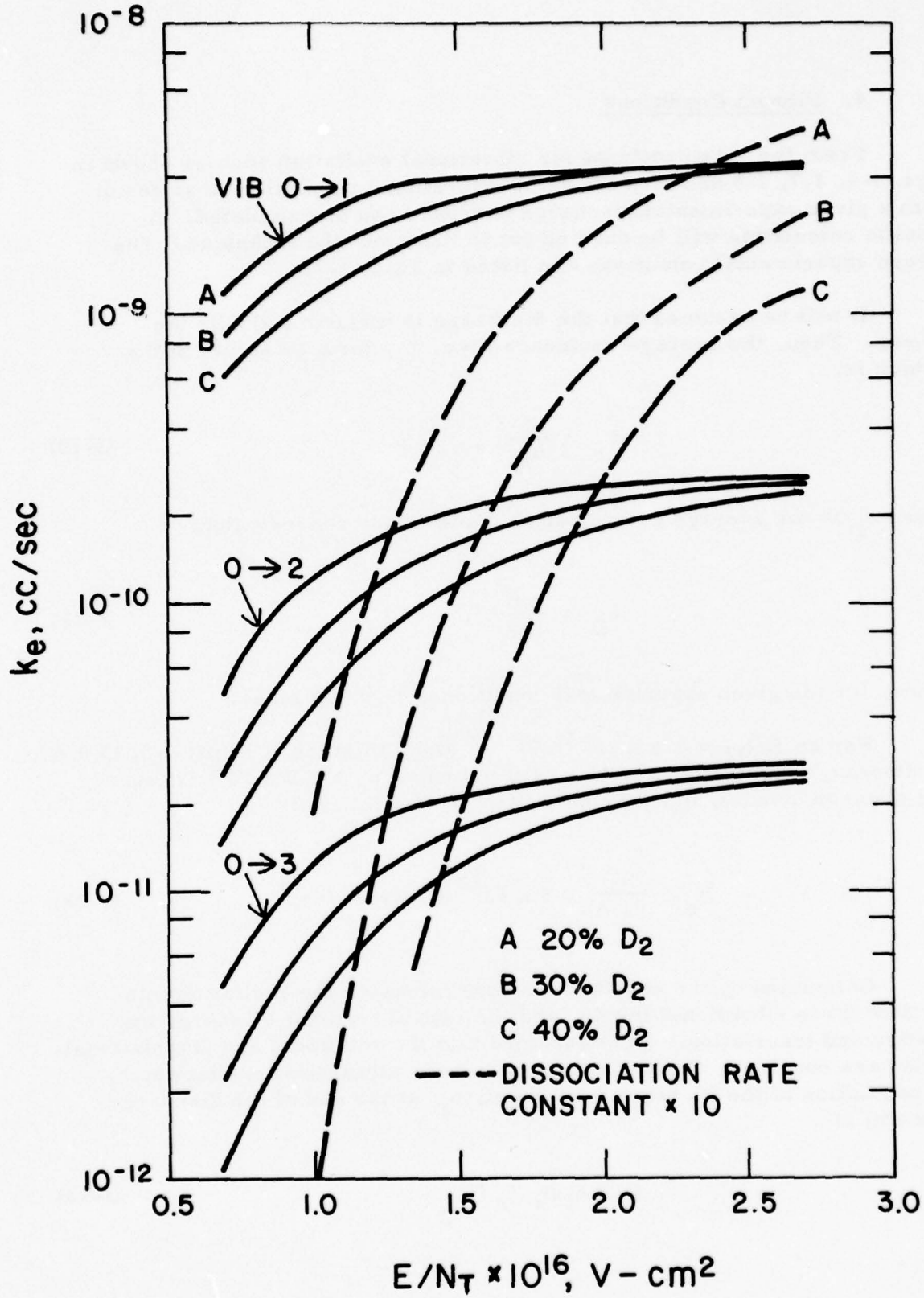

Fig. I-12 Comparison of Excitation Rate Constants of D_2 for Various D_2/He Mixtures.

4. Plenum Conditions

From the rate constants for vibrational excitation such as shown in Figs. I-4, I-7, I-9 and I-12 the actual vibrational populations that result from a given experimental discharge condition can be calculated. A specific calculation will be carried out to illustrate the technique. The chosen experimental conditions are listed in Table I-2.

It will be assumed that the discharge is uniform and fills the plenum. Then, the average residence time, τ_r, for a molecule in the plenum is:

$$\tau_r = \frac{L}{u_D} \quad , \tag{I-10}$$

where u_D is the average gas velocity. From mass conservation:

$$u_D = \frac{\dot{m}}{\rho A} \quad . \tag{I-11}$$

Hence, for the given experimental conditions, $\tau_r = 1.8$ msec.

For an $E/N_T = 0.8 \times 10^{-16}$ V-cm^2 and a mixture of D_2:He = 0.33:0.67, the discharge calculations yield a drift velocity, $u_e = 1.9 \times 10^6$ cm/sec. The electron density, n_e, may be determined as follows:

$$n_e = \frac{I}{u_e A} = 5 \times 10^{10} \text{ electrons/cm}^3 \tag{I-12}$$

Calculated by the code are the rate constants for excitation into the first three vibrational levels, and the rate of transfer of energy into rotation and translation. (It is assumed that the rotational and translational modes are coupled). Given a rate constant for vibrational excitation, k_i, the population of the ith vibrational level, n_i, at the end of the discharge (plenum) is

$$n_i = k_i \, n_e \, \tau_r \, N_{D_2} \tag{I-13}$$

TABLE I-2

NOMINAL EXPERIMENTAL DISCHARGE CONDITIONS

Length of Discharge = L = 20 cm

Cross Sectional Area of Discharge = A = 1.9 x 28 cm^2 = 53.2 cm^2

$E/N_T \sim 8 \times 10^{-17}$ V-cm^2

Discharge Current = 8 amps

N_T = Total Gas Density in particles/cm^3 of D_2/He Mixture

Plenum Pressure = 53 torr

Flow Rates of Gases:

$\dot{m}_{He}$ = 0.82 moles/sec

$\dot{m}_{D_2}$ = 0.41 moles/sec

Total Gas Density in Plenum (53 torr at 400°K) = $\rho = 2.13 \times 10^{-6}$ moles/cm^3

For the particular experimental conditions the vibrational populations that result are:

$$n_1 = 4 \times 10^{16} \text{ part/cm}^3$$

$$n_2 = 1.3 \times 10^{15} \text{ part/cm}^3$$

$$n_3 = 1 \times 10^{14} \text{ part/cm}^3$$

The estimate of rotational/translational heating is $\Delta T \sim 20^{\circ}K$.

The above calculation neglects V → T deactivation from D_2. We estimate a relaxation time of τ_{VT} for D_2 of ~ 100 msec for the plenum conditions. Clearly, $\tau_{VT} \gg \tau_r$ and V → T processes can be neglected. However, the intramode V → V exchange time for D_2 is estimated to be ~ 1 msec for the given conditions, and considerable rearrangement of quanta can occur within the D_2 while the gas flows through the plenum. Since the excitation rates to vibrational levels of D_2 higher than v = 3 are not known, and since the V → V rates are fast, we have assumed that the distribution found in the discharge will probably approach a Boltzmann distribution and can be characterized by an approximate vibrational temperature:

$$T_V = \theta_{D_2} / \ln (n_o/n_1) \approx 1700^{\circ}K \qquad \text{(I-14)}$$

where θ_{D_2} is the characteristic vibrational spacing for $D_2 = 4300^{\circ}K$.

A more exact calculation would have to include the combined finite kinetics of electron excitation together with finite vibrational exchange rates as the D_2/He mixture flows through the plenum. This type of calculation is possible by a modification of the present code, but was not pursued in the present contract.

C. D_2/HCl LASER MODELING

1. Assessment of Vibrational Energy Transfer Rates

In order to perform model calculations for the D_2/HCl laser it is necessary to determine the kinetic rates for vibration→translation (V→T) and vibration→vibration (V→V) energy transfer processes for this molecular system. Considerable experimental data is available for the D_2, HCl, and D_2/HCl mixtures, and this data base has been reviewed to determine the best kinetic rate package. Almost all of these data provide kinetic information on the rates for the lowest vibrational levels (v = 1). Therefore, a combination of empiricism and theory has been used to extend the rates to the upper vibrational levels for the anharmonic oscillator model (A. H. O.).

The mechanism considered for vibrational energy exchange in the D_2/HCl system is shown in Table I-3. It can be seen that this is a complex mechanism with many rates.

a. V→T Processes

Considerable experimental data exist for the V→T processes for the D_2/D_2 and HCl/HCl interactions for v = 1. For D_2, data exist at high temperatures (1500 - 3000°K) from shock tube experiments of Kiefer and Lutz[17] and Bird and Breshears.[18] At room temperature a number of measurements[19-21] have been performed. Quite recently Lukasik and Ducuing[22] have performed a Raman excitation technique to measure the V→T relaxation of D_2 over the temperature range of 50→400°K. The totality of this data provide a consistent set of measurements and define the V→T rate constant and its temperature dependence to better than a factor of two. A curve fit to these data is used as the rate for the process:

$$D_2\ (v = 1) + D_2 \rightarrow D_2\ (v = 0) + D_2\ . \qquad \text{(I-15)}$$

For the HCl/HCl V→T process data also exist over a wide range of temperature.[23-25] Figure I-13 summarizes these data and shows the resulting curve fit. It is seen that this rate exhibits a minimum around room temperature. This phenomenon is typical of the hydrogen halides and is presumably due to the dominance of attractive forces in the molecular interaction at lower temperatures.

TABLE I-3

ANHARMONIC OSCILLATOR KINETIC MECHANISM FOR D_2/HCl

V → T PROCESSES:

$$A\ (v = 1) + B \rightarrow A\ (v = 0) + B$$
$$A\ (v = 2) + B \rightarrow A\ (v = 1) + B$$
$$\vdots$$
$$A\ (v = n) + B \rightarrow A\ (v = n-1) + B$$

(4 combinations: A/A, A/B, B/B, B/A)

V → V PROCESSES:

INTRAMODE

$$A\ (v = 1) + A\ (v = 1) \rightarrow A\ (v = 2) + A\ (v = 0)$$
$$A\ (v = 2) + A\ (v = 1) \rightarrow A\ (v = 3) + A\ (v = 0)$$
$$\vdots$$
$$A\ (v = n) + A\ (v = 1) \rightarrow A\ (v = n + 1) + A\ (v = 0)$$
$$\vdots$$
$$A\ (v = n) + A\ (v = m) \rightarrow A\ (v = n + 1) + A\ (v = m - 1)$$

(A = D_2 or HCl, two sets of rates)

INTERMODE

$$A\ (v = 1) + B\ (v = 0) \rightarrow A\ (v = 0) + B\ (v = 1)$$
$$\vdots$$
$$A\ (v = n) + B\ (v = m) \rightarrow A\ (v = n-1) + B\ (v = m + 1)$$

(A = D_2, B = HCl)

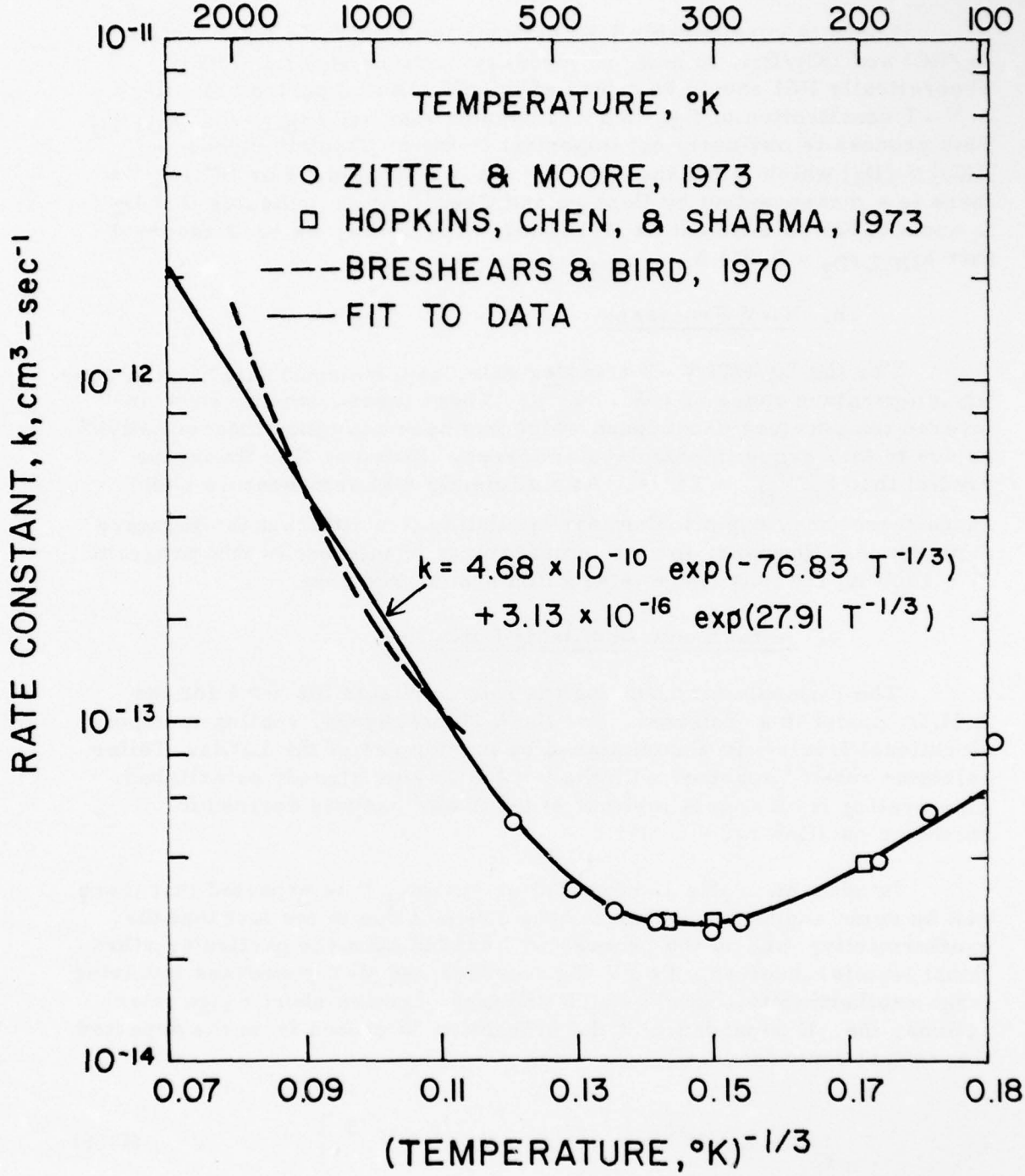

Fig. I-13 V→T Data for HCl/HCl Collisions as a Function of Temperature and Assumed Curve Fit.

There is considerably less data for the mixed V→T processes D_2/HCl and HCl/D_2. In fact, no measurements exist for D_2/HCl. Theoretically HCl should be a less efficient collision partner than D_2 in V→T deactivation of D_2. We will assume that $k_{D_2/HCl} = 0.2\ k_{D_2/D_2}$. This process is obviously not important in the mechanism unless $[HCl] > [D_2]$ which is not the optimum laser condition. For HCl/D_2 there is a measurement by Hopkins and Chen[19] which indicates that D_2 is about 0.025 as efficient as HCl itself. Therefore, we have assumed that $k_{HCL/D_2} = 0.025\ k_{HCl/HCl}$.

b. V→V Processes

For the D_2/HCl V→V transfer rate, experimental data[24] exist over the temperature range of 196 - 342°K. These measurements show an inverse temperature dependence which has been explained theoretically[24] as due to long range intermolecular forces. Based on this theory we predict that $k^{V\to V}_{D_2/HCl} \propto T^{-1/2}$. At sufficiently high temperature short range forces may begin to dominate resulting in a different temperature dependence. However, for the temperatures of interest in this program ($T < 1000°K$) the long range interaction should dominate.

c. Anharmonic Oscillator Rates

The rationale for choosing the rate constants for $v > 1$ for the A.H.O. model is as follows: For the V-T processes, scaling to upper vibrational levels was accomplished by making use of the Landau-Teller selection rules[26] together with the $v = 1 \to 0$ rates already established. This scaling is an approximation, since it was initially derived for harmonic oscillators.

In addition to this Landau-Teller scaling, it is expected that there will be some additional change in rate constant due to the fact that the exothermicity, ΔE, of the process will depend upon the particular vibrational level(s) involved. For V-T processes and V-V processes involving large exothermicity, both of which primarily involve short range interactions, the ΔE dependence of the probability is scaled from the expected theoretical dependence.[27]

$$k \propto T^{-1} \exp\left[-C\,(\Delta E)^{2/3}\,T^{-1/3}\right] \qquad \text{(I-16)}$$

The constant C is determined from the temperature dependence of the $v = 1$ process.

For V-V processes involving small ΔE ($\leq 200\ cm^{-1}$), the energy and temperature dependence is scaled according to long range interaction theory:[28]

$$k \propto T^{-1} \exp\left[-C\left|\Delta E\right|\right], \qquad (I\text{-}17)$$

where the constant C has been determined from empirical correlations or from experimental data[29-31] where available.

By this combination of experimental data, empirical correlations, and theory, the complete A.H.O. kinetic package was derived and is summarized in Table I-4. Due to their complexity, the A.H.O. kinetic rate constants are obviously an approximation at this stage, and further experimental and theoretical investigation are required to improve our understanding of these processes for the D_2/HCl molecular system. The rate constants listed in Table I-4 are those that were used in the modeling discussed in this report.

Toward the end of this program, additional data became available that would modify some of the rate constants derived above. In particular, under another program at PSI, Rosen et al[32] have recently measured the high temperature (1000-2000°K) HCl/H_2 V→T rate. Combined with the lower temperature data of Bott and Cohen,[33] these results show that the HCl/H_2 V→T process has a steeper temperature dependence than that for HCl/HCl. Thus, the assumption of $k_{HCl/D_2} = 0.025\ k_{HCl/HCl}$ is probably not correct, although the difference in the vicinity of room temperature, where the present modeling is concerned, is not expected to be very significant. In addition, Bott and Cohen[33] have also measured the D_2/HCl V→V rate over the temperature range of 300 -750°K. Their result shows a less steep temperature dependence than the data of Hopkins et al.[24] However, in the vicinity of 300°K the results are nearly identical.

It has not been possible to evaluate the quantitative significance of these revised rate constants on the laser calculations presented in this report. For the cavity conditions of interest in this study $T \leq 300°K$. At 300°K, there is little difference in the rate interpretations. However, at lower temperatures, one would expect that using the more recent rates would lead to less HCl/D_2 V→T deactivation and perhaps somewhat lower D_2/HCl V→V pumping. These effects are expected to be small and of minor importance in the overall conclusions.

TABLE I-4

LIST OF RATES FOR D_2/HCl A.H.O. MODEL

(all k's in units of cm^3-sec^{-1})

FOR D_2 $\omega_e' = 3118.4\ cm^{-1}$

$\omega_e'x_e' = 64.09\ cm^{-1}$

$\omega_e' - 2\omega_e'x_e' = 2990.22\ cm^{-1}$

Vibrational Levels → $u \leq 10$

$\Delta E' = \omega_e' - 2u\,\omega_e'x_e'$

HCl $\omega_e = 2989.74\ cm^{-1}$

$\omega_e x_e = 52.05\ cm^{-1}$

$\omega_e - 2\omega_e x_e = 2885.64$

Vibrational Levels → $v \leq 15$

$\Delta E = \omega_e - 2v\,\omega_e x_e$

1) $D_2(u) + D_2 \rightarrow D_2(u-1) + D_2$

$$k^{u,u-1}(D_2, D_2) = (u)\ 2.90 \times 10^{-9} \exp\left[-0.5963\,(\Delta E')^{2/3}\,T^{-1/3}\right]$$

$$k^{u-1,u}(D_2, D_2) = k^{u,u-1}(D_2, D_2) \exp\left[-1.4388\,(\Delta E')\,T^{-1}\right]$$

2) $D_2(u) + HCl \rightarrow D_2(u-1) + HCl$

$$k^{u,u-1}(D_2, HCl) = 0.200\ k^{u,u-1}(D_2, D_2)$$

$$k^{u-1,u}(D_2, HCl) = k^{u,u-1}(D_2, HCl) \exp\left[-1.4388\,(\Delta E')\,T^{-1}\right]$$

TABLE I-4 (Cont.)

3) $HCl\,(v) + HCl \rightarrow HCl\,(v-1) + HCl$

$$k^{v,v-1}(HCl, HCl) = (v)\left\{4.676 \times 10^{-10} \exp\left[-0.379\,(\Delta E)^{2/3}\,T^{-1/3}\right] + 3.130 \times 10^{-16} \exp(27.91\,T^{-1/3})\right\}$$

$$k^{v-1,v}(HCl, HCl) = k^{v,v-1}(HCl, HCl) \exp\left[-1.4388\,(\Delta E)\,T^{-1}\right]$$

4) $HCl\,(v) + D_2 \rightarrow HCl\,(v-1) + D_2$

$$k^{v,v-1}(HCl, D_2) = 0.025\,k^{v,v-1}(HCl, HCl)$$

$$k^{v-1,v}(HCl, D_2) = k^{v,v-1}(HCl, D_2) \exp\left[-1.4388\,(\Delta E)\,T^{-1}\right]$$

5) $D_2\,(u) + HCl\,(v-1) \rightarrow D_2\,(u-1) + HCl\,(v)$

$$k^{u,u-1}_{v-1,v}(D_2, HCl) = (u)\,(v)\left\{8.89 \times 10^{-11}\,T^{-1} \exp\left[(-1.633 \times 10^{-3})\,\Delta E''\right]\right\}$$

$$\Delta E'' = \Delta E' - \Delta E = \omega_e' - 2u\omega_e'x_e' - \omega_e + 2v\omega_e x_e$$

$$k^{u-1,u}_{v,v-1}(D_2, HCl) = k^{u,u-1}_{v-1,v}(D_2, HCl) \exp\left[-1.4388\,(\Delta E'')\,T^{-1}\right]$$

6) $HCl\,(v) + HCl\,(v'-1) \rightarrow HCl\,(v-1) + HCl\,(v')$

$$|\Delta E| = (2v' - 2v)\,\omega_e x_e$$

$$k^{v,v-1}_{v'-1,v'}(HCl, HCl) = (v)\,(v')\left\{6.769 \times 10^{-11}\,T^{-1/2} \exp\left[-4.638 \times 10^{-3}\,|\Delta E|\right] + 1.941 \times 10^{-12}\,T^{1/2} \exp\left[-(0.495\,|\Delta E|^{2/3} + 40.246)\,T^{-1/3}\right]\right\}$$

$$k^{v-1,v}_{v',v'-1}(HCl, HCl) = k^{v,v-1}_{v'-1,v'}(HCl, HCl) \exp\left[-1.4388\,|\Delta E|\,T^{-1}\right]$$

TABLE I-4 (Cont.)

7) $D_2(u) + D_2(u'-1) \rightarrow D_2(u-1) + D_2(u')$

$$|\Delta E'| = (2u' - 2u)\,\omega_e' x_e'$$

$$k^{u,u-1}_{u'-1,u'}(D_2, D_2) = 0.200\; k^{v,v-1}_{v'-1,v'}(HCl, HCl)$$

$$= (u)(u')\left\{1.354 \times 10^{-11} T^{-1/2} \exp\left[-4.638 \times 10^{-3} |\Delta E'|\right]\right.$$

$$\left. + 3.882 \times 10^{-13} T^{1/2} \exp\left[-(0.495 |\Delta E'|^{2/3} + 40.246) T^{-1/3}\right]\right\}$$

$$k^{u-1,u}_{u',u'-1}(D_2, D_2) = k^{u,u-1}_{u'-1,u'}(D_2, D_2) \exp\left[-1.4388 |\Delta E'| T^{-1}\right]$$

2. Characteristic Times

Before embarking on a detailed calculation of the laser cavity, it is useful to examine the characteristic times for various energy transfer reactions and for the major fluid mechanical process of mixing. Since the D_2/HCl EDL modeling involves many parameters such as area ratio, plenum pressure, P_o, and temperature, T_o, gas composition, cavity temperature, etc. some of which are not independent quantities, a complete optimization is very complex. Instead, we will carry out a simple analysis concentrating on establishing the approximate optimum Mach number at the exit plane of the nozzle bank, M_e, for the given plenum conditions, gas composition, and experimental dimensions.

For simplicity we will assume that all energy transfer reactions occur after the gas enters the cavity. For a given plenum condition and gas composition, the flow is assumed to isentropically expand through the nozzle. Hence, the thermodynamic properties at the nozzle exit plane can be parameterized by the nozzle expansion ratio, or equivalently M_e.

We consider the five fundamental vibration transfer reactions, i.e.,

$$
\begin{aligned}
&D_2^* + HCl \xrightarrow{k_1} D_2 + HCl^* \\
&D_2^* + D_2 \xrightarrow{k_2} 2\ D_2 \\
&D_2^* + HCl \xrightarrow{k_3} D_2 + HCl \\
&HCl^* + D_2 \xrightarrow{k_4} D_2 + HCl \\
&HCl^* + HCl \xrightarrow{k_5} 2\ HCl
\end{aligned}
\qquad \text{(I-18)}
$$

The asterisk indicates that the molecule is in a vibrationally excited state. In this approximate analysis, we consider the molecules in the harmonic oscillator limit, hence intramode pumping of HCl (processes I-2) is omitted. The characteristic times, τ's, associated with the reactions, I-18, can be calculated assuming constant temperature and density. For example, the characteristic pumping time $\tau_1 \sim 1/(k_1\,[HCl])$ where $[HCl]$ is the number density of HCl. The characteristic time of a reaction is equivalent to the vibrational relaxation time for that process at the particular exit temperature and density that result from the expansion.

In addition to the reaction times, there are also the characteristic flow time, $\tau_f = L_c/u_e$, where L_c is the cavity length and u_e is the exit velocity and the characteristic mixing time, τ_M. For the experimental conditions, the mixing process will probably be dominated by turbulent transport. Sato[34] has shown that the transition distance in a shear flow is 40 to 50 times the momentum thickness at the trailing edge in a low turbulence wind-tunnel, and the size of the nozzle in the NRL device is about 1 mm while $L_c \sim 30$ cm. From a detailed calculation of turbulent mixing in a shear layer[35], the half-width of the shear layer is determined to be linear in x, i.e., $\delta \sim 0.07\,x$. The density ratio between the two shear layers for this calculation is comparable to the present experiment. Using the above linear growth result, one can now estimate the turbulent mixing time, τ_M, which is defined as the time for the shear layer to grow to the width of the nozzle at the exit plane.

For the conditions of P_o = 60 torr, $T_o = 300^oK$, and $HCl/D_2 = 0.1/0.9$, the various characteristic times are shown in Fig. I-14. The V-V pumping time is seen to be fast compared with all V-T deactivation times. Also shown are τ_f corresponding to $L_c \sim 30$ cm and τ_M. As one may observe, $\tau_M < \tau_f$ which is desirable. However, the pumping time approaches τ_f with increasing M_e. For this case, it appears that the optimum condition should be approximately $1 < M_e < 2$. Under these conditions the device would be mixing limited.

As shown in Fig. I-15 - I-17, similar maps have been calculated for P_o = 1 atm, $T_o = 300^oK$ and mixtures of 10%, 5% and 2% HCl respectively. Also shown on Fig I-15 are lines for effective exit or cavity temperature, T_e, and area ratio, A_o/A^*.

A comparison between Figs. I-14 and I-15 shows the following features: For the 1 atm. plenum pressure (I-15), all the characteristic times for the energy transfer processes are considerably smaller at the same value of M_e due to the higher cavity pressure. However, the cavity flow times are identical. In addition, we assume that the turbulent mixing time is essentially independent of pressure,[36] and, hence, that τ_m is the same for both conditions. The advantage of the higher plenum pressure is that the pumping time may be made much smaller than τ_f and τ_m for considerably larger exit Mach number. The larger M_e leads to lower cavity temperature which enhances gain. Of course, a different discharge technique would be necessary to provide volumetric excitation of the vibrational mode of D_2 at this high, i.e., atmospheric, pressure.

The effect of varying HCl mole fraction is seen in Figs. I-15, 16, and 17. As the HCl concentration is decreased, the V→V pumping time

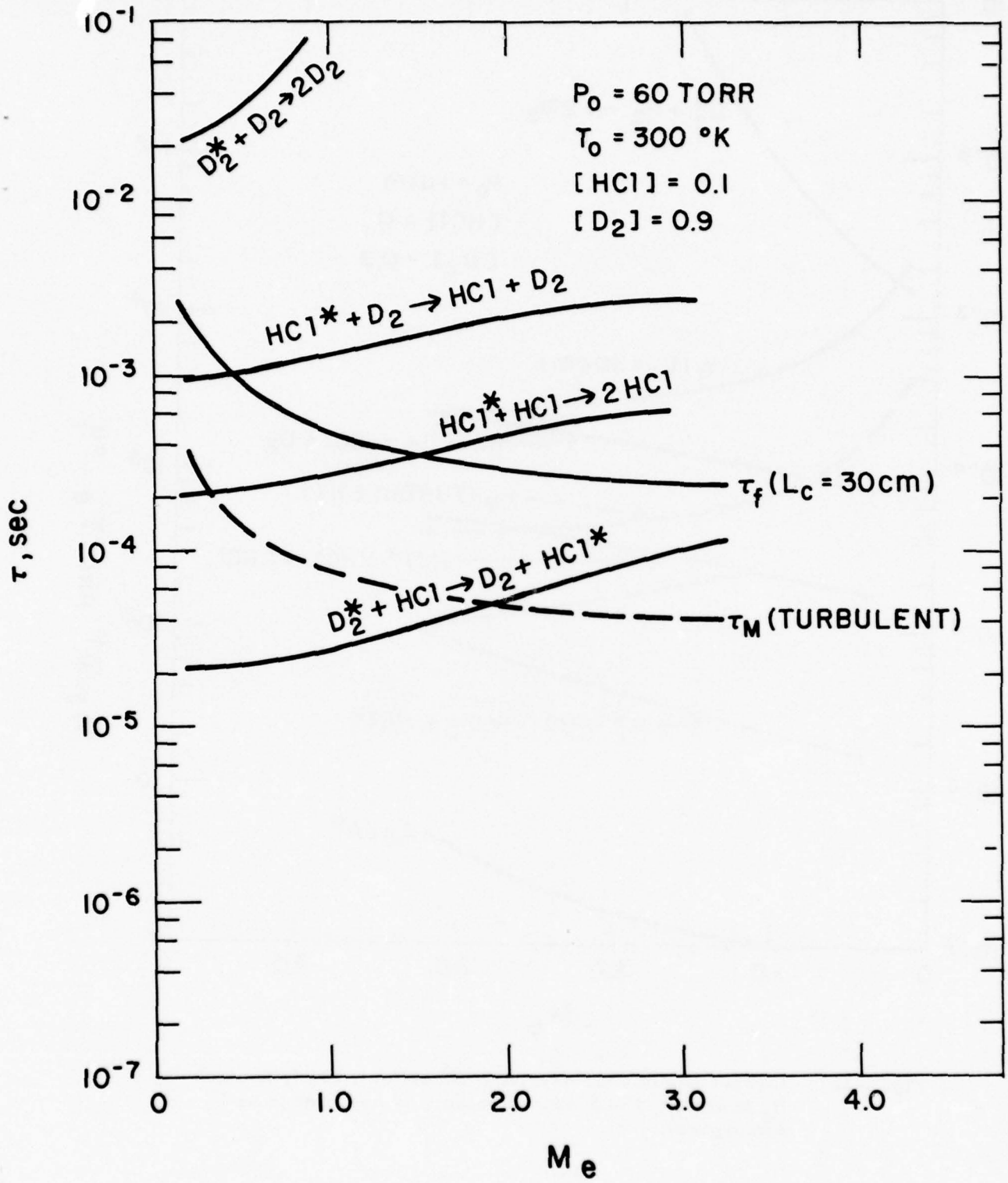

Fig. I-14 Comparison of Characteristic Times for Major Kinetic Processes with Turbulent Mixing Time and Cavity Flow Time for a 10% HCl - 90% D_2 Mixture. The Plenum Pressure is Assumed to be 60 Torr.

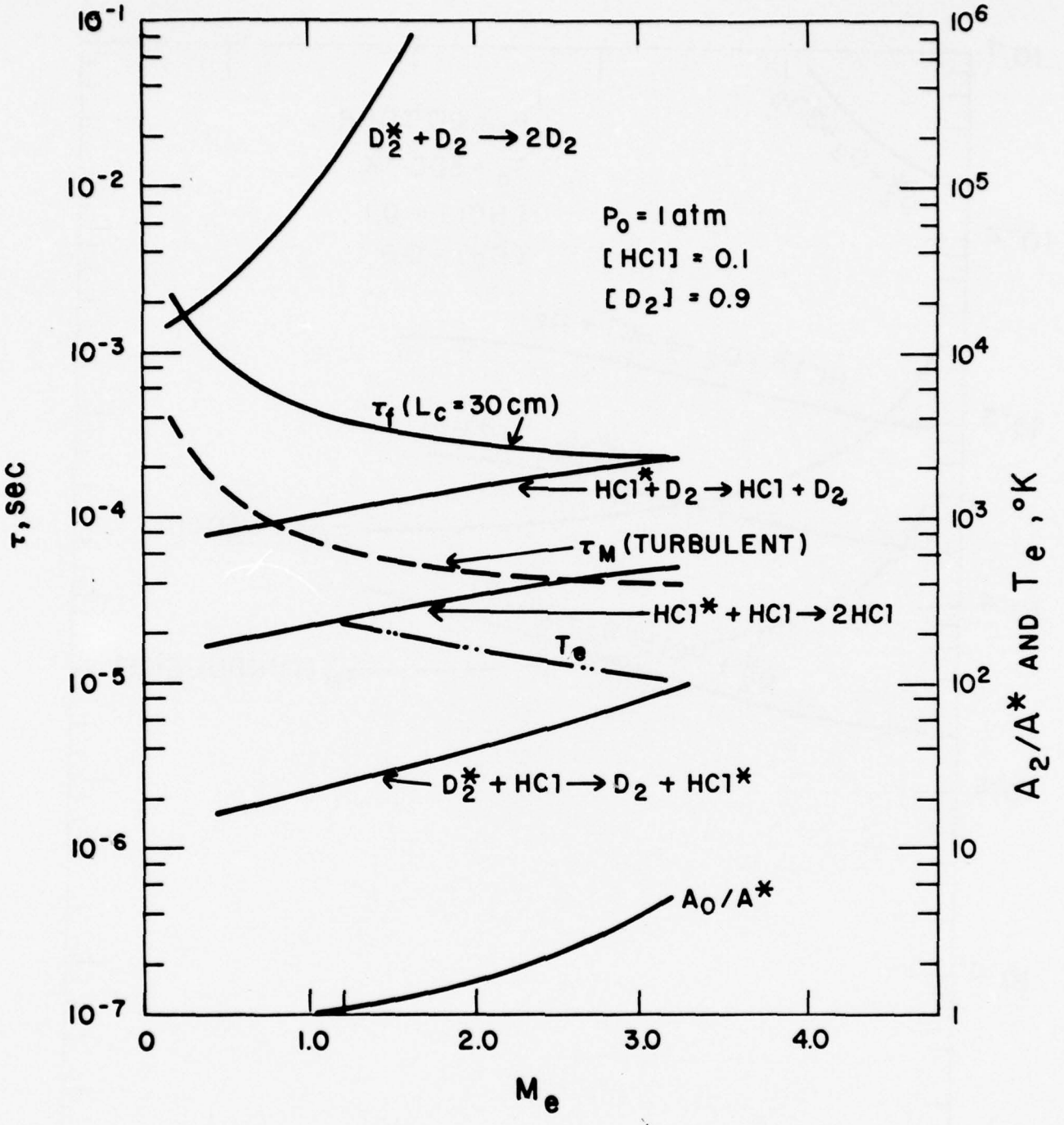

Fig. I-15 Comparison of Characteristic Times for a 10% HCl - 90% D_2 Mixture. The Plenum Pressure is Assumed to be 1 Atmosphere.

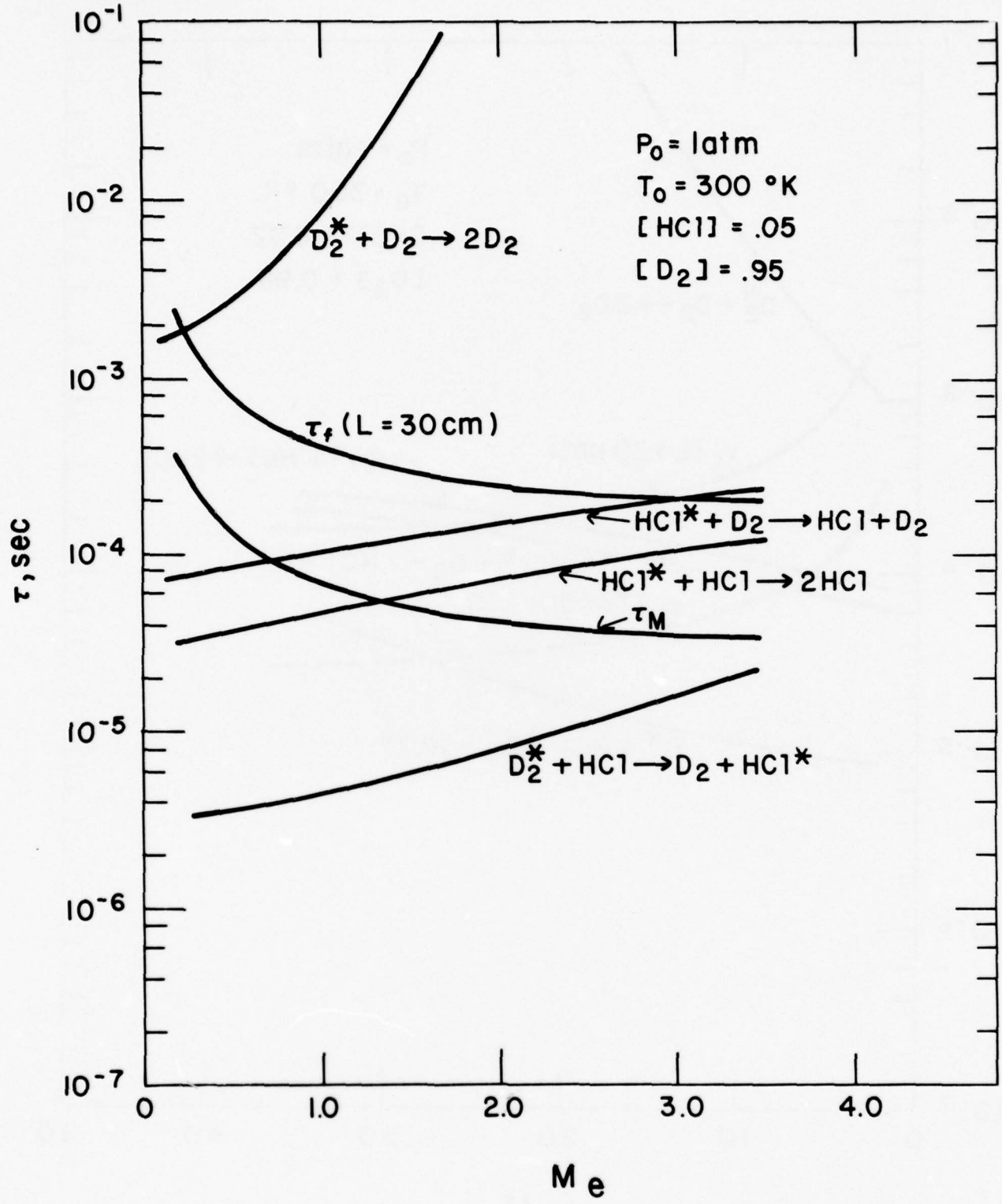

Fig. I-16 Comparison of Characteristic Times for a 5% HCl - 95% D_2 Mixture. The Plenum Pressure is Assumed to be 1 Atmosphere.

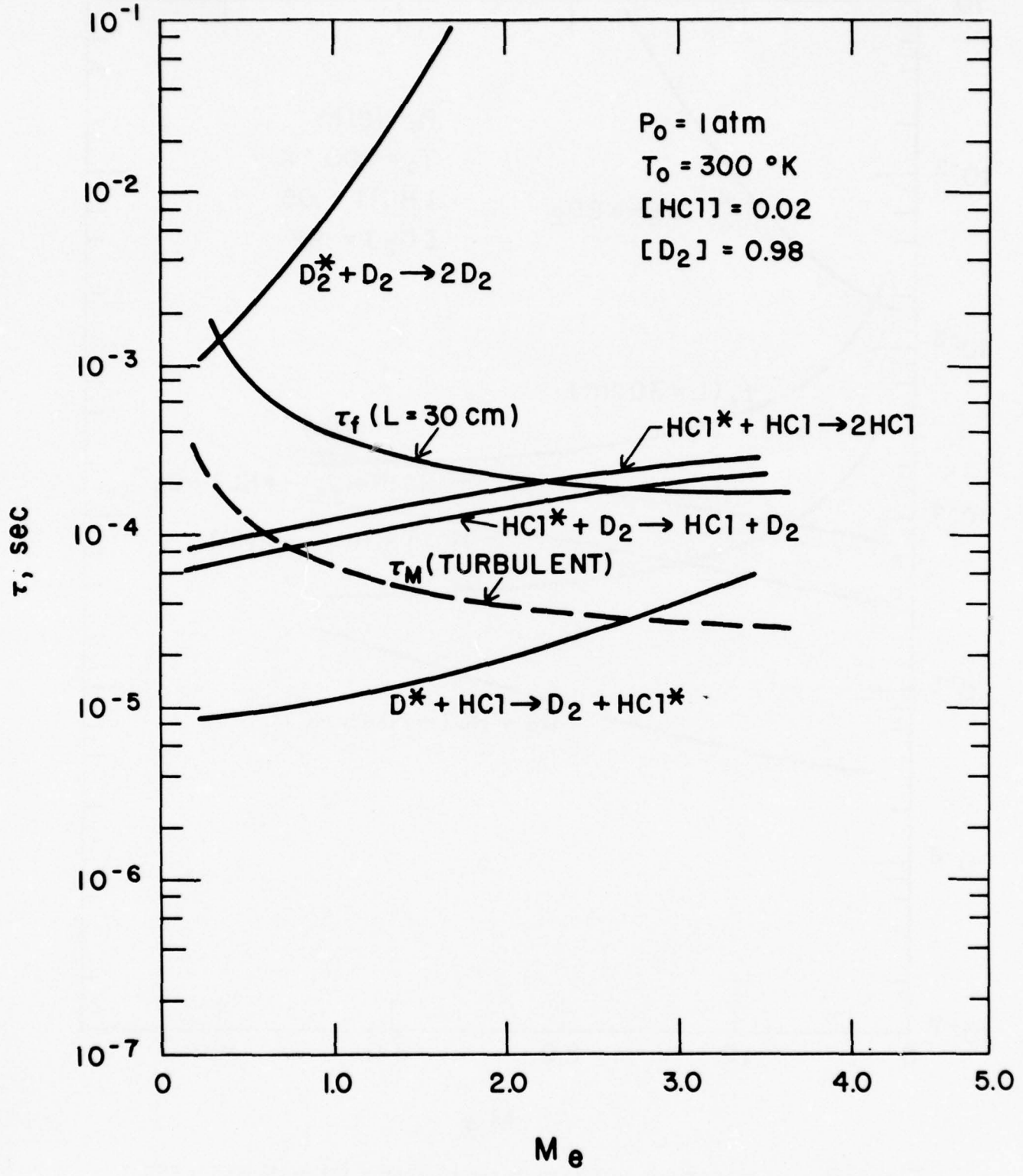

Fig. I-17 Comparison of Characteristic Times for a 2% HCl - 98% D_2 Mixture. The Plenum Pressure is Assumed to be 1 Atmosphere.

increases, and the dominant V→T deactivation process changes from HCl/HCl to HCl/D_2. As mentioned previously, this analysis ignores the HCl/HCl V→V pumping. It is difficult to estimate a characteristic time for this process, since it depends both upon the concentration of vibrationally excited HCl and the number of vibrational levels being considered. Even though the rate for this process is considerably faster than for the D_2/HCl pumping process (Table I-IV), it clearly adds to the overall time to pump HCl to a sufficiently high level for maximum gain. Thus, the times required to produce gain and lasing will be considerably larger than shown in Figs. I-14-17.

The major conclusion to be drawn from this analysis is that for the NRL experimental device designed to operate at $M_e > 2$, insufficient flow time may be available to provide for optimum pumping. A higher value of P_o would be desirable, but would require a major change in the excitation technique.

3. Mixing Analysis

The analysis presented in the preceeding section indicated that the mixing time, $\tau_m \ll \tau_f$. Hence, to a good approximation the gases mix instantaneously at some exit properties at the nozzle exit plane. This approximation is not reasonable if the pumping time (and other energy transfer times) are smaller than τ_m. For this latter condition, the details of the mixing clearly influence the vibrational kinetics. However, examination of Figs. I-14-17 indicates that conditions can be found for which $\tau_{pump} \sim \tau_m \ll \tau_f$. Accordingly, we have developed a simple mixing model which calculates the average properties at the nozzle exit plane by assuming that the secondary injection mixes instantaneously with the main flow.

A sketch of a nozzle with secondary injection is shown in Fig. I-18. Plenum gas (D_2 plus diluent) enters at station 1 with pressure P_1, density ρ_1, and velocity u_1. Cold HCl is injected at station 2. The gases are assumed to be uniformly mixed at station 3, the nozzle exit plane. The following analysis will provide the average gas properties at station 3.

Assuming one-dimensional steady nozzle flow, the governing equation, for the Mach number variation between stations 1 and 2 can be written as[37]

$$\frac{dM^2}{M^2} = \frac{\left(1 + \frac{\gamma-1}{2} M^2\right)}{(1 - M^2)} \left[(1 + \gamma M^2) \frac{dT_s}{T_s} - 2 \frac{dA}{A}\right] \qquad \text{(I-19)}$$

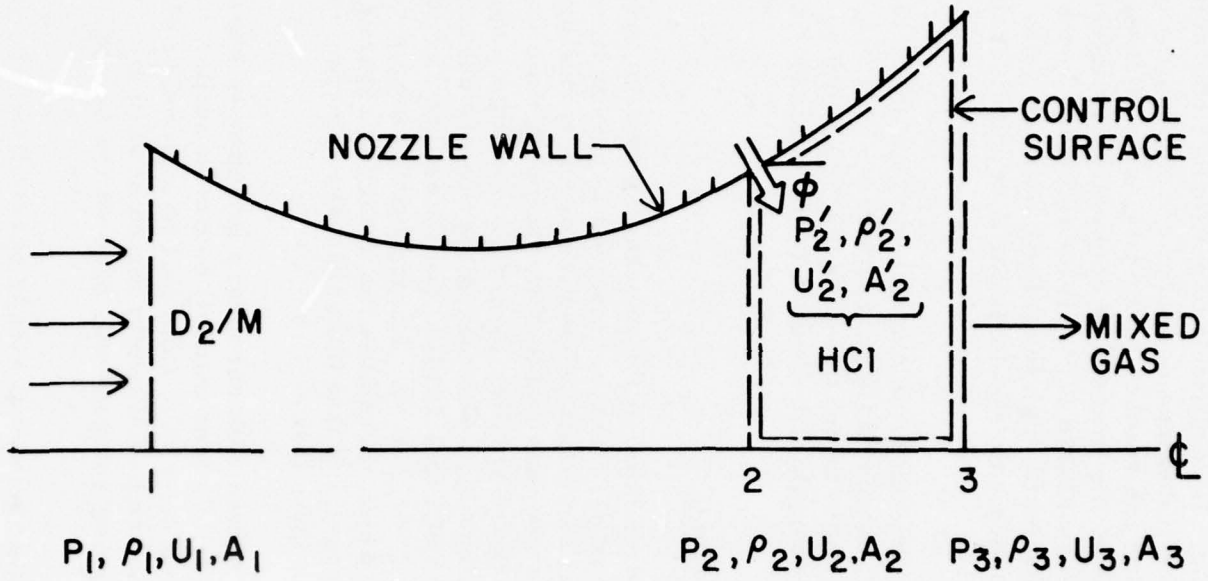

Fig. I-18 Schematic Representation of NRL Mixing Nozzle Configuration used in Describing Instantaneous Mixing Analysis.

where γ is the ratio of specific heats, and A is the nozzle cross-sectional area. Any change in plenum temperature T_s is due to V-T energy transfer. With an assumed D_2 vibrational temperature distribution one can readily calculate the Mach number distribution and consequently, P and ρ, with the aid of the continuity equation and the equation of state.

Now, consider the flow through the control surface of Fig. I-18. We shall write the physical equations governing the flow in such a way as to obtain relations between the properties at stations 2 and 3:

Continuity:
$$\rho u A = \rho_2 u_2 A_2 + \rho_2' u_2' A_2' \tag{I-20}$$

Momentum:
$$P_2 (A_2 + A_2' \cos\varphi) + \frac{P_2 + P}{2} (A - A_2 - A_2' \cos\varphi) - PA$$

$$= \rho u^2 A - \rho_2 u_2^2 A_2 - \rho_2' u_2'^2 A_2' \cos\varphi \tag{I-21}$$

Energy:
$$\rho u A H = \rho_2 u_2 A_2 H_2 + \rho_2' u_2' A_2' H_2' + \Delta Q \tag{I-22}$$

Perfect Gas Law:
$$P = \frac{R}{MW} \rho T , \tag{I-23}$$

where φ is the angle between the secondary injection and the axis (see Fig. I-18), R is the universal gas constant, MW is the average molecular weight of the mixture, H is the total enthalpy:

$$H = C_p T + \frac{1}{2} u^2 , \tag{I-24}$$

and ΔQ is the heat addition term which results from the vibrational energy transfer between stations 2 and 3.

$$\Delta Q = \frac{X_{D_2} R}{MW} \left[\frac{1}{e^{\theta_{D_2}/T_{v2}} - 1} - \frac{1}{e^{\theta_{D_2}/T_{v3}} - 1} \right] \left[\theta_{D_2} (1 - f_v) + (\theta_{D_2} - \theta_{HCl}) f_v \right] \tag{I-25}$$

where quantities without subscript indicate the properties at station 3, X is the mole fraction, θ is the vibrational spacing, T_v is the vibrational temperature of D_2 and f_v is the fraction of vibrational quanta transfered from D_2 to HCl. The above set of equations, Eq. I-20 to I-23, is sufficient for determining the unknowns P, T, ρ and u. Knowing the properties of the secondary flow, one can rearrange the continuity, momentum and energy equation and after some algebra, obtain

$$\frac{MW\ Pu}{RT} \cdot \frac{A}{A_2} = (1 + w_2') \rho_2 u_2 \tag{I-26}$$

$$u = \frac{1}{1 + w_2'} \left[u_2 + w_2' u_2' \cos\varphi + \frac{P_2 - P}{2 \rho_2 u_2} \left(1 + \frac{A_2'}{A_2} \cos\varphi + \frac{A}{A_2}\right)\right] \tag{I-27}$$

$$C_P T = \frac{C_{P_1} T_2}{1 + F_2'} + \frac{F_2' C_{P_2}' T_2'}{1 + F_2'} + X_{D_2} \left[\theta_{D_2} - \theta_{HCl} f_v\right] \left[\frac{1}{e^{\theta_{D_2}/T_{v2}} - 1} - \frac{1}{e^{\theta_{D_2}/T_{v3}} - 1}\right] + \frac{1}{2R} \left[\frac{MW}{1 + F_2'} u_2^2 + \frac{F_2' MW_2'}{1 + F_2'} u_2'^2 - MW \cdot u^2\right] \tag{I-28}$$

where w is the mass flow rate, F is the molar flow rate, and C_P is the specific heat at constant pressure. With a known nozzle contour, A/A_2, one can iterate on P. Assuming P, one can calculate u from Eq. (I-27) and consequently T from Eq. (I-28). Finally, from Eq. (I-26), one can calculate P which is then compared with the assumed value. Iteration

continues until a converged solution is obtained. The properties of the secondary flow can be determined from the isentropic relations if we know the stagnation pressure and temperature, the gas composition, the mass flow rate and the exit temperature. The results of the above instantaneous mixing model, namely the thermodynamic state of the mixture at station 3, can be used as inputs for the D_2/HCl EDL cavity calculations.

4. Cavity Model

To model the D_2/HCl EDL in the cavity region a generalized laser kinetics code developed under another program[38] was used. This code can integrate a large number of kinetic equations under a variety of fluid dynamic constraints. For the present calculations the cavity region was assumed to be a constant area duct with no radial gradients (one dimensional). Heat addition to the gas from V→T and V→V processes is accounted for throughout the flow.

The model assumed 11 vibrational levels in D_2 and 16 in HCl. This rather large number of levels was chosen to avoid "barrier reflection" at the top of the vibrational ladder as the intramode V→V pumping takes place. The results suggest that a smaller number of levels, particularly in D_2, could have been used with some small reduction in computer running time. The vibrational kinetics package and spectroscopic constants used in this modeling are given in Table I-4.

As a function of flow distance (time), the code calculates the populations of the various vibrational levels, small signal gain (or absorption) on each rotational level of each vibrational level, and fluorescence emission per particle. In addition, a subroutine can be used to simulate power extraction in the gain equals loss approximation.[39] The oscillator strengths and line width cross section for HCl are those developed for the H_2/HCl GDL modeling.[39]

A calculation to simulate a D_2/HCl EDL experiment is performed as follows: (i) Given the discharge parameters and plenum gas conditions, the Boltzmann code is used to determine the excitation rate constants and electron drift velocity as functions of E/N. (ii) From the results of (i) a plenum calculation is performed as outlined in Section I.B.4. This yields the vibrational distribution of D_2 and gas translational temperature at the end of the plenum or entrance to the nozzle. (iii) Given the secondary gas injection conditions and nozzle geometry, the instantaneous mixing model is used to specify the properties of the fully mixed gas at the exit of the nozzle. Vibrational relaxation and further heat addition to the gas can be accounted for as outlined in Section I.C.3. (iv) The output

conditions from (iii) are then used as input to the cavity model. In principle, the various codes (i) - (iv) can be combined so that the entire calculation would be performed in sequence. However, as is usually the case for complex modeling problems, it is much more efficient to do each calculation separately and provide some evaluation before proceeding onto the next step.

To illustrate the cavity model a sample calculation will be presented. The discharge and plenum conditions are essentially those discussed in Sections I.B. 3 and 4. As will be remembered, this yielded a vibrational temperature of $D_2 \sim 1700^{\circ}K$. HCl at $300^{\circ}K$ is injected at the nozzle and the input conditions for the cavity calculation are shown in Table I-5.

Results of vibrational population distributions of HCl at various distances downstream of the nozzle exit are shown in Fig. I-19. This figure shows the effect of anharmonic pumping as quanta in the lower vibrational levels of HCl are pumped up the ladder by the exothermic V→V transfer mechanism, process (I-2), resulting in increased population on higher vibrational levels. Because of the complexity of the rate structure, it is difficult to assess the exact mechanisms involved. There are also effects of V→V transfer from D_2 to HCl and of internal transfer in D_2. At the last station shown (x = 20 cm), the translational temperature has risen to $205^{\circ}K$, so there has also been some small translational heating due to V→ T deactivation and non-resonant V→V transfer processes.

The small signal gain, G_o, resulting from these population distributions is shown in Fig. I-20. For each vibrational band only the particular transition of maximum gain has been plotted. It can be seen that as the V→V pumping of HCl occurs, the gain increases and shifts to higher vibrational levels. The absolute magnitude of G_o ($\approx 10^{-3} - 10^{-4}$ cm^{-1}) is clearly too small for a practical laser. This is to be expected from the low initial D_2 vibrational temperature ($T_{V_{D_2}} = 1700^{\circ}K$). However, it is possible to calculate the spontaneous radiation (fluorescence) from such vibrational distributions and compare these results with experimental data.

TABLE I-5

Input to D_2/HCl EDL Cavity Calculation

$[HCl]$	=	0.029 mole fraction
$[D_2]$	=	0.333 " "
$[H_e]$	=	0.638 " "
$T_{v_{D_2}}$	=	1700°K
P_e	=	0.013 atm
T_e	=	195°K
u_e	=	1.1 km/sec

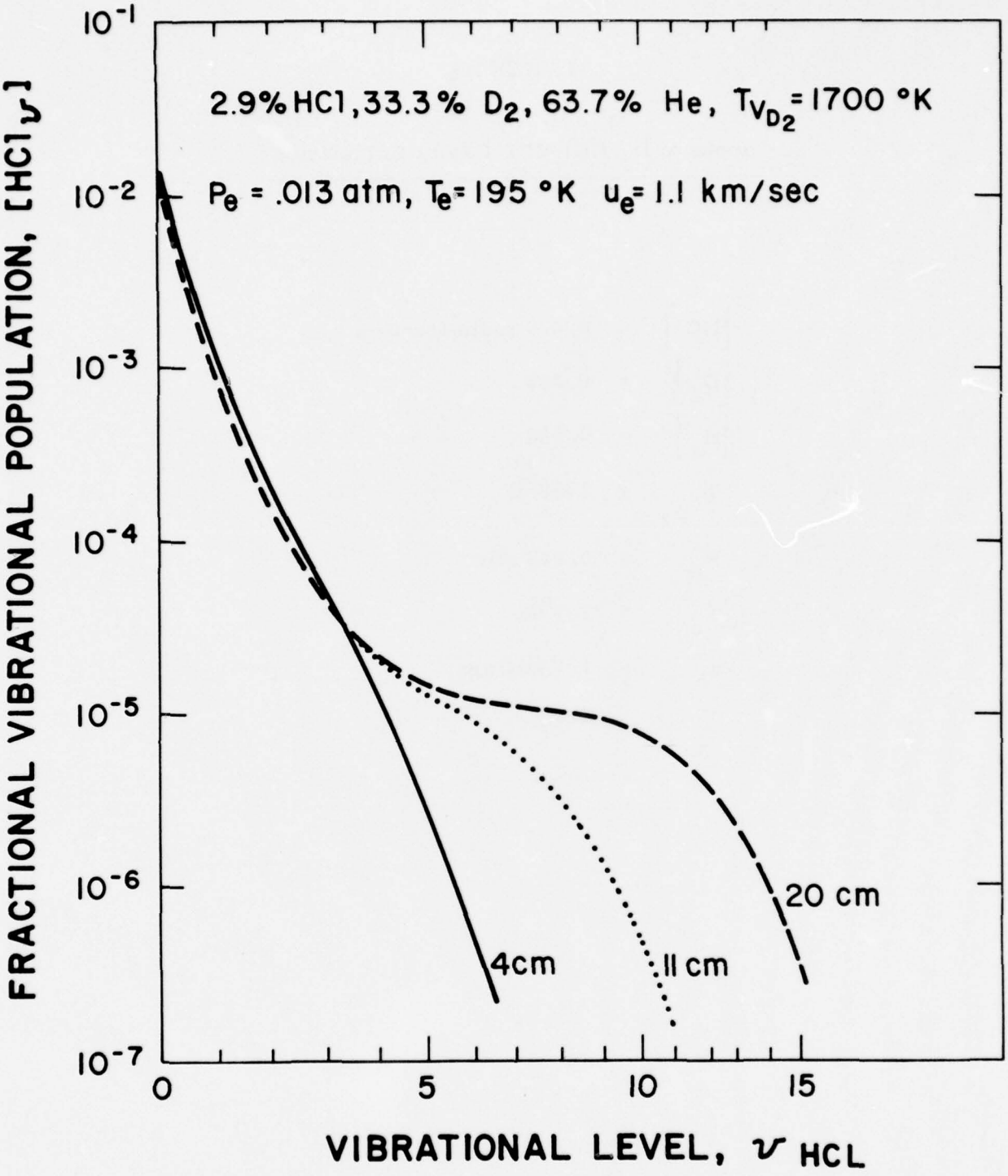

Fig. I-19 Vibrational Population Distributions for HCl at Various Distances Downstream of the Nozzle Exit. A Straight Line on such a Figure would Indicate a Boltzmann Distribution.

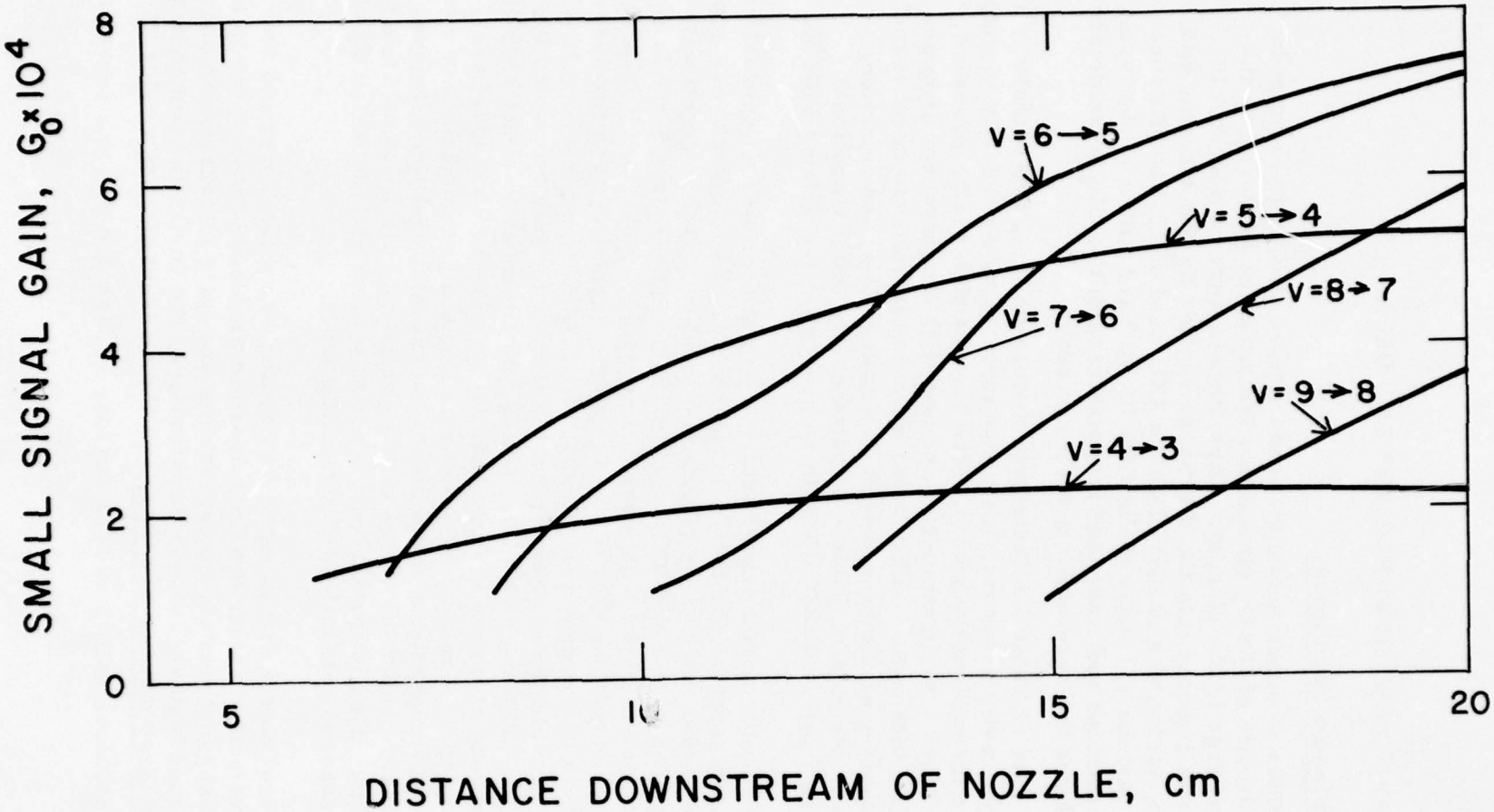

Fig. I-20 Small Signal Gain for Various Vibrational Transitions as a Function of Distance Downstream of the Nozzle. The Maximum Gain for each Vibrational Transition has been Plotted. In General the Specific Rotational Transition for Maximum Gain will Change with Distance; this has not been Indicated on the Figure.

D. COMPARISON WITH EXPERIMENTAL DATA

1. Plenum Conditions

A series of experiments were performed at NRL to attempt to obtain an estimate of the D_2 vibrational temperature produced by the electric discharge in the plenum. Experiments were carried out in which CO_2 was injected into the discharge excited D_2/He stream, and, downstream, lasing was observed on the CO_2 band at 10.6 μ. By measuring the gain on various v, J lines of the CO_2 10.6 μ band with a probe laser, both the vibrational and rotational temperatures of the CO_2 were determined. Table I-6 shows the results for a series of runs.

The data of Table I-6 distribute themselves into two classes. The runs with low cavity pressure, i.e., 6-8 torr, show a gradually increasing temperature throughout the cavity. The runs at high cavity pressure, i.e., 12-14 torr, show a rapid temperature jump with a subsequent drop or leveling off downstream.* This latter behavior is believed to be associated with some choking of the flow at high secondary (CO_2) gas injection. Nevertheless, the data of Table I-6 indicate CO_2 (001) vibrational temperatures from 1000-2200°K with an average value around 1700°K.

The results of this experiment can be used to infer an approximate vibrational temperature for the D_2 in the cavity. Two different assumptions can be made: (i) The D_2 vibrational level (v = 1) is energetically in close energy resonance with CO_2 (01^11). Thus, the D_2 (v = 1) mode can be assumed to be in rapid V→V equilibrium with CO_2 (01^11). If it is further assumed that the CO_2 (01^10) is rapidly quenched, then for every quanta of D_2 (v = 1) energy lost to CO_2, the CO_2 (001) mode will gain ~70% of that energy. Simple analysis indicates that under this situation, for a measured CO_2 (001) T_v of 1700°K, the T_v of D_2 must be about 2300°K. (ii) In the second case, we assume that D_2 (v = 1) and CO_2 (001) are directly coupled by a rapid V→V process. For the gas conditions of a high D_2 vibrational temperature compared to the translational temperature, the Teare-Trainor[40] relation may be used to relate T_v for D_2 to that measured for CO_2 (001). This latter analysis leads to a value of 1100°K for T_v of D_2 for a measured value of 1700°K for CO_2 (001).

Several points can be made concerning this experiment and the resulting analysis. First, the fluid dynamic problems encountered in the experiment suggest that the measurements and their interpretation should not be assigned high accuracy. Nevertheless, the device did demonstrate lasing for a large number of gases, and the measurement of a value of

* The temperature values at 12.1 cm may be high due to some systematic error.

TABLE I-6

Vibrational/Rotational Temperature Inferred from CO_2 Gain*

Mixture $He/D_2/CO_2$ (Mole Fraction)	Gas Pressure Plenum (torr)	Gas Pressure Cavity (torr)	Distance (cm)	T_V CO_2 (001) (^oK)	T_R (^oK)
.760/.215/.025	97	14.1	23	1650	240
.767/.217/.016	97	6.7	23	2200	245
.761/.215/.024	97	14.0	16	1700	230
.766/.216/.018	97	7.8	16	1825	235
.768/.217/.015	97	6.6	16	1950	240
.768/.208/.024	97	12.4	5.6	1300	190
.775/.210/.015	97	6.9	5.6	1075	140
.768/.208/.024	97	12.4	12.1	2200	290
.775/.210/.015	97	7.2	12.1	1850	245

*Further details of this experiment may be found in J. Stregack, B. L. Wexler and G. A. Hart, Appl. Phys. Lett. 27, 670 (1975).

of 1700°K for CO_2 (001) is reasonable for a laser situation. Secondly, the two analyses give a wide range of possible D_2 vibrational temperatures: 1100-2300°K. It is noted that our discharge modeling calculation gave an intermediate value, ~1700°K. Thirdly, a reasonable choice between the two chosen D_2/CO_2 energy transfer mechanisms cannot be made at present on the basis of existing experiment or theory. Finally, a more complex analysis using a finite kinetic analysis and the measured rate constants for the D_2/CO_2 molecular system could be performed, but does not seem justified on the basis of the uncertainty of the data.

In conclusion, this experiment and analysis offers no detailed verification of the plenum discharge modeling. The results show that substantial excitation of the D_2 vibrational mode must occur, and this conclusion is consistent with the results of Sec. I. B. Measurements on a system more amenable to detailed analysis would be needed to provide a more accurate determination of D_2 vibrational temperature.

2. Fluid Dynamics

In the early stages of the experiment it was recognized by NRL that for certain values of secondary mass injection, the measured cavity pressure suddenly increased, suggesting a choked flow in the cavity. It was also believed that for values of mass injection less than these critical values, the flow was reasonably well characterized. It was these latter (normal) conditions for which the modeling was planned. However, as experimental data became available it was clear that, in general, the measured cavity pressure did not closely correspond to the expected values based on known plenum pressure and nozzle area ratio even in the non-choked situation. A simple analysis illustrates this point.

The detailed nozzle dimensions for the NRL EDL are shown in Fig. I-21. The nozzle throat height, A^*, is nominally 1 mm, so that the overall geometric area ratio is 7. The case chosen for analysis used a primary flow of 0.33 D_2/0.67 He molar mixture through the nozzle configuration shown in Fig. I-21. For this gas mixture the theoretical flow rate (in the absence of boundary layers) is given by

$$(\rho u)^* = 157\ p_o / \sqrt{T_o}\ \text{gm/cm}^2\text{-sec} \qquad \text{(I-29)}$$

at the throat, where p_o (atm) and T_o (°K) are the plenum pressure and temperature, respectively. In the discharge region, where the flow area $\approx 7\ A^*$, the Mach number is ~.08 and $T/T_o \approx .998$, $p/p_o \approx .995$. Thus, a static pressure measurement in the discharge region yields p_o within 0.5%. The selected plenum conditions are shown in Table I-VII. For $p_o = 53$ torr and $T_o = 300$°K, the mass flow is thus 0.632 gm/sec per unit area of primary throat, yielding 4.24 gm/sec total flow ($A^* = 6.7\ \text{cm}^2$), or ~ 1.06 moles/sec, comparable with observed flow rates.

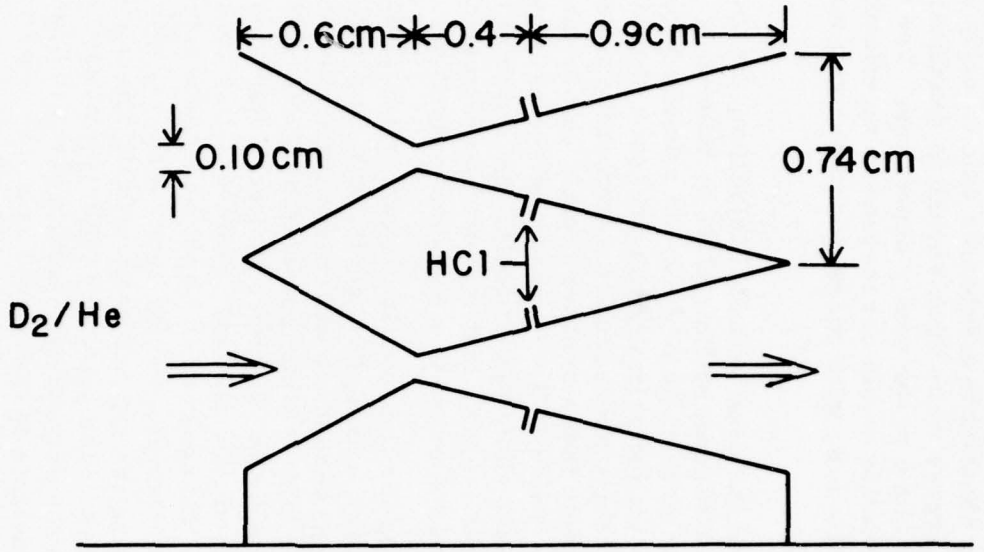

Fig. I-21 Schematic of NRL EDL Mixing Nozzle Array. The Dimensions are Nominal.

For the case of no secondary injection, if this D_2-He mixture were expanded supersonically to an area ratio of 7, the downstream pressure would be $\sim .009\ p_o$. Observed cavity pressures were in the range $0.2\ p_o > p > 0.1\ p_o$, (see Table I-7). This behavior would imply either that the flow had been shocked to a subsonic exit velocity or that nozzle and cavity wall boundary layers were thick enough to drastically reduce the effective area of flow close to the cavity centerline. The observed cavity pressures for this situation would correspond to an effective area ratio A/A^* in the range 1.3 - 1.8, with corresponding cavity temperatures $0.57\ T_o > T > 0.44\ T_o$.

For analysis of the case with HCl injection, the instantaneous mixing model was used with a secondary flow of 3% by volume of HCl (or 27% mass ratio) introduced at an area ratio of 2.32, or roughly 3 mm downstream of the throat. At this point the primary gas pressure should already be less than $.06\ p_o$, and the cavity pressure for a uniformly mixed supersonic flow should be $\sim .02\ p_o$. Both these pressure levels are lower than the observed cavity pressures (see Table I-7). However, diagnostics employed with CO_2 injected as the secondary gas establish that some of the cavity gas is cold ($\sim 200^oK$ see Table I-6), so that it must be assumed that the entire cavity flow has <u>not</u> been shocked to a subsonic velocity.

Various causes for this poorly characterized flow might be listed: (i) nozzle wall boundary layers, (ii) cavity wall (top and bottom) boundary layers, (iii) inefficient secondary injection with associated incomplete mixing, and (iv) poor diffuser/pump operation. Estimates of most of these phenomena were made and none, by itself, appeared to be sufficient to produce the observed flow effects. However, this analysis did suggest several experimental changes which might be implemented to improve the fluid dynamics. For example, cavity boundary layer effects could be minimized by diverging the top and bottom walls slightly to account for the displacement thickness of the boundary layers. An estimate of the behavior of the HCl flow from the secondary injection ports indicated that the HCl stream would not penetrate to the nozzle axis. Penetration improvement could be obtained by using fewer injection ports of smaller diameter, or by using an inert carrier gas to permit higher values of secondary gas injection.

Toward the end of the present program, NRL was able to improve the flow in the device substantially. This was accomplished by first recognizing that the steam injector line was limiting the pressure in the device to about 2 torr. More importantly, the top and bottom cavity walls were wedged at an angle of 1.7^o each to compensate for boundary layer growth. An example of these improved flow conditions is shown in Table I-8. These data are for CO/He/C_2H_2 flows, but it is clear that substantial secondary injection produces no discernable choking effects as was shown in the earlier data. Hence, (in retrospect) there appears no evidence for incomplete mixing in the NRL EDGDL.

TABLE I-7

Comparison of Calculated and Observed Flow Properties

	Calculated	Experimental
P_o (torr)	----	53
T_o (^oK)	----	300
$\dot{m}$ (gm/sec)	4.24	4
p/p_o (no secondary injection)	0.009	0.1 - 0.2
p/p_o (with secondary injection)	0.02	0.1 - 0.2

TABLE I-8

Flow Conditions with and without Wedged Cavity

Gauge Pressure (PSIG)			Mass Flows (moles/sec)			Plenum Pressure (torr)	Cavity Pressure (torr)	
He	CO	C_2H_2	He	CO	C_2H_2			
180	110	--	2.57	.24	0.0	127.6	2.4*	
		10			.112	127.7	3.4	New Cavity
		5			.089		3.23	750 ma current thru gas
		0.0			.067		3.06	
		-2.5			.055		2.91	
180	105	--	2.57	.215	0.0	125	5.8	Old Cavity
		0.0			.067		7.8	500 ma discharge current

Note: The mass flow calculations use the following sonic orifices, He .128", CO .079", C_2H_2 .125"

* Because of steam ejector vent valve (upstream of the laser, near the pump), the minimum pressure in the device is about 2 torr.

3. Cavity Fluorescence Data

It was decided that these aerodynamic issues associated with the experiment as it first existed, precluded a detailed comparison of the results of the analysis with the data. Therefore, it was decided to provide some calculations which would encompass a range of possible experimental operation and to provide a preliminary design of an improved device to be used for further assessment of the viability of the D_2/HCl EDL.

A series of measurements were performed by NRL on the infrared fluorescence from HCl using an optical system which could be translated parallel to the flow during a run. These data consist of records of infrared intensity in selected bandpasses versus distance downstream of the nozzle. Examples of these data are shown in Fig. I-22 for an optical bandpass of approximately 3.0 - 4.0μ. The top trace (a) is illustrative of an unchoked flow, while the bottom trace, (b) obtained at a higher HCl injection rate, shows an abrupt leveling off of the signal which is not due to optical or electronic saturation. This latter fluorescence behavior was always associated with the abrupt jump in cavity pressure and was believed due to the presence of shocks or choked flow in the cavity as described previously.

Although it was decided not to perform detailed comparison of these data with the calculations, several qualitative conclusions can be made. (i) For the more normal run Fig. I-22 (a), the fluorescence intensity continues to rise throughout the observation distance of about 12 cm. More recent fluorescent data (DARPA-NRL Laser Program Semiannual Technical Report, 1 Jan. 1975-30 June 1975, NRL Memorandum Report 3217, 1976) show that in the non-choked situation the intensities actually do not show a leveling off until about 20-25 cm downstream of the nozzle exit. This observation can be compared to the calculations of Fig. I-20. The conditions are not identical, but, nevertheless, for these low cavity pressure, $\sim$8 torr, the HCl is calculated to be at a low level of excitation with small values of gain at distances of 10 cm downstream of the nozzle. Considerably longer flow lengths and/or higher cavity pressures would be required to provide optimum pumping and gain. (ii) No lasing of HCl could be obtained. This result is also consistent with the results of Fig. I-20. (iii) Observations at longer wavelength 4.0 - 4.5 μ showed much less radiation intensity than in the 3-4μ bandpass. Again this result is consistent with the low level of HCl vibrational excitation expected. As the gas flows down the cavity, HCl/HCl V$\rightarrow$V pumping should populate the higher vibrational levels of HCl and the fluorescence should shift to longer wavelength. (iv) The typical E/N for the runs of Fig. I-22 is 1×10^{-16} V-cm^2. This is close to the optimum discharge condition for this mixture as seen from Fig. I-11.

These qualitative comparisons of the fluorescence data combined with the plenum comparison (Sec. I.D.1) do indicate a general consistency with the modeling results. Excitation of the D_2 vibrational mode in the discharge appears to occur, and it may be possible to channel as much as 70% of the discharge energy into the vibrational mode by operating at optimum E/N. V$\rightarrow$V transfer from D_2 to HCl does occur as evidenced by the HCl fluorescence. However, to demonstrate lasing, higher density operation is required.

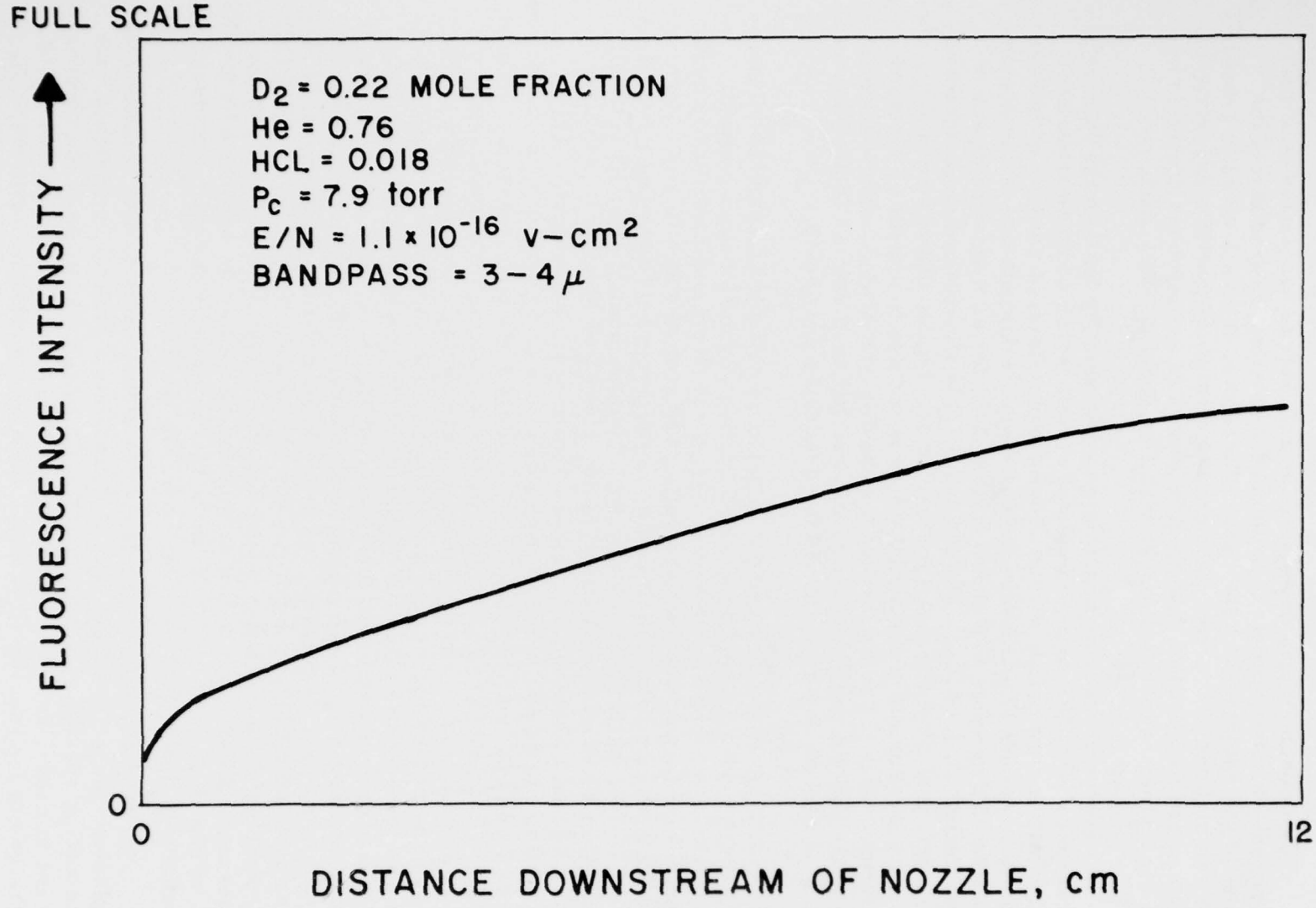

(a)

Fig. I-22(a) HCl Infrared Fluorescence Trace from D_2/HCl EDL Experiment. The Experimental Conditions are Given in the Figure.

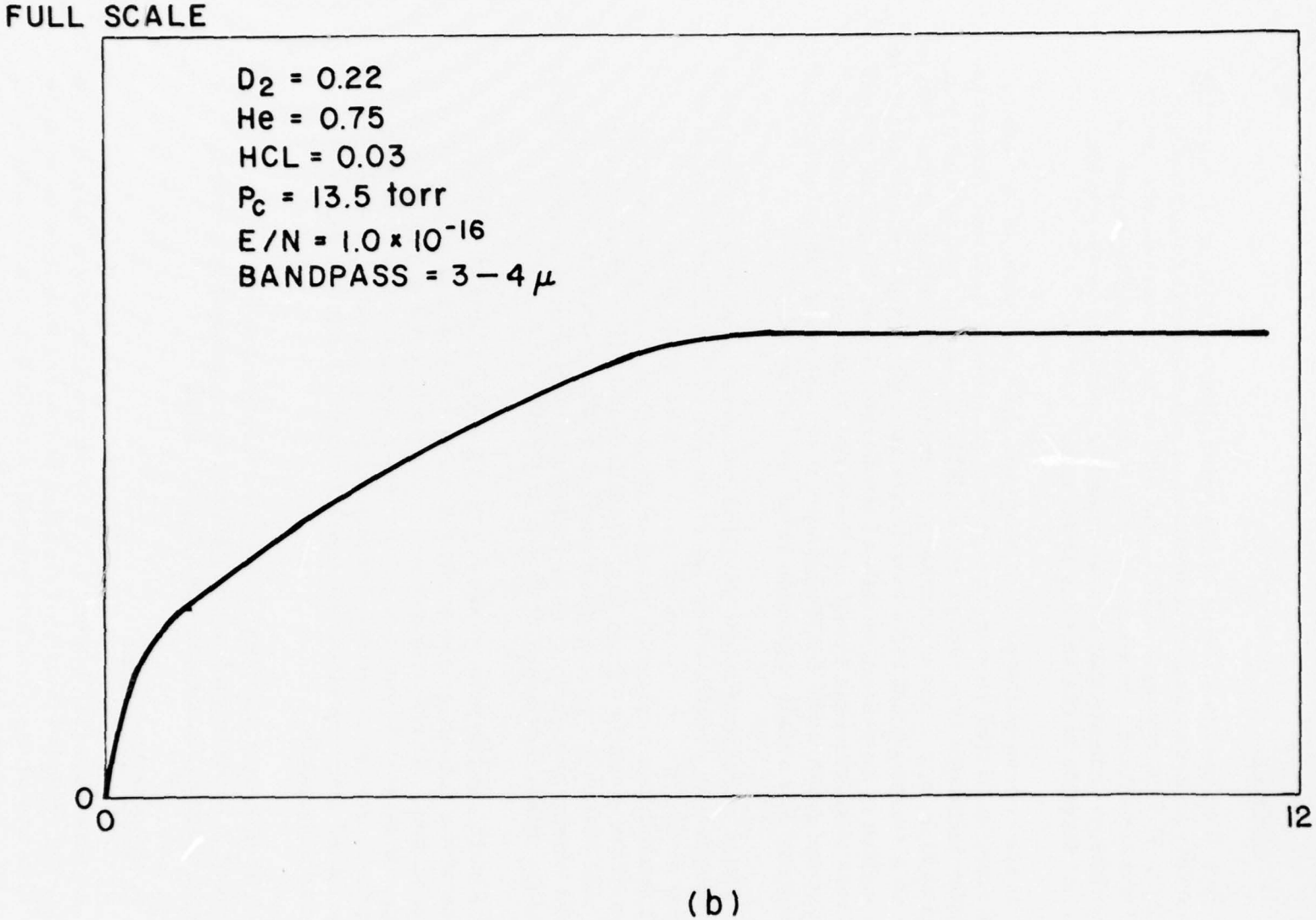

(b)

Fig. I-22(b) HCl Infrared Fluorescence Trace from D_2/HCl EDL Experiment. The Experimental Conditions are Given in the Figure. The Major Experimental Difference Between (b) and (a) is the Higher Secondary Mass Injection for Trace (b).

E. DESIGN OF NEW EXPERIMENT

1. Concept

Based on the discussions of the proceeding section, it is clear that a new facility is necessary for a meaningful experimental demonstration of the D_2/HCl EDL concept. First, the flow in the present device cannot be well characterized. In addition, even if the flow could be improved, the calculations indicate that a higher density operation is desireable. This is not feasible in the existing apparatus.

In the course of the present program, NRL had planned to replace the pin-type, ballasted glow discharge with an e-beam sustained discharge. This latter technique is a recognized scalable excitation method which can be used at high, e.g., one atmosphere, pressure. Therefore, it was decided to take as a starting point for a new device concept an atmospheric pressure plenum excited by an e-beam sustained discharge. Using the comparison of the various characteristic times for the major kinetic processes with the fluid dynamic constraints for the high pressure operation, the overall cavity Mach number and nozzle expansion ratio can be estimated.

There were insufficient time and resources available at this point in this program to provide extensive discharge modeling for the e-beam sustainer discharge. However, there is no reason to believe that the overall conclusions of the glow discharge modeling, i.e., that a large fraction of the electron energy can be channeled into the D_2 vibrational mode, will change for an e-beam sustained discharge. Therefore, a series of kinetic calculations were performed for various assumed values of T_v of D_2 within the range $1000^o \leq T_v \leq 2000^oK$.

Finally, it has been shown for the N_2/CO_2 mixing GDL[41] that injection of the secondary gas at the throat of the nozzle provides more efficient mixing. Therefore, it was decided to design a nozzle for this new experiment that would provide for throat injection as well as meet the requirements for providing optimum cavity temperature and pressures as determined from the kinetics. A preliminary design of such a nozzle array was undertaken.

The following sections present the results of this design study and can be used to provide guidance in planning an upgraded experimental facility in which to demonstrate the D_2/HCl EDL.

2. Kinetic Modeling

As was discussed in Sec. I.C.2, a comparison of the characteristic times for the various vibrational transfer processes with the approximate mixing time and cavity flow time provides a method for quickly optimizing the overall fluid dynamics of the device. Various maps for one atmosphere

plenum pressure and several HCl concentration were shown in Figs. I-15 to I-17. These maps did not consider any diluent in the plenum gas. An additional map for Ar diluent is given in Fig. I-23. Although the bulk of the measurements with the existing device were done with He diluent, Ar would be a better choice for the new experiment. Ar would provide more stopping power than He for the high energy electrons of the e-beam in the plenum, and, also, the Ar/D_2 mixture would provide a better molecular weight match with the HCl secondary flow and thereby reduce dissipative effects in the mixing.

Figure I-23 shows that for $M_e > 2$ the mixing time is less than the D_2/HCl V→V transfer time and both time are much shorter than the flow time for a 30 cm long cavity. For purposes of a design point we have chosen to select $M_e = 2.5$ to produce the required cavity conditions. This requires a nozzle of area ratio ~ 3.3.

A series of full vibrational kinetic calculations were performed under the following assumptions: (i) The plenum gas is a D_2/Ar mixture of molar ratio 1/2, P_o = 1 atm., and $T_o = 300^oK$. Various D_2 vibrational temperatures were assumed covering the range of 1000 - 2000°K. (ii) For each value of D_2 T_v, three different amounts of HCl are injected at the throat, and the instantaneous mixing model (Sec. I.C.3) is used to specify the fully mixed conditions at the exit of the nozzle. The expansion area ratio is chosen to be 3.3 to provide a nominal cavity Mach number of 2.5. It is further assumed that no vibrational kinetics occur in this mixing process. (iii) The fully mixed gas enters the cavity, the vibrational kinetics occur, and small signal gains for HCl v, J transition are calculated as a function of flow distance through the cavity.

An example of such a calculation is shown in Fig. I-24 for an assumed D_2 T_v of 1500°K and a final HCl mole fraction of 0.006 (comparable to the conditions of Fig. I-23). It should be noted that to preserve clarity in the figure, not all the vibrational transitions showing gain have been plotted. Several points can be made from Fig. I-24. First, the gain peaks a few cm downstream of the throat. This is to be compared with the results of Fig. I-20 and is due primarily to the much higher cavity pressure (45 torr) compared to the previous condition (~ 1.0 torr). Second, the predicted small signal gains are high, > 1% cm^{-1}, and lasing should be possible with reasonable values of optical cavity parameters.

To illustrate the effect of D_2 vibrational temperature, a typical transition was selected (v = 3 → 2), and the peak value of gain for that transition obtained in each calculation plotted against the assumed D_2 T_v for that case; the result is shown in Fig. I-25. It can be seen that even for rather modest values of $T_v = 1250^oK$, reasonable gains are obtained. From the results of the discharge modeling as well as the D_2/CO_2 gain measurements presented previously, we have every reason to believe that values of D_2 T_v from 1000 - 2000°K are obtainable via practical discharge

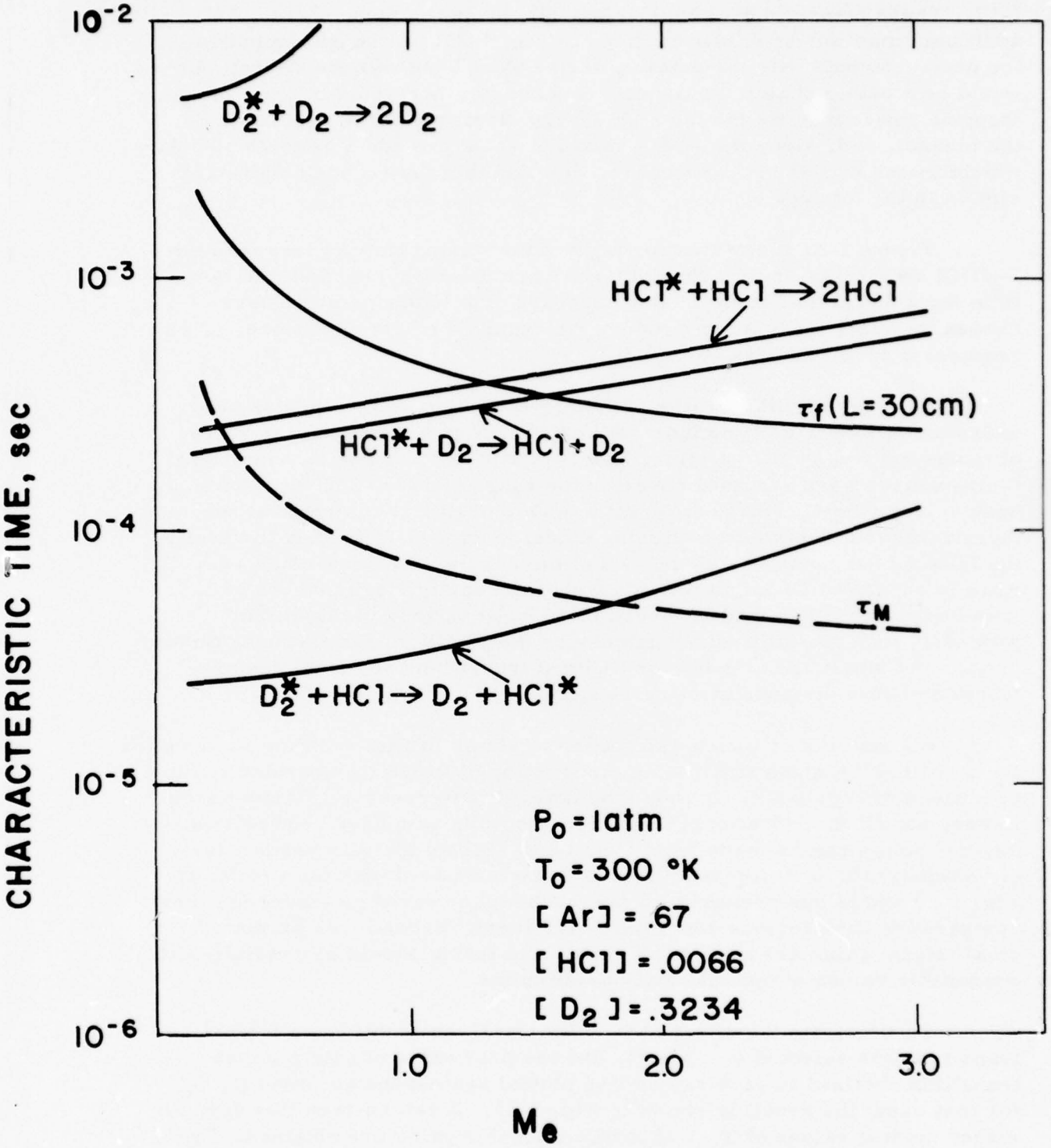

Fig. I-23 Comparison of Characteristic Times for a 0.7% HCl - 32.3% D_2 - 67% Ar Mixture with an Assumed Plenum Pressure of 1 Atmosphere.

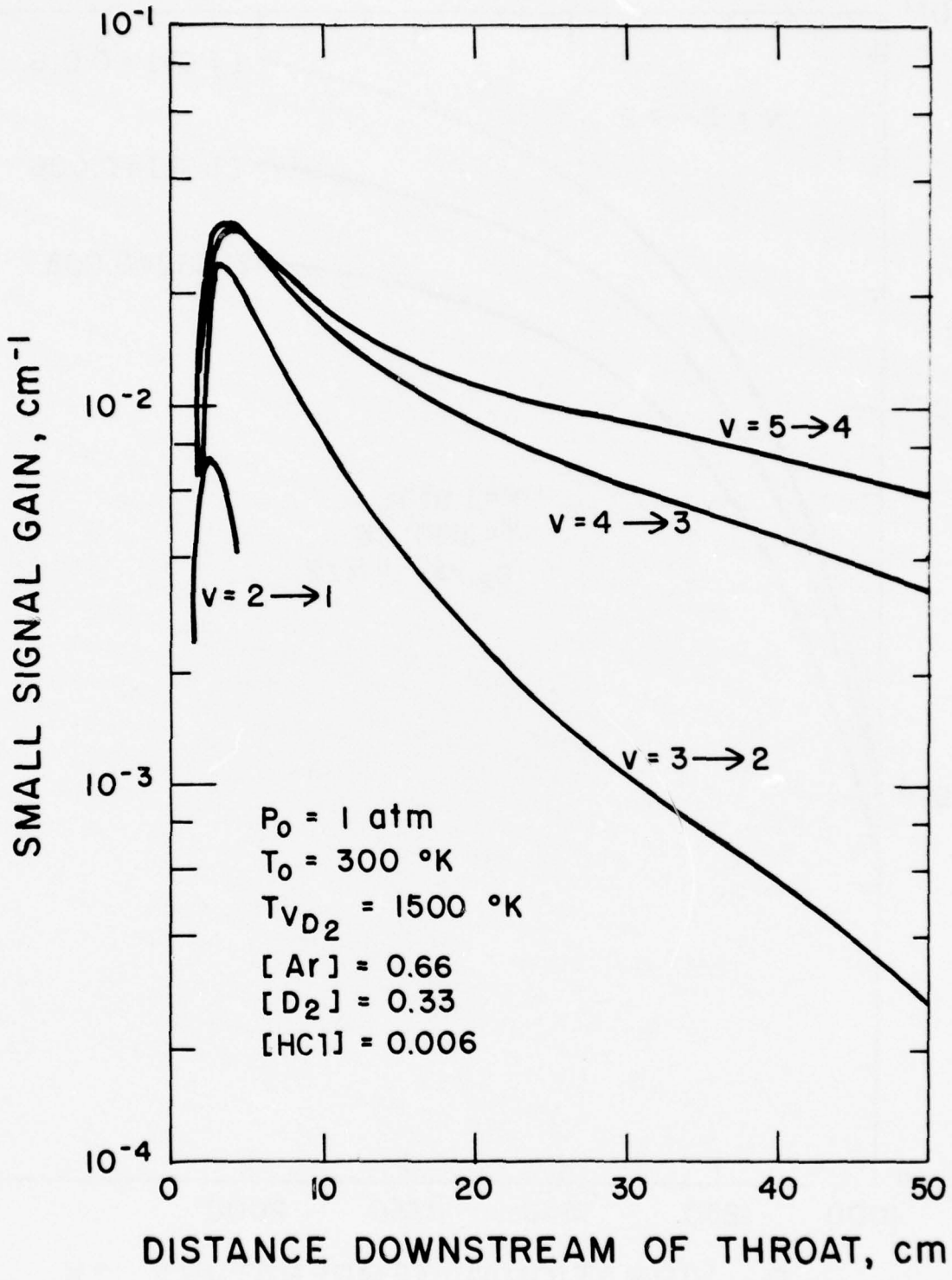

Fig. I-24 Small Signal Gain for Selected Vibrational Transitions of HCl as a Function of Distance Downstream of the Nozzle.

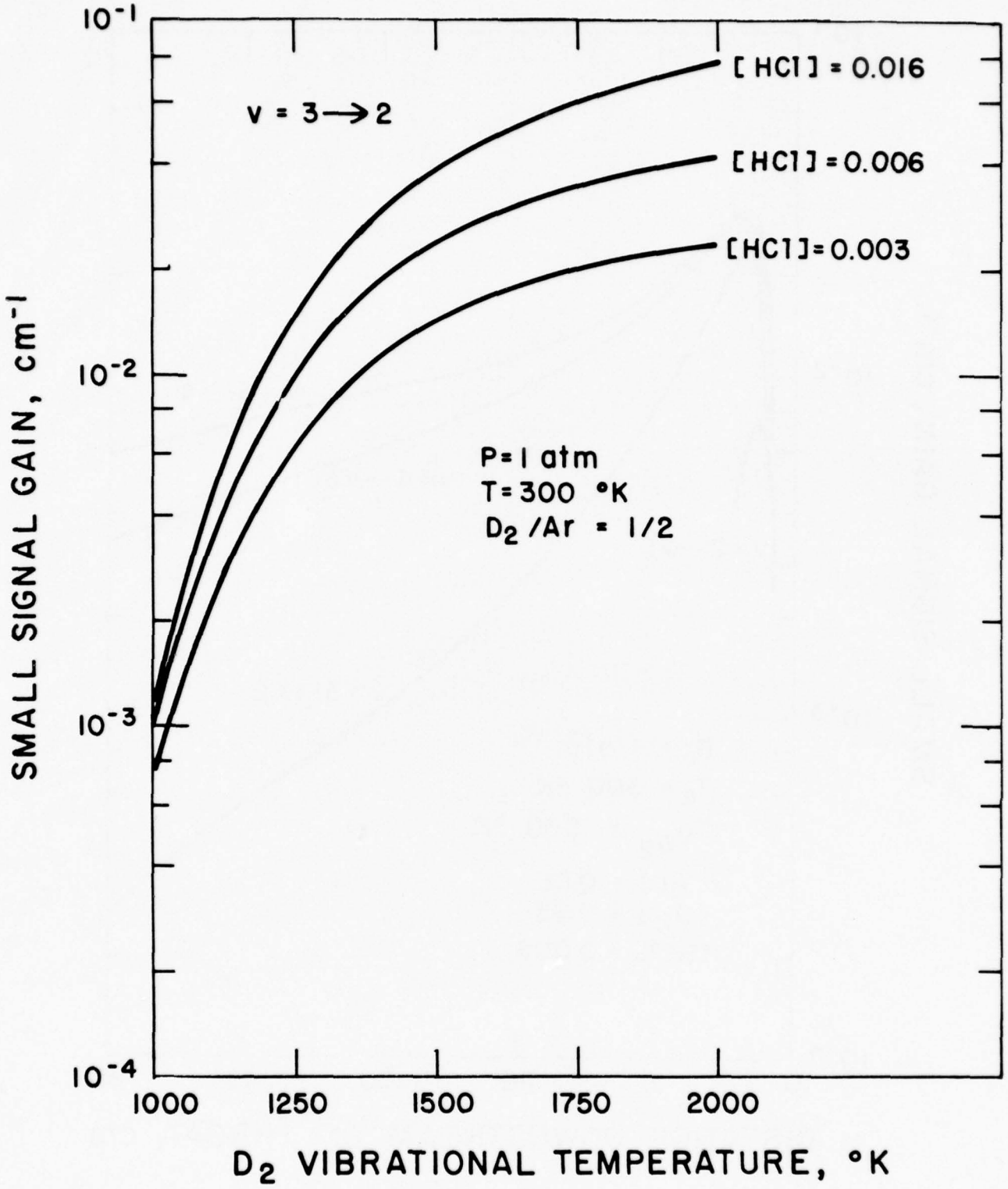

Fig. I-25 Maximum Small Signal Gain for the v = 3 → 2 Vibrational Transition of HCl as a Function of the Plenum Vibrational Temperature of D_2 Assumed in the Calculation.

techniques. Therefore, the results of this kinetic analysis indicate that a D_2/HCl EDL operated at high density using e-beam sustainer discharge excitation would be feasible.

3. Nozzle Design

One of the possible configurations for a D_2/HCl mixing EDL would be to expand the D_2 through a two-dimensional supersonic nozzle, while the HCl is injected at the throat. Taran et al[41] have shown theoretically and experimentally that this configuration gives excellent results for the N_2/CO_2 EDL. It is shown that satisfactory mixing can be obtained with an increase of the freezing efficiency over simple expansion nozzles or premixed flow.

We have chosen to design a nozzle for the next D_2/HCl EDL device incorporating throat injection. A complete turbulent mixing calculation is beyond the scope of the present program, but we will use an existing PSI laminar mixing code with appropriate modifications as a design tool for this nozzle. The turbulent transport will be modeled by the eddy viscosity approximation.

There are various successful eddy viscosity models, each developed for a different flow situation.[36,42,43] For planar, free turbulent mixing in a coflowing stream, we choose Schetz's[44] model in order to account for the variable-density situation through the appropriate definition for the mass flow defect (or excess):

$$\epsilon \approx 0.0036\, \rho_e\, u_e \int_0^\infty \left| 1 - \frac{\rho u}{\rho_e u_e} \right| dy \quad , \tag{I-30}$$

where ϵ is the eddy viscosity, ρ is the density, u is the velocity, and subscript e indicates the external condition.

Before we apply this model to our case, it was verified against two turbulent wake-flow measurements, one of which is subsonic and the other supersonic. Turbulence measurements in the wake of a thin flat plate were performed by Chevray and Kovasznay[45] in a low-speed wind tunnel. This experiment offers a critical test of the present model, since it corresponds to the development of a turbulent boundary layer with zero pressure gradient when the wall shear is suddenly removed at the trailing edge. The results of the model comparison with the data are shown in Fig. I-26. The decay of the center line velocity defect

$$W = 1 - \frac{u}{u_e} \tag{I-31}$$

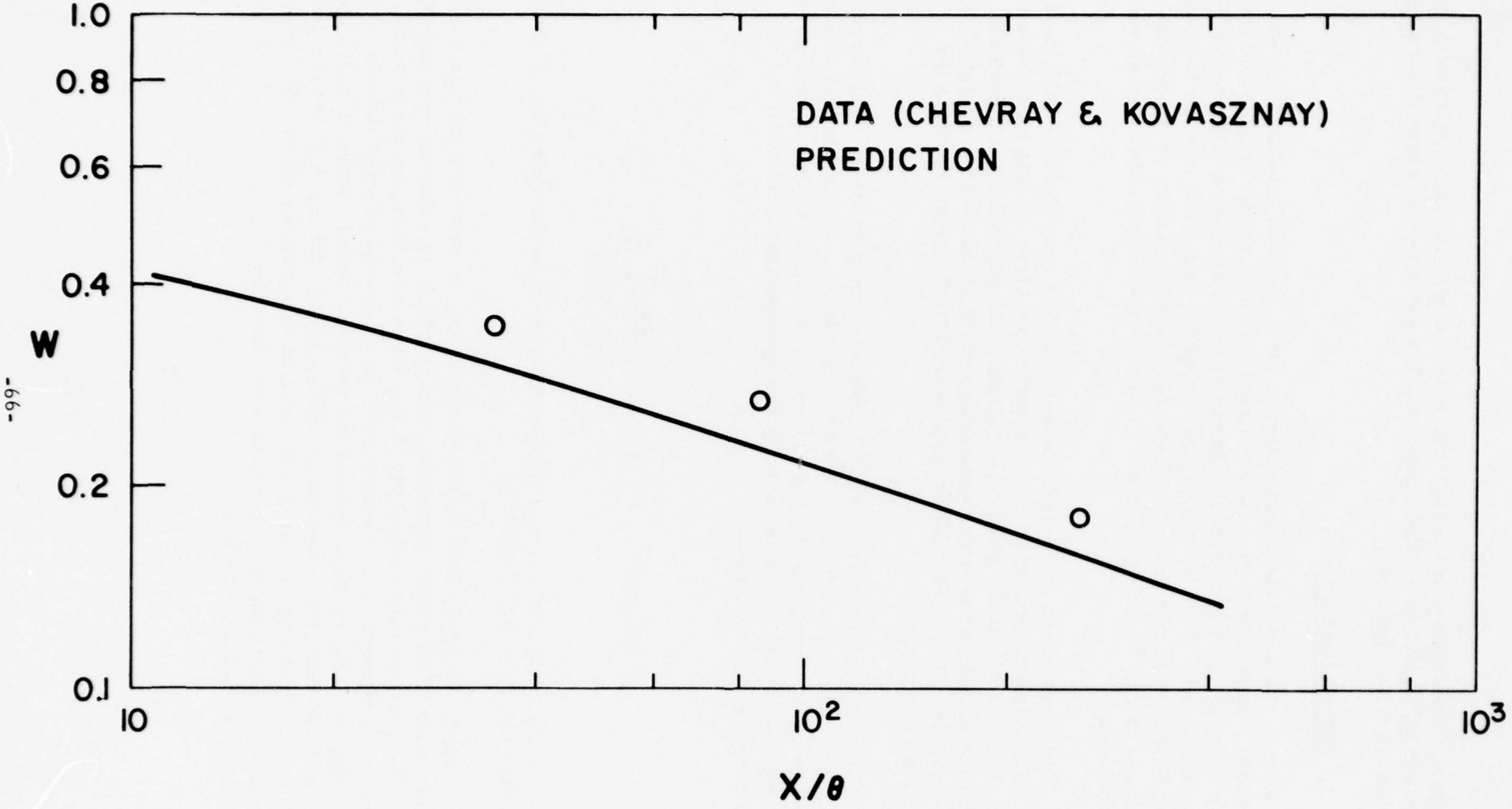

Fig. I-26 Comparison of Predictions of Schetz's Model with Subsonic Data.

is plotted as a function of x/θ where θ is the momentum thickness at the trailing edge. The adequacy of Schetz's eddy viscosity model for this low speed case is clearly demonstrated by these results.

Although the two-dimensional turbulent wake has been extensively studied at low speed, information for supersonic turbulent wakes is scarce. Measurements with cylinders placed normal to a Mach 6 air stream have been made by McCarthy and Kubota[46] and Behrens.[47] In these two experiments, the combination of high Mach number and severe body bluntness produced large gradients in the flow immediately adjacent to the wake. Under such circumstances the turbulent wake mean flow becomes indistinguishable from that of the inviscid wake. To restore the prominence of the turbulence core, the inviscid gradients must be reduced. This can be accomplished by using a very slender body. Demetriades[48] has made some mean-flow measurements in the supersonic wake of a very slender, two-dimensional body in a continuous open-circuit wind tunnel at Mach 3 with a stagnation pressure of 730 mm Hg absolute and a stagnation temperature of 38°C. Under these conditions, the role assumed at low speeds by the cylinder diameter as a gaging length of the wake flow is assumed by the wake drag thickness. If the body drag coefficient, C_D, is associated with a lateral dimension h, then the wake drag per unit span is:

$$\frac{1}{2} \rho u^2 C_D h = \int_{-\infty}^{\infty} \rho u (u_e - u) \, dy = \text{constant} \quad . \tag{I-32}$$

The constant quantity $C_D h$, called "the virtual body thickness", can be obtained from this expression if we assume that the lateral velocity distribution is similar. From the experimental data, the constant $C_D h$ is found to be 0.00909 cm, and this value is used to nondimensionalize the axial distance. As shown in Fig. I-27, the rate of decay of the centerline velocity defect is accurately predicted by Schetz's eddy viscosity model for the turbulent transport in this supersonic flow situation.

Having demonstrated by these comparisons with turbulent flow data that Schetz's model is reasonably accurate, we can now apply it to determine the appropriate mixing nozzle for the D_2/HCl EDL. A sketch of the assumed nozzle configuration is shown in Fig. I-28. The HCl injection port is located at the sonic point of the nozzle and provides co-axial injection of HCl or HCl/Ar mixtures. In practice, the position of the HCl injection relative to the throat could be varied to provide for some empirical optimization of the mixing. The nozzle throat height is assumed to be 1.0 mm with a nominal A/A^* of 3.3 to provide for the required expansion to $M_e = 2.5$.

For this calculation, the laminar coefficient of viscosity, which can be readily calculated from the molecular properties[49], was determined, and was found to be small compared with the eddy viscosity. Thus, our assumption that shows that turbulent mixing occurs appears to be valid.

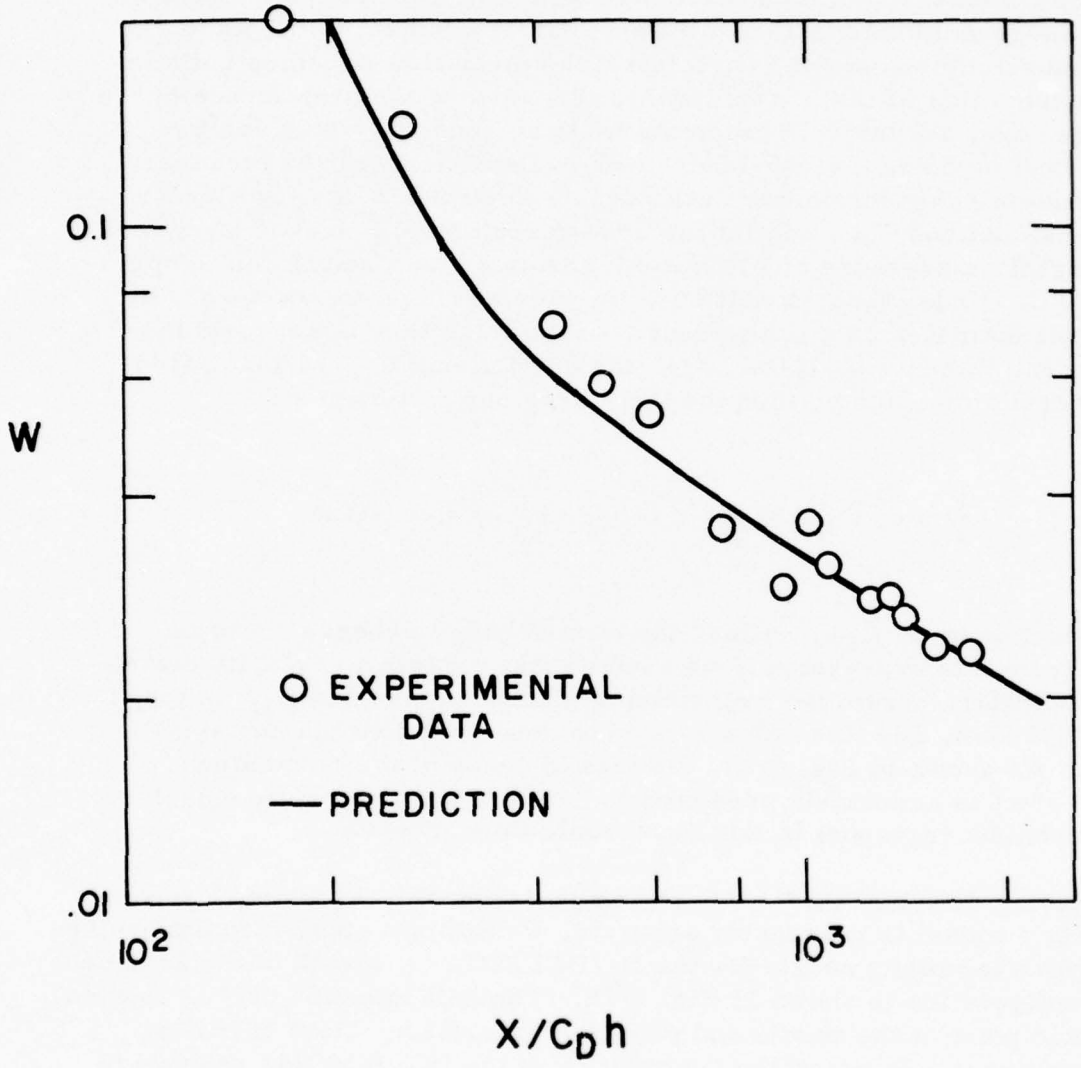

Fig. I-27 Comparison of Predictions of Schetz's Model with Supersonic Data.

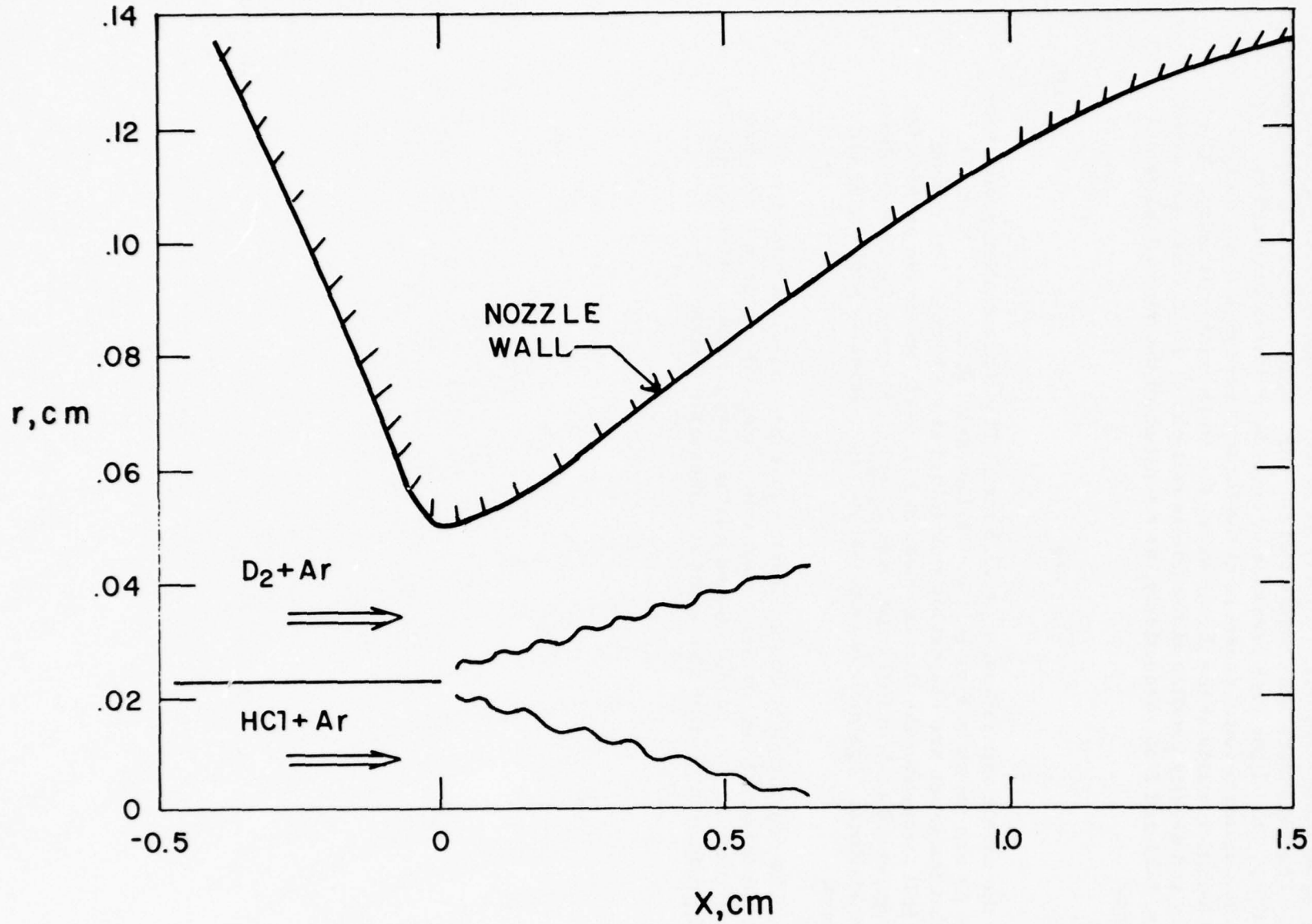

Fig. I-28 Schematic of Mixing Nozzle with Axial Injection at Throat. This Configuration was used in the Mixing Calculation Described in the Text.

We have modeled a case in which the plenum flow contains approximately equal mole fractions of D_2 and Ar at one atmosphere pressure and 300°K. The secondary flow consists of HCl/Ar = 0.18/0.82 at 1.02 atmospheres and 300°K. The slight over pressure of secondary flow is required to maintain a uniform static pressure at the throat where both flows merge. The calculation starts at the throat where the Mach number is unity. The velocity and density profiles at the nozzle exit plane, x = 1.5 cm, are given in Figs. I-29 and I-30 respectively, as a function of the normalized radial distance,

$$\bar{r} = r/r_e \quad , \tag{I-33}$$

where the nozzle exit radius, r_e = 13.5 mm. The concentration profiles for D_2 and Ar are shown in Fig. I-31 for various axial distances. It can be seen that the gases are reasonably well mixed at x ≥ 10 cm. The mixing of the HCl throughout the flow is shown in Fig. I-32, where the profiles for HCl, expressed as % of HCl relative to $\underline{D_2 \text{ only}}$, are given for several downstream stations. Again, it is seen that HCl is reasonably well mixed for x ≥ 10 cm.

The conclusion of this analysis is that for centerline injection of HCl at the throat of the nozzle, reasonable mixing will occur in a distance of about 10 cm for gas conditions and mixture compositions which kinetically should produce high gains and lasing at comparable distances.

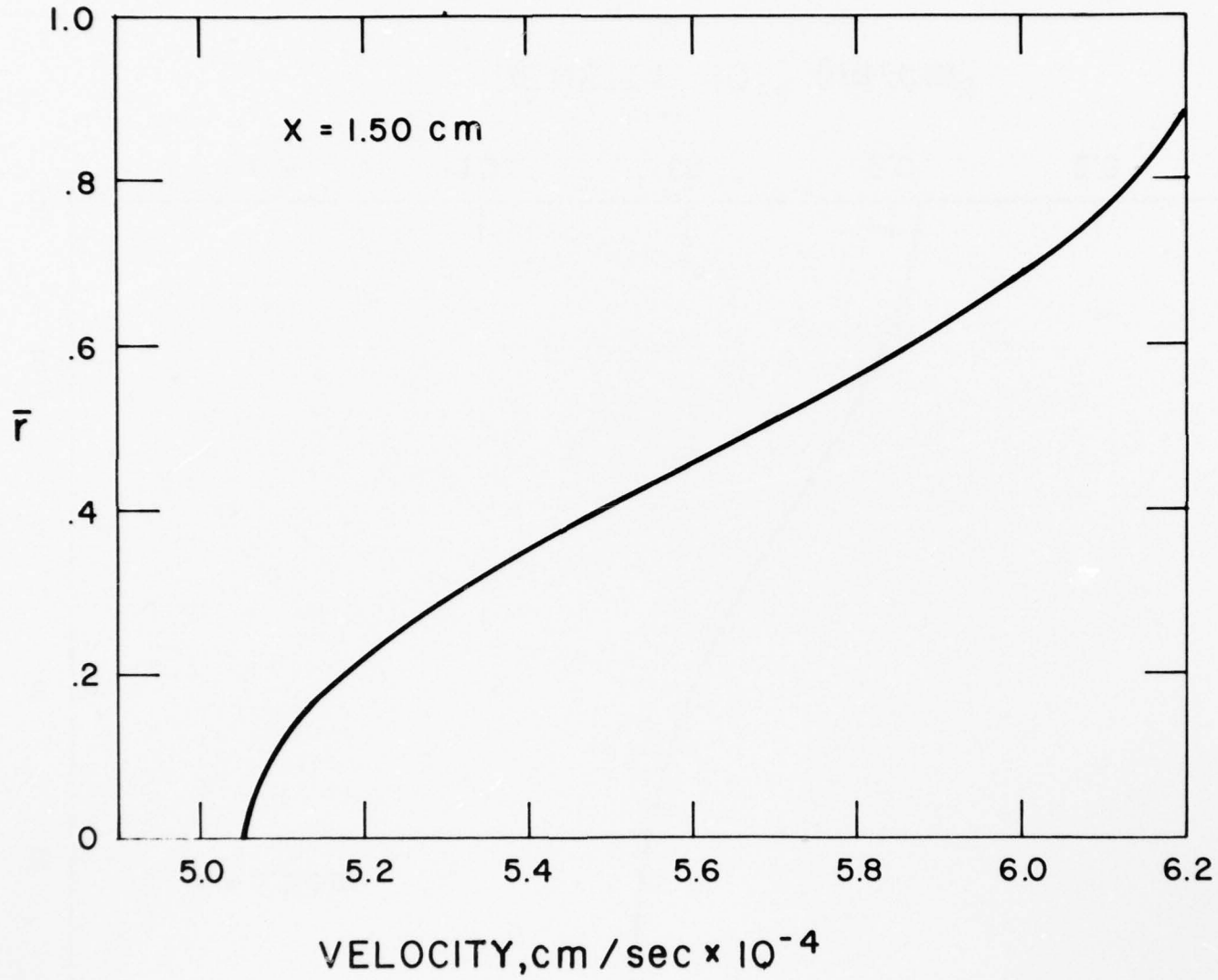

Fig. I-29 Velocity Profile at Exit of Nozzle as Determined from Mixing Calculation.

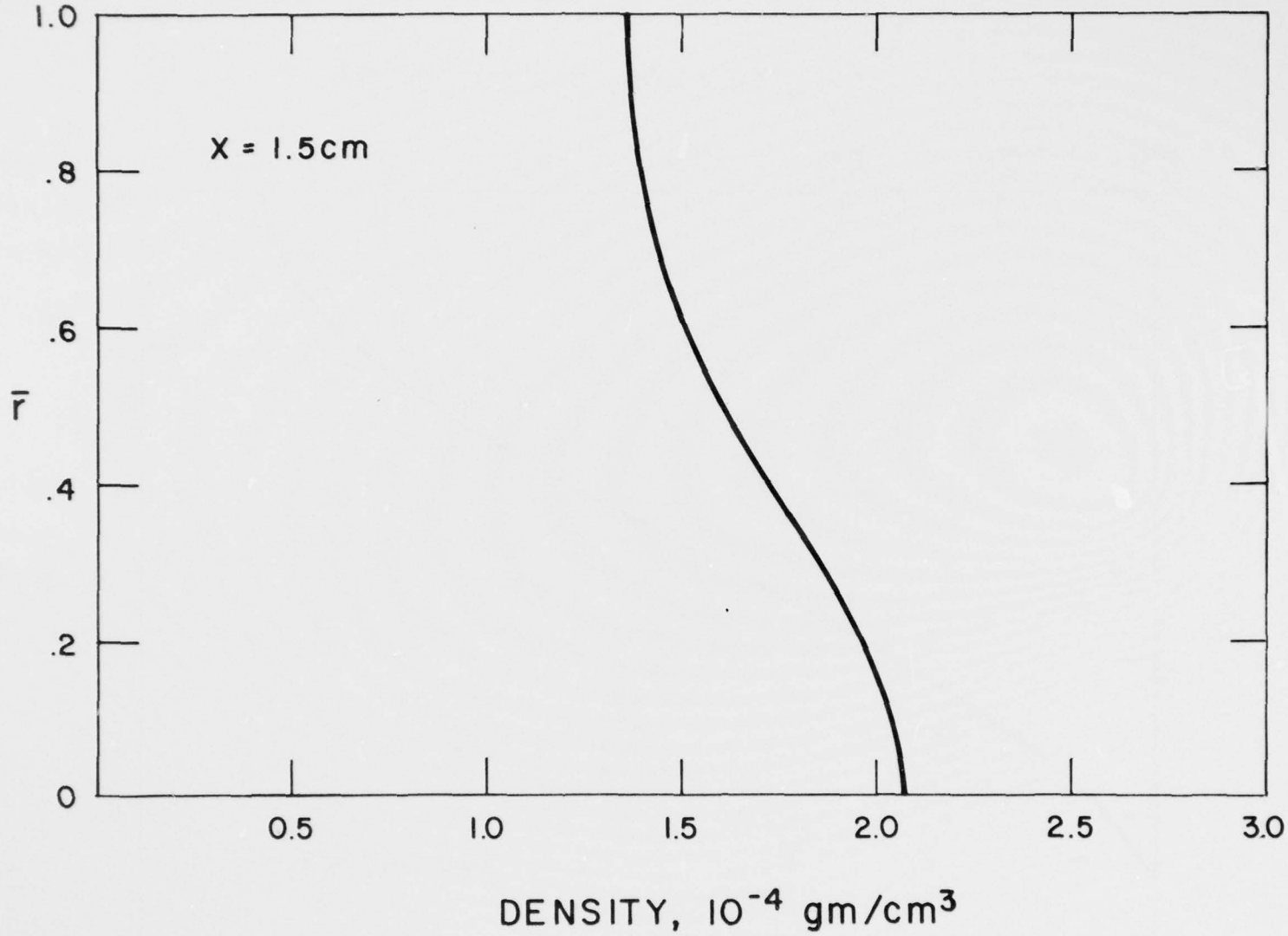

Fig. I-30 Density Profile at Exit of Nozzle as Determined from Mixing Calculation.

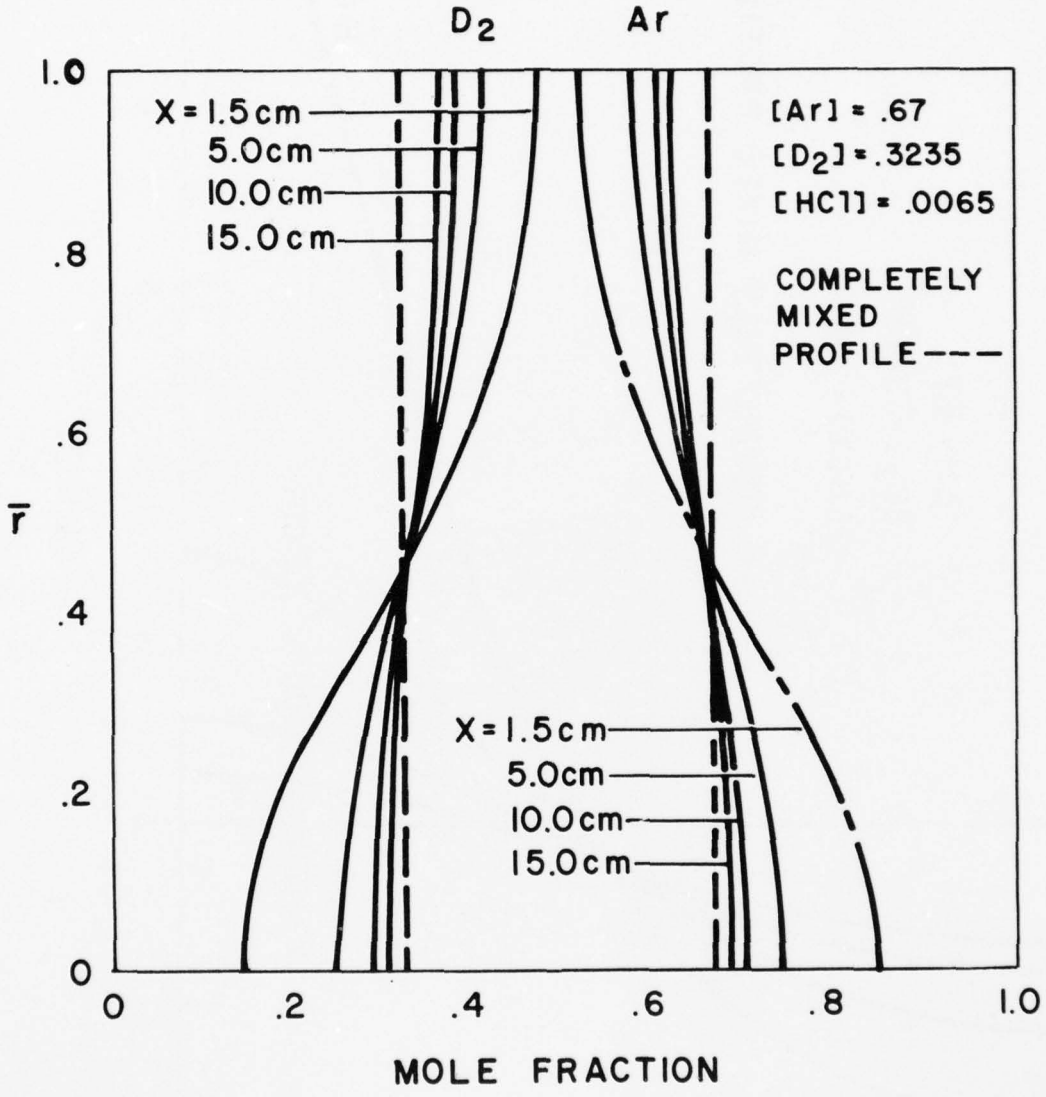

Fig. I-31 Concentration Profiles for D_2 and Ar at Various Distances Downstream of Nozzle Throat.

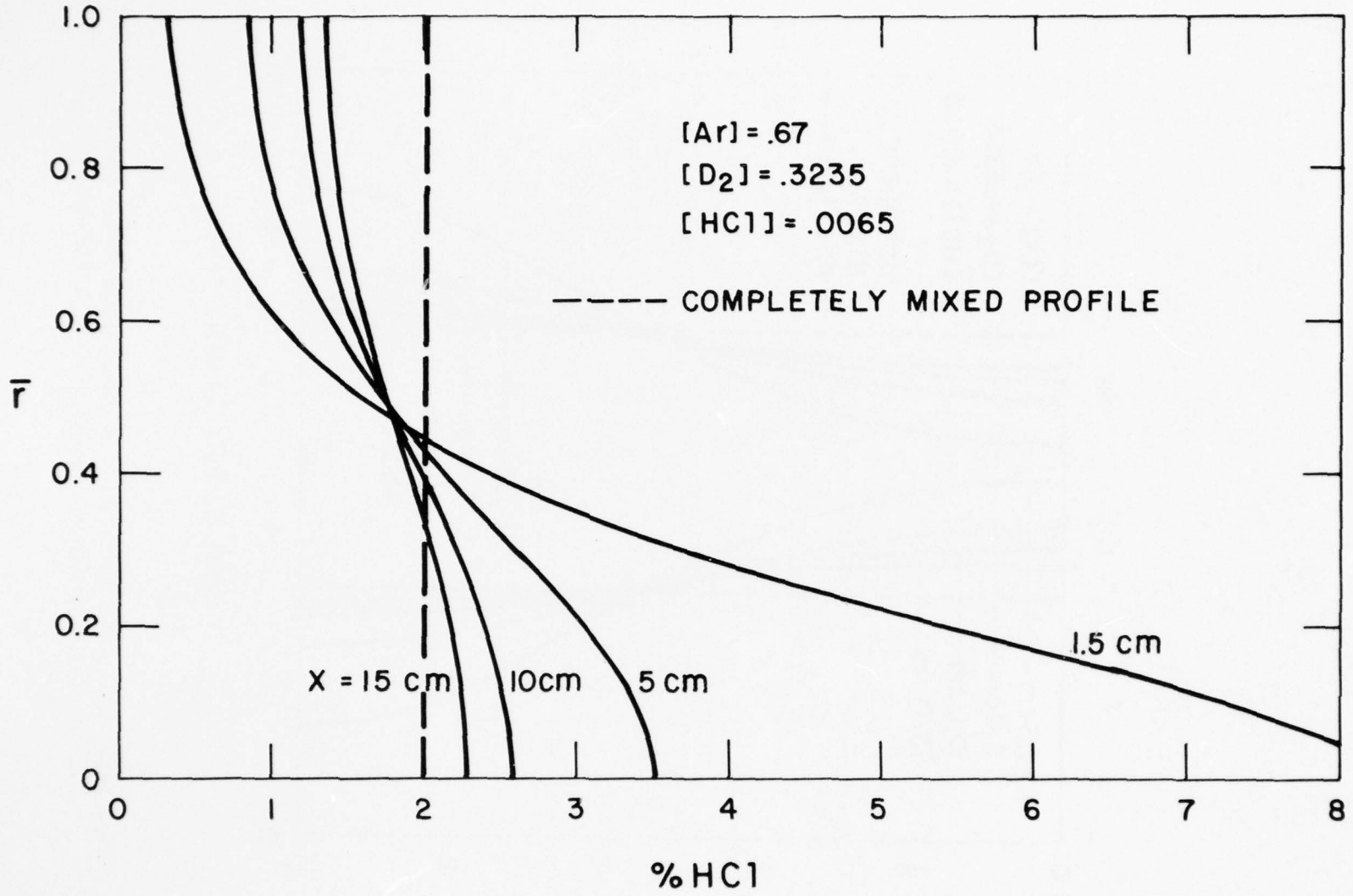

Fig. I-32 Concentration Profiles for HCl at Various Distances Downstream of Nozzle Throat. Note that these Profiles are Expressed as % HCl Relative to D_2.

F. CONCLUSION AND SUMMARY

An initial goal of this program was to develope an analytic capability to model the D_2/HCl EDL experiment. This code development consisted of three major separate tasks: (i) a model of the discharge or plenum conditions, (ii) a technique to handle secondary injection and subsequent gas mixing, and (iii) a vibrational kinetic code to calculate gain on vibrational/rotation transitions in the cavity. These codes were developed and successfully operated under this program.

To specify the discharge conditions, an existing Boltzmann transport code was modified and used. State-of-the-art cross sections for electron impact excitation of H_2 were determined by a careful review of available data and theory, and by comparison of predicted transport properties of H_2 discharges with measurement. A cross section data package for D_2 was determined primarily by analogy to the data for H_2. With these data packages, the capability exists to calculate the transport properties, excitation rate constants, and energy deposition into the various internal modes for a wide range of experimental discharge conditions in pure H_2 and D_2 and in mixtures of these gases with He or Ar.

The results of a discharge calculation for conditions comparable to those used in the NRL EDL device indicated that a D_2 vibrational temperature of about 1700°K was expected. No direct experimental determination of this temperature was possible. However, approximate D_2 vibrational temperatures could be inferred from D_2/CO_2 laser gain experiments and indicated a range of temperatures from 1100 - 2300°K. It is undoubtedly a coincidence that the median of this temperature range agrees with the prediction.

An approximate mixing analysis was developed to provide for injection of HCl within the nozzle and the instantaneous mixing of the gas, with the calculation of new, appropriate flow conditions at the nozzle exit with the specification of any heat input to the gas due to vibrational kinetics. This model seemed appropriate for the NRL EDL, since it was estimated that the mixing time was probably short compared to the characteristic time for V→V pumping of HCl by D_2. This mixing code uses as input the plenum conditions (as specified by the Boltzmann code) and calculates the input conditions for the cavity analysis.

A complete set of vibrational energy transfer rate constants for the D_2/HCl molecular system was developed from a combination of experimental data, theory, and empirical correlation. These rate constants

were used with an existing anharmonic oscillator laser code to calculate HCl vibrational populations and small signal gain as the gas flowed down the cavity. In addition, infrared fluorescence per molecule and simulated power extraction are other available options from such a calculation.

The second major goal of this research effort was to use the predicted results of the analytic model to compare with experimental data and to guide the experimental effort. An early calculation performed for appropriate device conditions indicated that at the low gas densities expected in the cavity, the gain was not expected to peak until well beyond the available, accessible viewing area. This prediction was qualitatively consistent with the data; infrared fluorescence (observed primarily from the lower levels of HCl) increased monotonically throughout the observation distance of about 23 cm and no lasing could be obtained.

More quantitative comparisons of the results of the calculations with data were inhibited by the realization that the fluid dynamic flow in the NRL EDL device as it then existed was difficult to characterize. It was determined that the cavity static pressures were much higher than expected on the basis of simple inviscid calculations. The reason for this discrepancy was eventually determined to be a combination of steam ejector and cavity wall boundary layer effects.

Because of these flow problems, a decision was made late in the program to use the remaining resources to conceptually design a better experiment. As a starting point, it was decided to consider an e-beam sustainer discharge operating at one atmosphere plenum pressure as the laser excitation source. By operating at a higher plenum pressure, higher cavity density is attainable. Although detailed discharge calculations were not performed for these higher pressures, it is expected that D_2 vibrational temperatures comparable to the glow discharge results should be attainable. A series of cavity kinetic calculations were performed for a range of D_2 T_v's from 1000 - 2000°K. These results indicate the high gains, i.e., $>1\%\ cm^{-1}$, can be achieved a few cm downstream of the nozzle.

In addition, a turbulent mixing calculation was performed to assess axial injection of secondary gas at the nozzle throat. It was determined that the gases should be reasonably well mixed 10 cm downstream of the injection position. Obviously, further iteration can be performed to provide the optimum device conditions, where the mixing length and HCl pumping length are comparable.

The conclusions of this conceptual design study are that the higher density operation is desirable and that a demonstration of a D_2/HCl EDL should be possible. The preliminary operating conditions, nozzle expansion ratio, and injection technique are determined. This information can be used to develop a detailed experimental design.

II. ANALYTICAL MODELING OF A PULSED ELECTRIC DISCHARGE HCl LASER

A. INTRODUCTION

This section of this report provides a description of research performed at PSI in support of the NRL pulsed electrical discharge HCl infrared laser experiment. This latter program involved studies of the electrical excitation of mixtures of HCl/Ar with the goal of determining the feasibility of developing an efficient laser operating on HCl vibration/rotation transitions. In this study the electrical excitation was provided by an electron beam sustained discharge utilizing the NRL Maxwell cold cathode e-beam sustainer device which has the capacity of operating at voltages of 300 kv with beam current densities of ~10 amps/cm^2. The laser test chamber in these experiments had an active length of 100 cm, height and depth of 10 cm, and a mirror/coupling configuration designed to allow observation of lasing at small signal gains of order 10^{-3} cm^{-1}.

The primary goal of the PSI research effort was to develop an electric discharge kinetic model for HCl to be used to provide predictions of system gain and optimum operating conditions. A detailed discussion of this electron kinetic model is presented in Sec. II-B and specific system gain predictions and comparison with data are discussed in Sec. II-C. Lastly, an analysis of infrared fluorescence measurements, performed early in the experimental program, is given in Sec. II-D.

B. ELECTRIC DISCHARGE KINETICS

It is well known that when a partially ionized gas is subjected to an electric field the resulting steady state electron velocity distribution need not be Maxwellian. Indeed the resulting velocity (energy) distribution is determined by the competition between the accelerating electric field and elastic and inelastic collisions between the electrons and bath gas molecules. The characteristics of such discharges are generally defined in terms of the bulk transport properties for given values of the Townsend parameter E/N, where E is the applied voltage per unit length and N is the gas number density. The two most commonly used transport properties are the electron drift velocity V_D and the characteristic electron energy ϵ_K. In the case of a Maxwellian velocity this latter quantity is the equivalent of $k T_e$ where k is Boltzmann's constant and T_e is the electron temperature.

In order to specify the excitation rate constants for specific electron/molecule interactions occuring in the discharge, which is the goal of the present analysis, the detailed electron velocity distribution is required. Although this distribution cannot be readily deduced experimentally, it can be predicted theoretically by solving the Boltzmann transport equation. This analytical technique, however, requires specification of the electron energy dependent cross sections for all of the important elastic and inelastic electron/molecule processes which occur in the discharge. Unfortunately, such detailed data is not commonly available for most gases.

If the transport properties of a gas are known as a function of the Townsend parameter, then unknown cross sections may be deduced by an inverse process, e.g., ref. 50. In this method, the Boltzmann transport equation is solved with a trial set of cross sections in order to provide predicted bulk transport properties as a function of the Townsend parameter. The predictions are then compared to the data and the trial cross sections are adjusted in a systematic manner in order to improve the agreement between prediction and data. This process is repeated iteratively until the difference between data and predictions is within the uncertainty of the data. This technique cannot provide a unique set of cross sections, and, therefore, considerable insight is required in choosing the trial cross sections. The selection process can be simplified somewhat if the analysis is limited to a range of Townsend parameter where only one or two inelastic processes are important.

In the case of HCl, the data base is relatively sparse. Only a few of the inelastic processes of interest in HCl have been studied, and, furthermore, the only measurement of the bulk transport properties of HCl discharges is the early work of Bailey and Duncanson.[51, 52] This latter study was performed

in pure HCl over the E/N range of 3 - 12 x 10^{-16} V-cm^2, and the observed values of drift velocity and characteristic energy are listed in Table II-1. In the present analysis these data will be used in conjunction with the available cross section information to deduce a self-consistent set of cross sections for HCl.

There is one caveat which should be mentioned before proceeding with this analysis. Although Bailey and Duncanson's[51] work is qualitatively valuable, their measured transport properties may not be as accurate as one might desire. In particular, the drift velocities were determined through use of a magnetic field, and the difference between electric and magnetic drift velocity was not appreciated at that time. Indeed, the actual drift velocity can be determined from their raw data only if a number of restrictive assumptions are made.[53] In the one instance where modern measurements can be compared with measurements performed by Baileys' group,the agreement is poor,[13] suggesting that the error associated with Baileys' experimental technique is large. Thus, a modern study of electron transport properties in HCl discharges is necessary to develop a cross section data base having high confidence limits. For the present analysis, the results of Bailey and Duncanson will be assumed to be correct; however, no effort will be made to provide "exact" agreement between the predicted and measured transport properties.

The first reported effort directed towards developing a set of collision cross sections for HCl which was compatible with the available transport data[51] was the work of Nighan and co-workers[54] at UTRC. This analysis was performed using the technique of Frost and Phelps[50] mentioned earlier, and included the collision processes of momentum transfer, rotational excitation, vibrational excitation, dissociative attachment and electronic state excitation. At the time of this analysis only the cross section for dissociative attachment had been measured.[56] Guidelines used in estimating the remaining cross sections included the theoretical study of Itikawa and Takayanagi[56] on rotational excitation and elastic scattering in HCl, and the electron-HCl excitation spectrum reported by Compton et al.[57]

The cross section base deduced by Nighan et al is shown in Fig. II-1 which is taken from Ref. 54. The dominant feature of this figure is the high cross section, ~10^{-15} cm^2, for vibrational excitation of HCl. It is interesting to note that although the onset energy for vibrational excitation of HCl is 0.36 eV, the predicted onset for this process from the UTRC analysis is at ~ 0.46 eV.

The availability of recent measurements[58-62] on the vibrational excitation cross sections for HCl, taken since the time of the UTRC analysis, has provided motivation for a new determination of the total cross section

TABLE II-1

MEASURED TRANSPORT PROPERTIES OF HCL DISCHARGES

$E/N \times 10^{16}$ v-cm^2	ϵ_K^*, eV	$V_D \times 10^{-6}$, cm/sec
3	0.084 - 0.093	3.5
4.5	0.145	4.4
6	0.162 - 0.172	4.5
9	0.294 - 0.32	5.0
12	0.54 - 0.56	6.0

* Lower values from Ref. 51. The higher values are reported in Ref. 52 as the results of Ref. 51. The cause of this discrepancy is not clear.

PRELIMINARY HCl CROSS SECTIONS

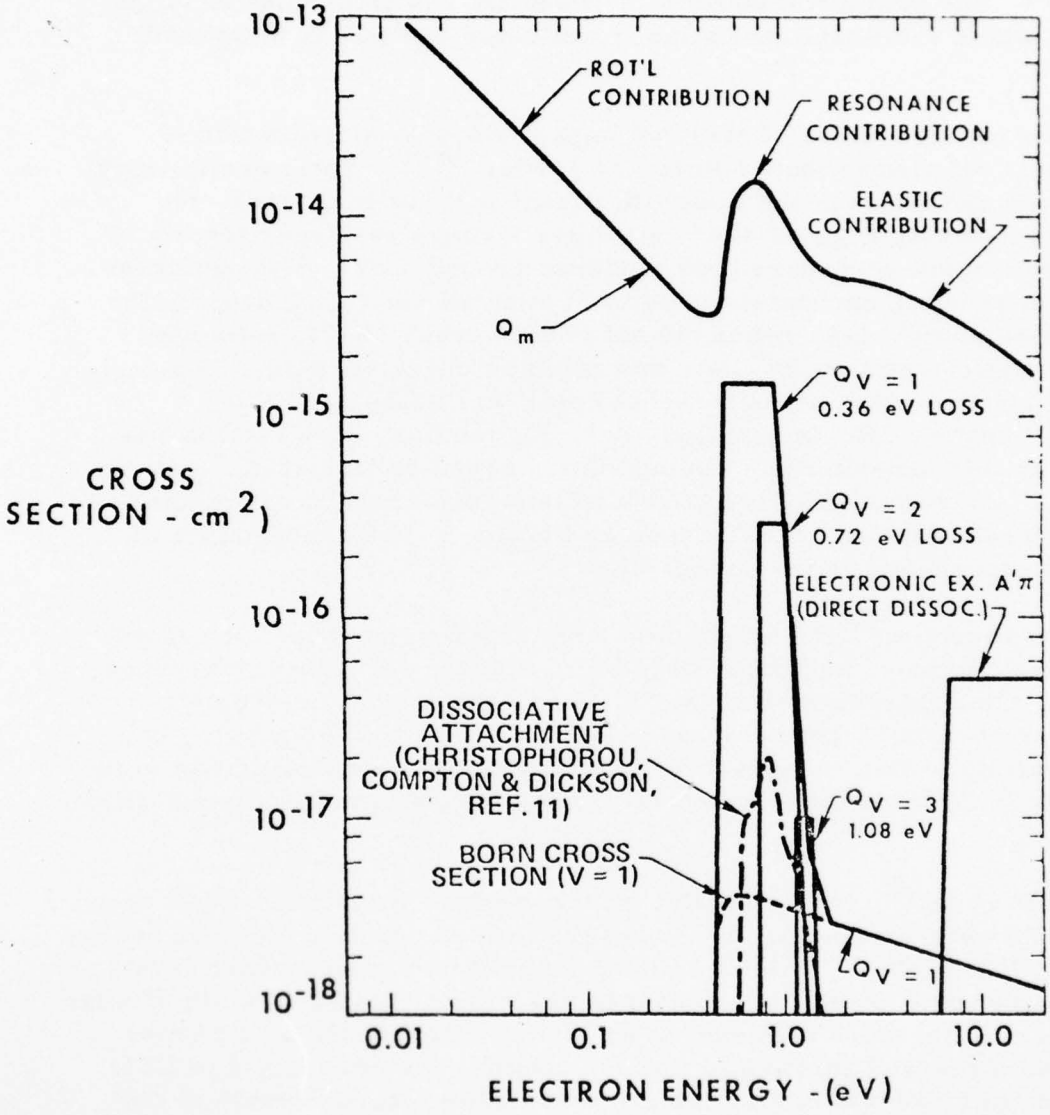

Fig. II-1 Electron Collision Cross Sections for HCl as Taken From Ref. 54.

base for HCl again by comparison with the transport data of Bailey and Duncanson. This redetermination has been performed by a technique similar to that of Frost and Phelps, but using a computer code for the solution of the Boltzmann transport equation which was originally developed by Carleton and Megill[11] and subsequently modified by Lenander[2] and by Yos et al.[63] The primary difference between the two techniques is in the manner in which rotational excitation is evaluated and this is discussed in Appendix B.

Of the recent studies of electron impact vibrational excitation of HCl the most detailed is that of Rohr and Linder.[58-59] Their preliminary results[58] for excitation of the first vibrational level of HCl, presented only for a scattering angle of 120°, exhibited a sharp peak near threshold followed by a broad secondary peak centered around 3 eV. Although these data had not yet been accurately integrated over all scattering angles, the cross section energy dependence did not seem to vary significantly with scattering angle, and the 120° data was taken as characteristic. The angle integrated cross section of the threshold peak was estimated to be 1.3×10^{-15} cm^2 ± 50%. In actuality, only the relative cross section was measured in this experiment. Their relative cross section at an electron energy of 10 eV was normalized to an absolute measurement of the total scattering cross section for HCl taken by Brüche.[64] The uncertainty in Brüches measurement is not specified.

More recently,[59] the differential cross section has been integrated over scattering angle, and it has been found that the secondary peak takes on more of the appearance of a plateau. Furthermore, the magnitude of the cross section at the threshold peak was raised to 2.18×10^{-15} cm^2. The uncertainty in this value is still not defined, being primarily due to the uncertainty in Brüches measurement. The resulting cross section is shown in Fig. II-2.

Ziesel et al.[60] have also studied the electron impact vibration excitation of HCl near threshold. Their results, which span the electron energy range of 0.36 - 0.50 eV, exhibit a sharp rise near threshold which levels off approximately 0.06 eV above onset in agreement with the results of Rohr and Linder. In the work of Ziesel et al, the vibrational excitation cross section was measured relative to that for dissociative attachment of HCl. As pointed out by Ziesel et al., the three available measurements of this cross section[55, 65, 66] differ by a factor of five, with that of Christophorou et al.[55] being the largest. Thus, the peak cross section near threshold as deduced from Ziesel et al's. measurements can vary between 2.5×10^{-16} - 1.25×10^{-15} cm^2 depending upon the choice of the dissociative attachment

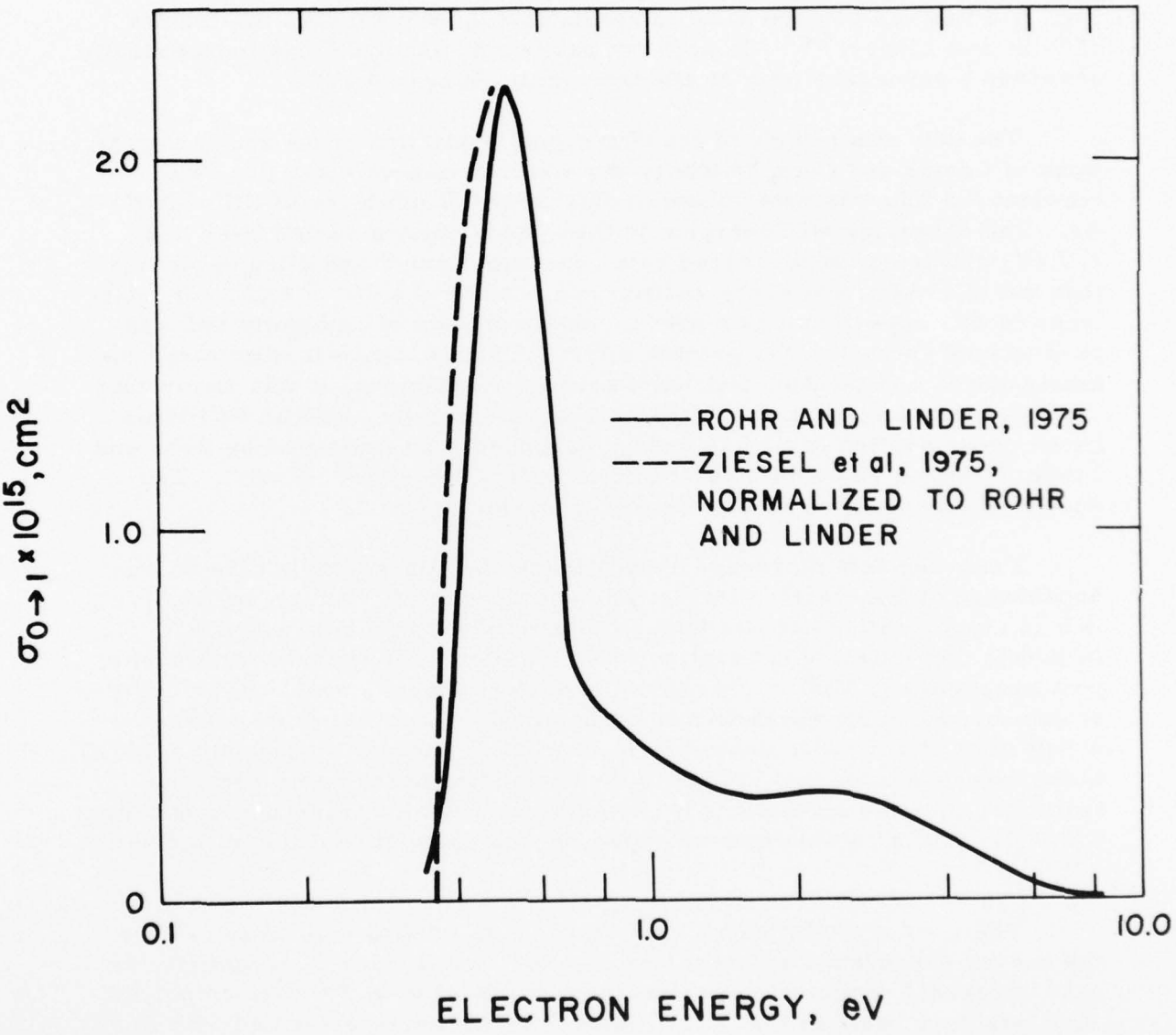

Fig. II-2 Experimental Electron Excitation Cross Sections for the HCl v = 1 → 0 Transition.

cross section. Furthermore, as discussed in Ref. 60, an additional factor of two uncertainty arises through the data analysis.* Thus, the magnitude of the cross section for vibrational excitation of HCl cannot be readily deduced from these data at the present time. The observed cross section, arbitrarily normalized to a peak value of 2.18×10^{-15} cm^2, is shown in Fig. II-2 and can be seen to be in reasonable agreement with the results of Rohr and Linder.[59] Although not published, Schultz[61] has independently observed a secondary peak at electron energies near 3 eV.

The only other study of the vibrational excitation cross section is the work of Center and Chen,[62] where the electron impact excitation rate constant for HCl was determined in discharges of mixtures of HCl-CO-N_2-Ar. The characteristic energies in these experiments varied from 0.8 - 1.7 eV, and from the measured rate constants, Center and Chen estimated that the HCl excitation cross section was ~ several x 10^{-16} cm^2. The data taken in this experiment exhibited a certain amount of ambiguity and was re-analyzed as part of the present effort. This re-analysis eliminated the ambiguities, and through detailed discharge predictions, it was shown that the measured excitation rate constants were consistent with an HCl vibrational cross section having an energy dependence as measured by Rohr and Linder[59] with a value near threshold of approximately 10^{-15} cm^2. The details of this analysis are presented in Appendix C.

From the data discussed above, it may be concluded that the energy dependence of the electron impact vibrational excitation cross section for HCl is significantly different than that deduced in the UTRC analysis,[54] (although this latter cross section was consistent with the measured transport properties of HCl discharges). However, there is still a large degree of uncertainty in the absolute magnitude of this excitation cross section. A new set of trial cross sections, incorporating these recent data discussed above was developed and used with the previously described Boltzmann transport equation computer code to provide predicted transport properties for HCl. These calculations are specific to a translational temperature of 300°K.

The $v = 0 \rightarrow 1$ vibrational excitation cross section was taken to have the energy dependence as prescribed by Rohr and Linder[59] except for the near threshold region where the results of Ziesel et al.[60] were employed. This was done because the latter measurements were performed with finer

---

* The situation is further complicated by the fact that the graphical and tabular data presented in Ref. 60 are inconsistent by a factor of two.

AD-A034 674 PHYSICAL SCIENCES INC WOBURN MASS F/G 20/5
ANALYTIC MODELING OF ELECTRICALLY EXCITED D2/HCL AND HCL LASER --ETC(U)
JUL 76 R TAYLOR, G CALEDONIA, P LEWIS, P WU N00014-75-C-0035

UNCLASSIFIED PSI-TR-58 NL

2 OF 2
AD
A034674

END

DATE
FILMED
2-77

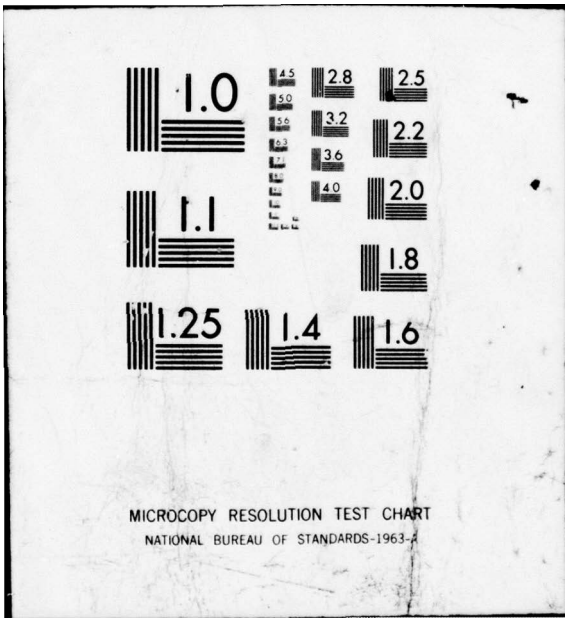
1.0
1.1
1.25
1.4
1.6
1.8
2.0
2.2
2.5
2.8
3.2
3.6
4.0
4.5
5.0
5.6
6.3
MICROCOPY RESOLUTION TEST CHART
NATIONAL BUREAU OF STANDARDS-1963-A

energy resolution than those of Rohr and Linder. There is very little information available on the $v = 0 \rightarrow 2$ vibrational excitation cross section. Ziesel et al. report that onset of this process occurs near threshold, and that the peak cross section is approximately one tenth that of $v = 0 \rightarrow 1$ excitation. Rohr and Linder report that at an energy of 3 eV the ratio of $v = 0 \rightarrow 2$ to $v = 0 \rightarrow 1$ cross sections is approximately one quarter. The cross section used in the present calculations was chosen to satisfy these criteria and to have an energy dependence similar to that observed for the $v = 0 \rightarrow 1$ cross section. The momentum transfer cross section used was similar to that developed in the UTRC analysis[54] except that the resonance contribution was shifted to lower energies in concert with the vibrational excitation cross section. Indeed, sharp structure in the differential cross section for elastic scattering of electrons from HCl has been observed to occur near 0.36 eV, the threshold for vibrational excitation.[67] The data used for the remaining inelastic processes were the dissociative attachment cross section of Christophorou et al.,[55] the electronic state excitation cross section determined in the UTRC analysis,[54] and the ionization cross section measured by Compton and Van Voorhis.[68] Rotational excitation was handled by the single level approximation as described in Appendix B.

The above set of cross sections was adjusted until "reasonable" agreement was obtained between measured and predicted transport properties. For the most part these adjustments were limited to variations in the magnitude of the vibrational excitation cross sections and to the shape and magnitude of the momentum transfer cross section in the resonance region. The final "best set" of vibrational and momentum transfer cross sections is shown in Fig. II-3. Note that the peak value of the vibrational excitation cross section is 1.3×10^{-15} cm^2 which is in the midrange of the available estimates.[54, 58-62] Predicted transport properties for HCl, developed from the cross sections shown in Fig. II-3, are compared with the measurements of Bailey and Duncanson[51] in Tables II-2 and II-3. Shown for comparison are the predictions from Ref. 54. As can be seen the present calculated results are reasonable, although the predicted values of ϵ_K and V_D are somewhat higher than the data at the highest values of E/N considered. Although much better comparison could have been achieved by further adjustment of the cross sections, the accuracy of the transport data does not warrant the effort. Interestingly enough, the difference between the present predictions and those of Ref. 54 are not large although the cross sections used are quite different.

Calculations have also been performed for mixtures of 10% HCl/90% Ar and 3.33% HCl/96.67% Ar. Standard values for the Ar cross sections were used, as listed in Ref. 4. The predicted characteristic energies and drift velocities for these mixtures are shown in Fig. II-4 vs E/N_{HCl}.

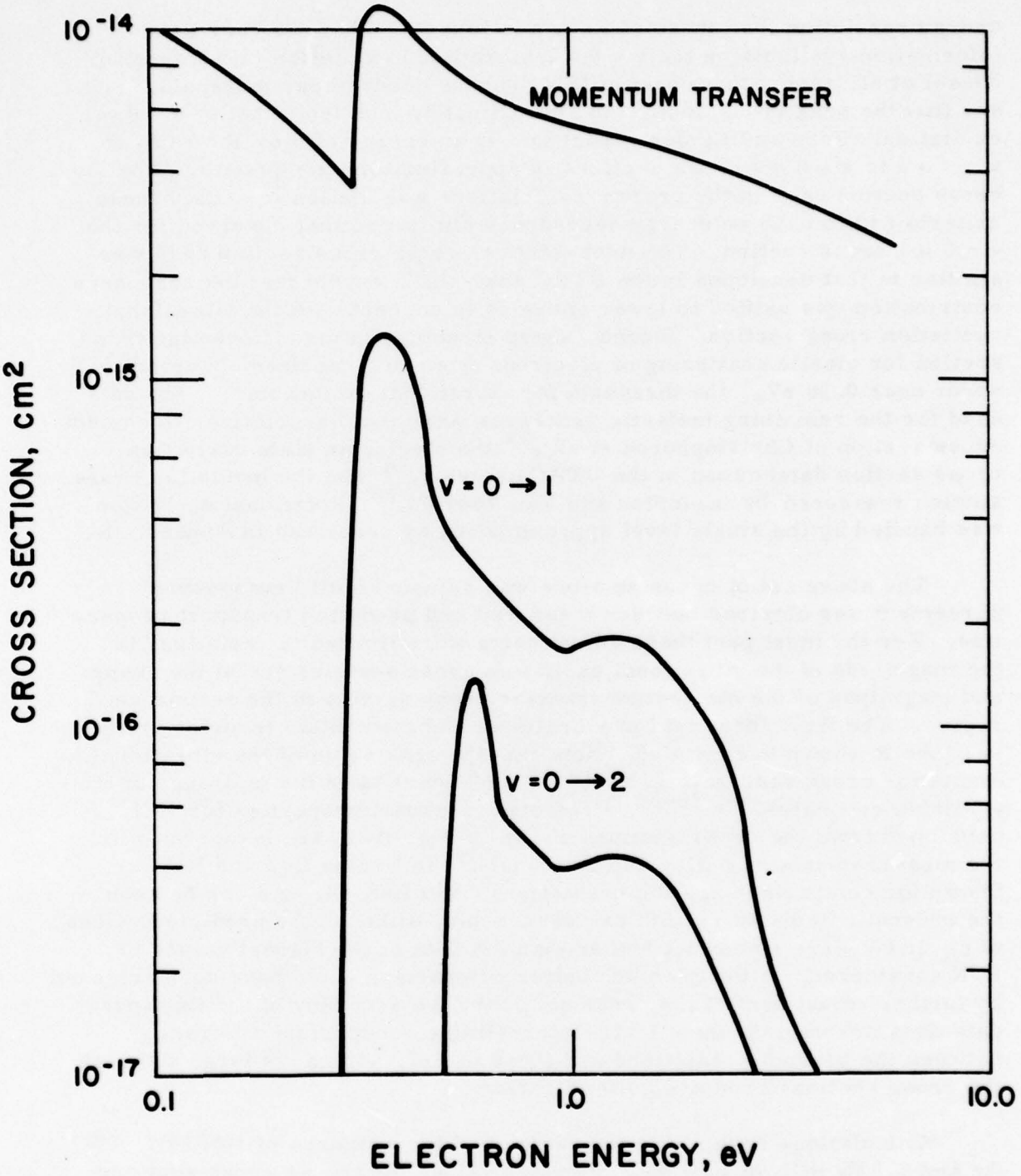

Fig. II-3 Electron Collision Cross Sections for HCl as Selected for the Present Study.

TABLE II-2

COMPARISON OF PREDICTED AND MEASURED CHARACTERISTIC ENERGIES IN HCL DISCHARGES

$E/N \times 10^{+16}$, V - cm^2	ϵ_K, eV		Present Analysis
	Data, Ref. 51	Prediction, Ref. 54	
3	0.084-0.093	0.09	0.08
4.5	0.145	(0.16)*	0.12
6	0.162-0.175	(0.21)	0.165
7	----	0.24	0.20
9	0.294-0.32	(0.36)	0.33
10	---	0.43	0.43
12	0.54 - 0.56	(0.74)	0.73
15	---	1.32	1.31

*( ) → Interpolated from Predictions Presented in Ref. 54

TABLE II-3

COMPARISON OF PREDICTED AND MEASURED DRIFT VELOCITIES IN HCL DISCHARGES

$E/N \times 10^{+16}$, V-cm^2	$V_D \times 10^6$, cm/sec		
	Data, Ref. 51	Prediction, Ref. 54	Present Analysis
3	2.5	2.7	2.5
4.5	4.4	(4.4)*	3.7
6	4.5	(4.95)	4.5
7	---	5.4	5.1
9	5.0	(6.0)	5.7
10	---	6.1	5.8
12	6.0	(6.25)	6.1
15	---	6.4	6.4

*( ) → Interpolated from Predictions Presented in Ref. 54

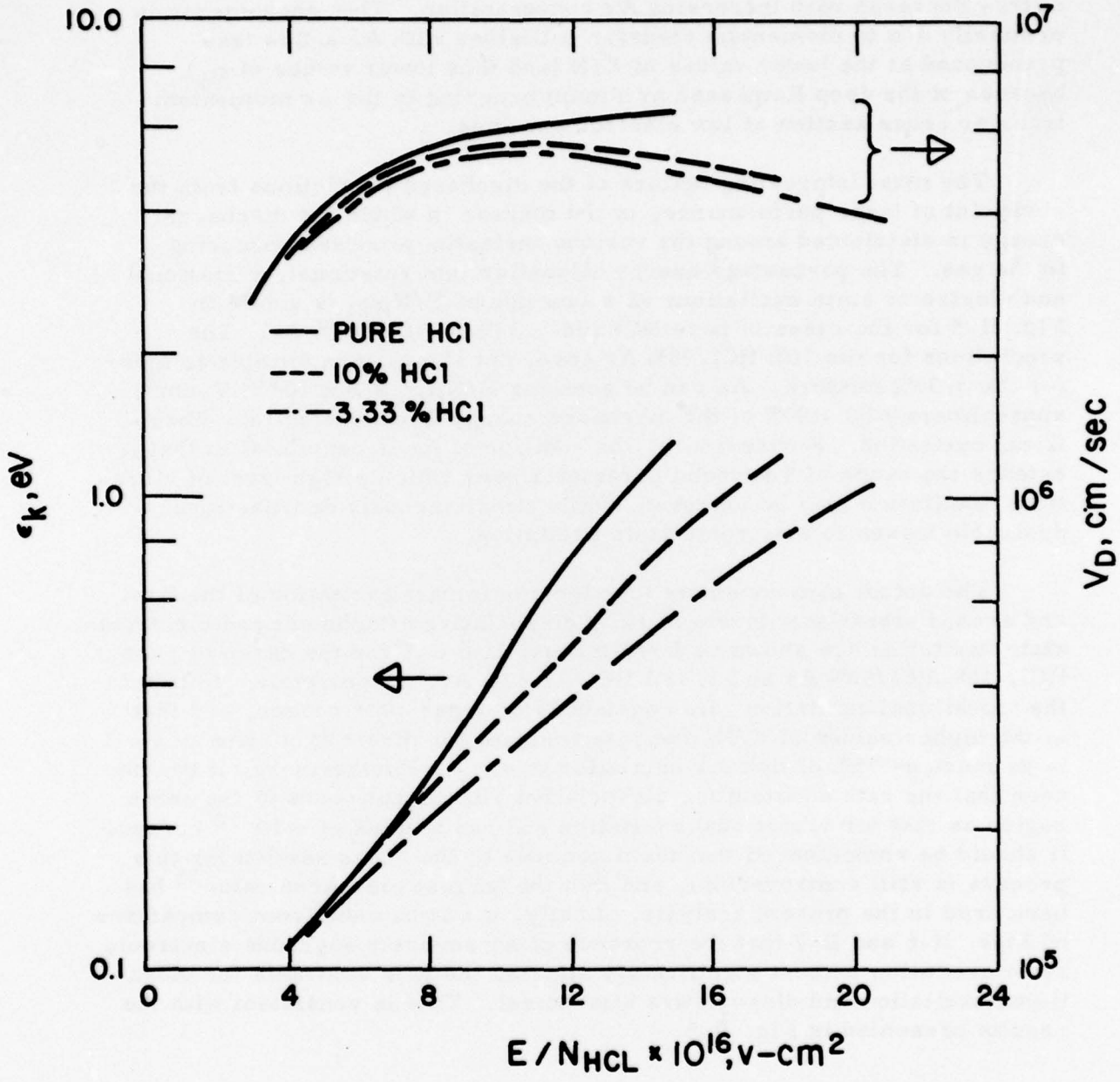

Fig. II-4 Predicted Discharge Transport Properties for Pure HCl and HCl/Ar Mixtures.

The results for pure HCl are also shown for purposes of comparison. As can be seen, the presence of Ar affects the transport properties at the higher values of E/N_{HCl} where both the drift velocity and characteristic energy decrease with increasing Ar concentration. This phenomenon is primarily due to momentum transfer collisions with Ar and is less pronounced at the lower values of E/N (and thus lower values of ϵ_K) because of the deep Ramsauer minimum occuring in the Ar momentum transfer cross section at low electron energies.

The most interesting feature of the discharge predictions from the viewpoint of laser performance, is the manner in which the discharge energy is distributed among the various inelastic processes occuring in the gas. The percentage energy allocation into rotational, vibrational and electronic state excitations as a function of E/N_{HCl} is shown in Fig. II-5 for the cases of pure HCl and 3.33% HCl/96.67% Ar. The predictions for the 10% HCl/90% Ar case, not shown, are similar to those for the 3.33% mixture. As can be seen for $E/N_{HCl} \geq 8 \times 10^{-16}$ V-cm^2, approximately 80 - 90% of the discharge energy is channeled into vibrational excitation. Furthermore, the addition of Ar is beneficial in that it extends the range of Townsend parameter over which a high level of vibrational excitation may be achieved, while simultaneously decreasing undesirable losses to electronic state excitation.

The actual rate constants for electron impact excitation of the first and second vibrational levels of HCl, dissociative attachment and electronic state excitation are shown vs E/N in Figs. II-6 to 8 for the cases of pure HCl, 10% HCl/90% Ar and 3.33% HCl/96.67% Ar, respectively. Note that the vibrational excitation rate constant is of order 10^{-8} cc/sec, and that at the higher values of E/N, the rate constant for direct excitation to v = 2 is as much as 15% of that for excitation to v = 1. Furthermore, it can be seen that the rate constant for dissociative attachment peaks in the same region as that for vibrational excitation and has a value of $\sim 10^{-10}$ cc/sec. It should be remembered that the magnitude of the cross section for this process is still controversial, and that the largest measured value[55] has been used in the present analysis. Lastly, it can be seen from comparison of Figs. II-6 and II-7 that the presence of Ar severely degrades electronic state excitation without significantly altering the rate constants for vibrational excitation and dissociative attachment. This is consistent with the results presented in Fig. II-5.

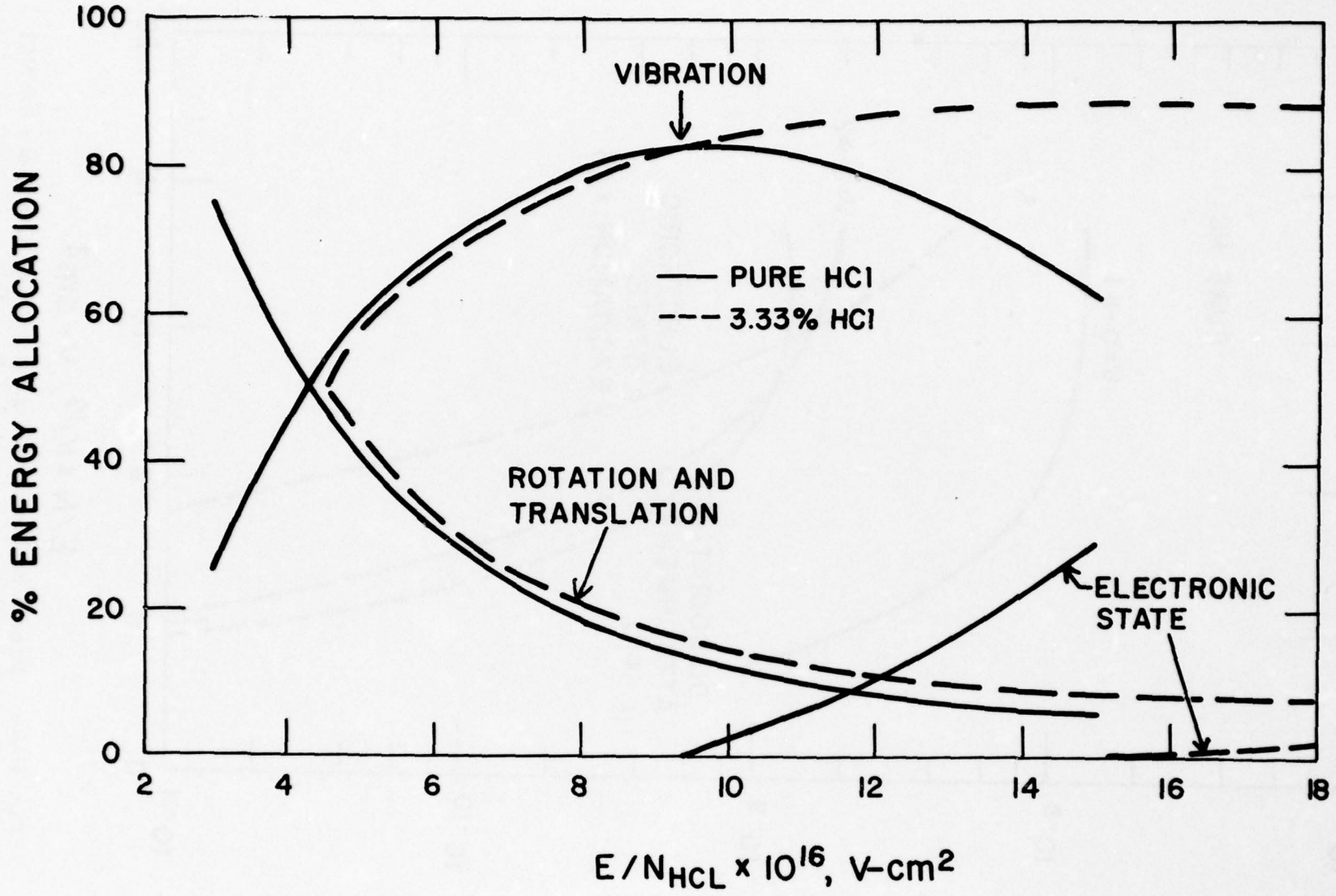

Fig. II-5 Predicted Percent Discharge Energy Deposition into Various Internal Modes of HCl in Pure HCl and a 3.33% HCl/96.67% Ar Mixture.

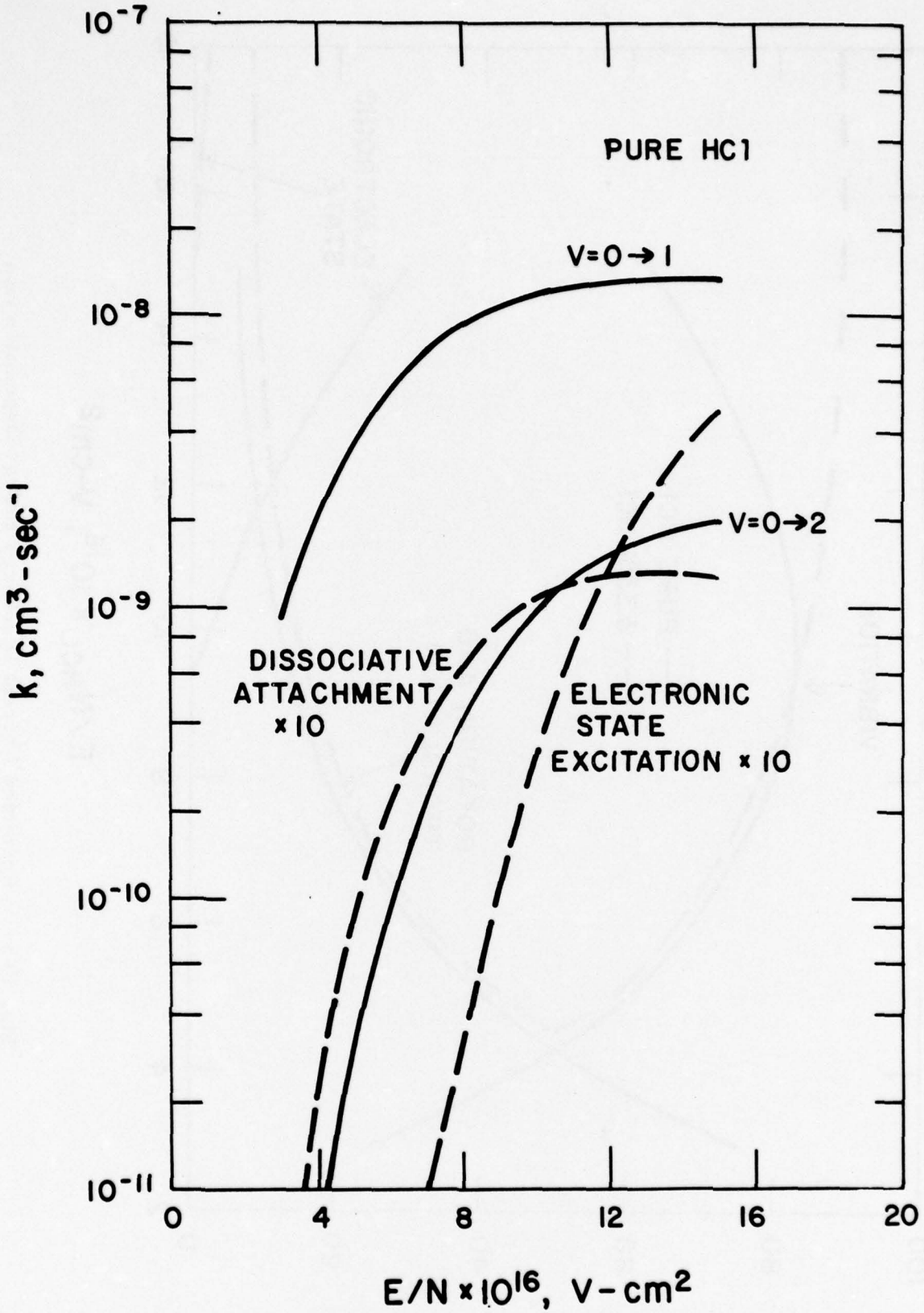

Fig. II-6 Predicted Electron Excitation Rate Constants for HCl as a Function of E/N for Pure HCl.

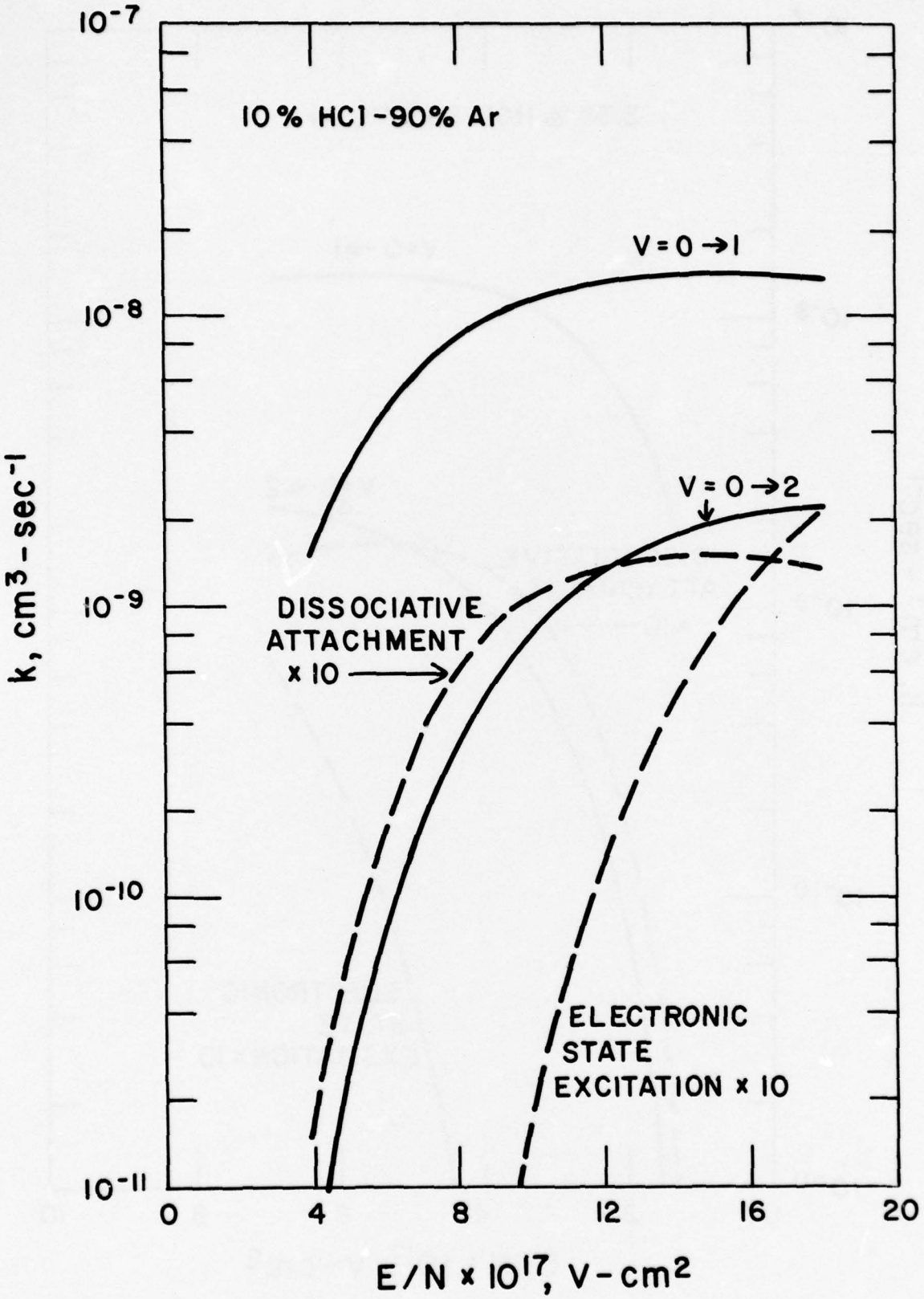

Fig. II-7 Predicted Electron Excitation Rate Constants for HCl in a 10% HCl/90% Ar Mixture.

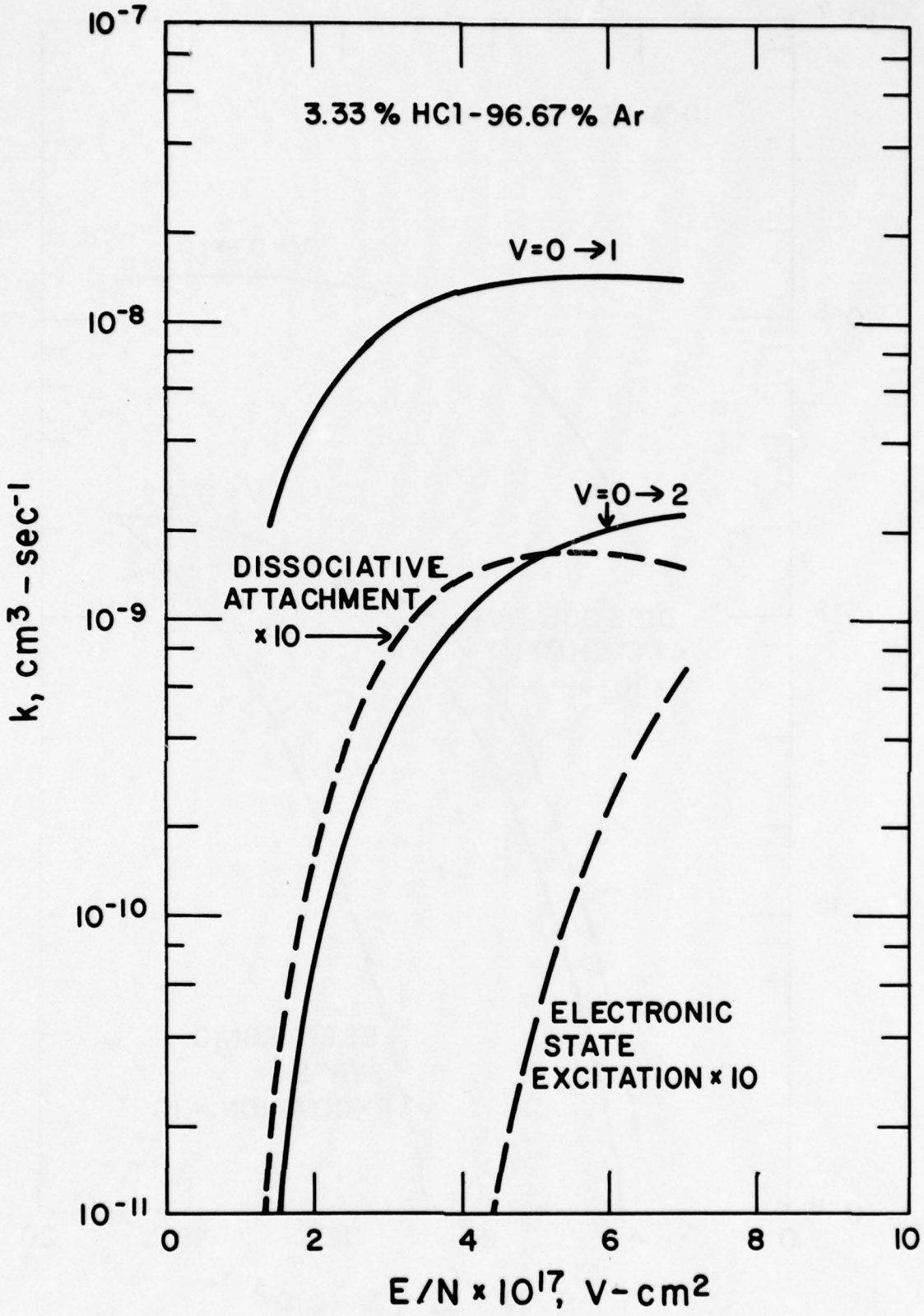

Fig. II-8 Predicted Electron Excitation Rate Constants for HCl in a 3.33% HCl/96.67% Ar Mixture.

C. LASER PERFORMANCE STUDIES

1. Gain Predictions

The results of the previous section have been coupled with a vibrational kinetics code in order to provide gain predictions for generic experimental conditions studied in the NRL program. The vibrational kinetics package employed, discussed in Section I.C.1 of this report, included all vibration-vibration and vibration-translation reactions of importance in HCl/Ar mixtures. The calculations were performed under the assumption of a uniform medium having an active length of 100 cm. Rotational equilibration with translation was assumed to be instantaneous, so that the energy supplied to the gas by electron impact rotational excitation was equi-partitioned between the translational and rotational degrees of freedom.

A specific case considered corresponded to a mixture of 10% HCl/90% Ar at a pressure of one atmosphere and initial temperature of 300°K. An E/N of 1.2×10^{-16} V-cm^2 was selected, a value corresponding to a predicted high efficiency for vibrational excitation (see Fig. II-5). The sustainer current was taken to be 6 amps/cm^2, a value typical of those realized experimentally. With a predicted drift velocity of 5.5×10^6 cm/sec this sustainer current would correspond to an electron density of $\sim 7 \times 10^{12}$/cm^3. The two vibrational excitation processes included in the calculation were

$$e + HCl\ (v) \rightarrow e + HCl\ (v + 1)$$

and (II-1)

$$e + HCl\ (v) \rightarrow e + HCl\ (v + 2)$$

having rate constants of 1.3×10^{-8} and 1.3×10^{-9} cm^3/sec, respectively. The e-beam pulse was taken to have a duration of 3 μsec.

The predicted small signal gain histories for this case are shown in Fig. II-9 for the lowest vibrational levels of HCl. As can be seen, the predictions exhibit small signal gains greater than 10^{-2} cm^{-1}. The decreasing gain shortly after pulse termination is a result of vibrational-translational deactivation with a commensurate increase in translational temperature. The total predicted increase in translational temperature over 20 μsec was ~80°K.

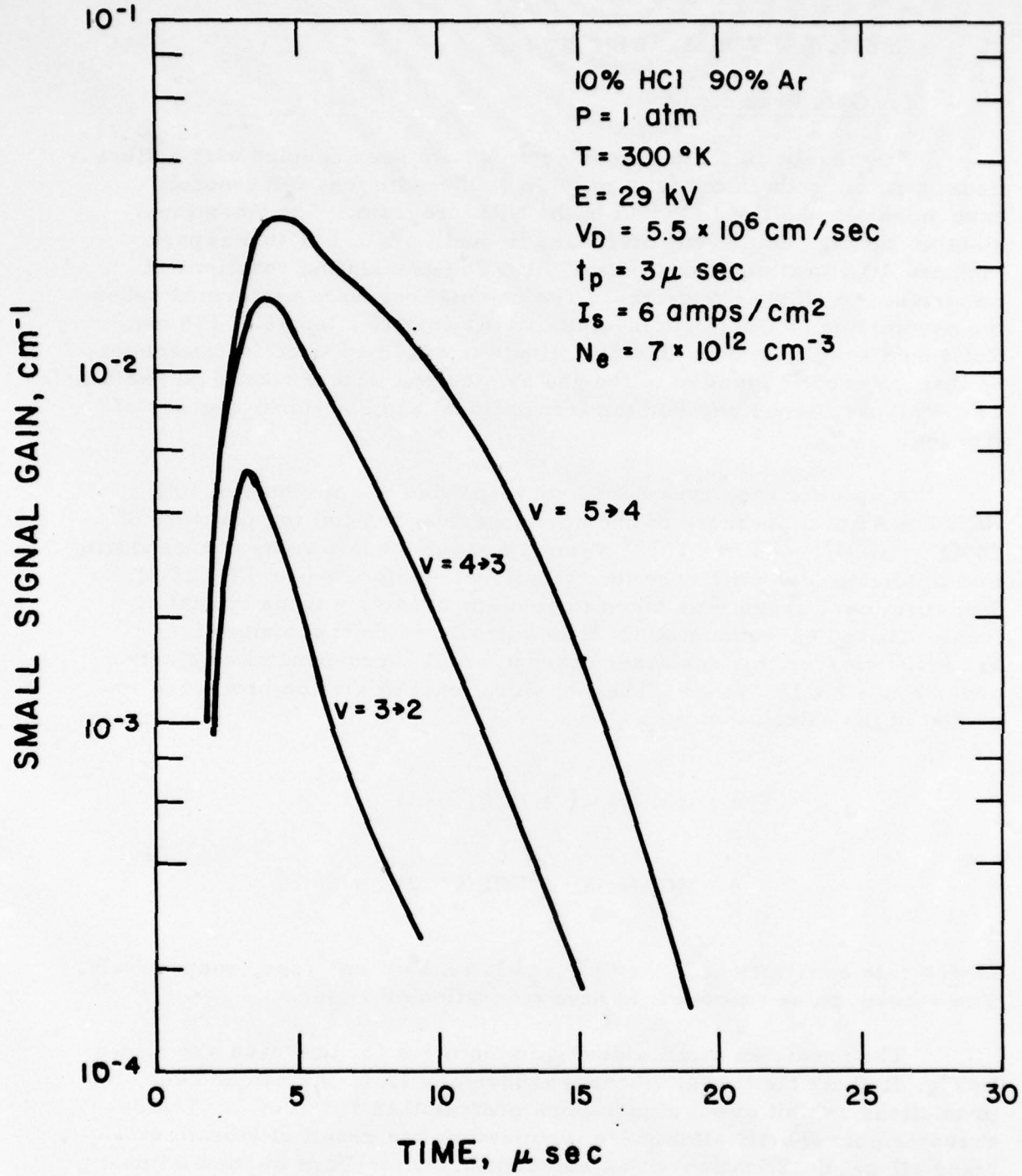

Fig. II-9 Calculation of Small Signal Gain of Several HCl Vibrational Transitions as a Function of Time After the Initiation of an E-Beam Sustainer Discharge in a 10% HCl/90% Ar Mixture. The Assumed Experimental Conditions are Listed on the Figure. No H or Cl-atoms are Assumed to be Present.

Unfortunately, such high gains were not realized experimentally. Indeed, as discussed in detail in Ref. 69, although a large range of mixture ratios, pressures and E/N's were studied, lasing was never observed to occur, suggesting that actual small signal gains were $\lesssim 10^{-3}$ cm^{-1}. This observation led to a review of the assumptions used in the modeling. One feature that had not been considered was the possible importance of atomic species, created in the discharge, which could vibrationally deactivate HCl.

Atomic species are created directly in the discharge via dissociative attachment, i.e.,

$$e + HCl \rightarrow H + Cl^- \quad . \qquad \text{(II-2)}$$

Under optimum operating conditions for vibrational excitation, the discharge is attachment dominated, and thus process (II-2) leads to the dissociation of one HCl molecule for every secondary electron created. An additional source of atomic species in the discharge is the reaction

$$Ar^+ + HCl \rightarrow ArH^+ + Cl \quad , \qquad \text{(II-3)}$$

which has recently been reported[70] to have a rate constant $\geq 1.3 \times 10^{-10}$ cm^3/sec. This reaction acts in competition to the Ar^+ clustering reaction

$$Ar^+ + 2\,Ar \rightarrow Ar_2^+ + Ar \qquad \text{(II-4)}$$

which has a rate constant[71] of $\sim 10^{-31}$ cm^6-sec^{-1}. The reaction between Ar_2^+ and HCl has not been studied, however, the branch to form ArH^+ would be close to thermoneutral and is perhaps not favorable. For a 10% HCl/90% Ar mixture at 1 atmosphere reaction (II-3) is favored over (II-4), and, thus, approximately one chlorine atom is created for every positive ion. In the instance when ArH^+ is the dominant ion, it most probably reacts with Cl^- to reform HCl, i.e.,

$$ArH^+ + Cl^- \rightarrow HCl + Ar \quad , \qquad \text{(II-5)}$$

and no additional free atom would be formed. Under conditions where Ar_2^+ is the dominant ion, it could recombine with Cl^- to form free Cl. Neither of these last two reactions have been studied.

Thus, it would appear that in the attachment dominated discharge, at least two atoms will be formed for every ion pair. For the beam operating conditions of V = 300 kV and I ≈ 6 amps/cm^2, the ion pair production rate is predicted to be ~ 3 x 10^{21}/cm^3-sec, and thus for a 3 μsec pulse ≥ 1.8 x 10^{16}, atoms will be formed. This is to be compared with an HCl concentration of 2.5 x 10^{18}/cm^3 for a 10% HCl mixture. From these two concentrations it can be seen that, if the rate constant for vibrational deactivation of HCl by atoms is > 150 times that for self deactivation, the atoms will provide the dominant vibrational loss mechanism.

The rate constants for vibrational deactivation of HCl (v = 1) by H[72] and Cl[73] have been reported to be 6.5 and 8.5 x 10^{-12} cm^3/sec, respectively, at room temperature. This is to be compared to a rate constant of 2.4 x 10^{-14} cm^3/sec for self deactivation of HCl, again at room temperature. Thus, a concentration of 1.8 x 10^{16} H and Cl atoms is sufficient to more than triple the overall HCl vibrational deactivation rate in a 1 atm mixture of 10% HCl/90% Ar. Gain predictions have been performed for the identical conditions of Fig. II-9 but with three times the HCl deactivation rate constant. The results of this calculation are shown in Fig. II-10, and it can be seen that the increased deactivation severely degrades the small signal gain to levels which would be only marginally observable in the experiment.

Thus it would seem that the presence of discharge created H and Cl atoms in the gas can inhibit laser action. There are several other possible sources of atom production which have not been considered in the above analysis. For example, in the case of the primary beam, HCl can be directly ionized, and the HCl$^+$ can later recombine dissociatively. Furthermore, direct dissociation or dissociative ionization can occur. For the secondary electrons, electronic state excitation leading to dissociation can be important at higher values of E/N as demonstrated in the discharge calculations presented earlier. Lastly, any Ar metastable states produced in the discharge could be collisionly quenched by HCl in a dissociative process. Such processes can only be conjectured at present because of the limited experimental evidence available.

2. Sustainer Current Measurements

If a high concentration of atomic species limits laser performance, one could envision either operating under conditions which minimize their importance or, alternately, introducing atomic scavengers into the gas mixture. Unfortunately, there is another aspect of the experimental measurements which is not understood at present; this has to do with the

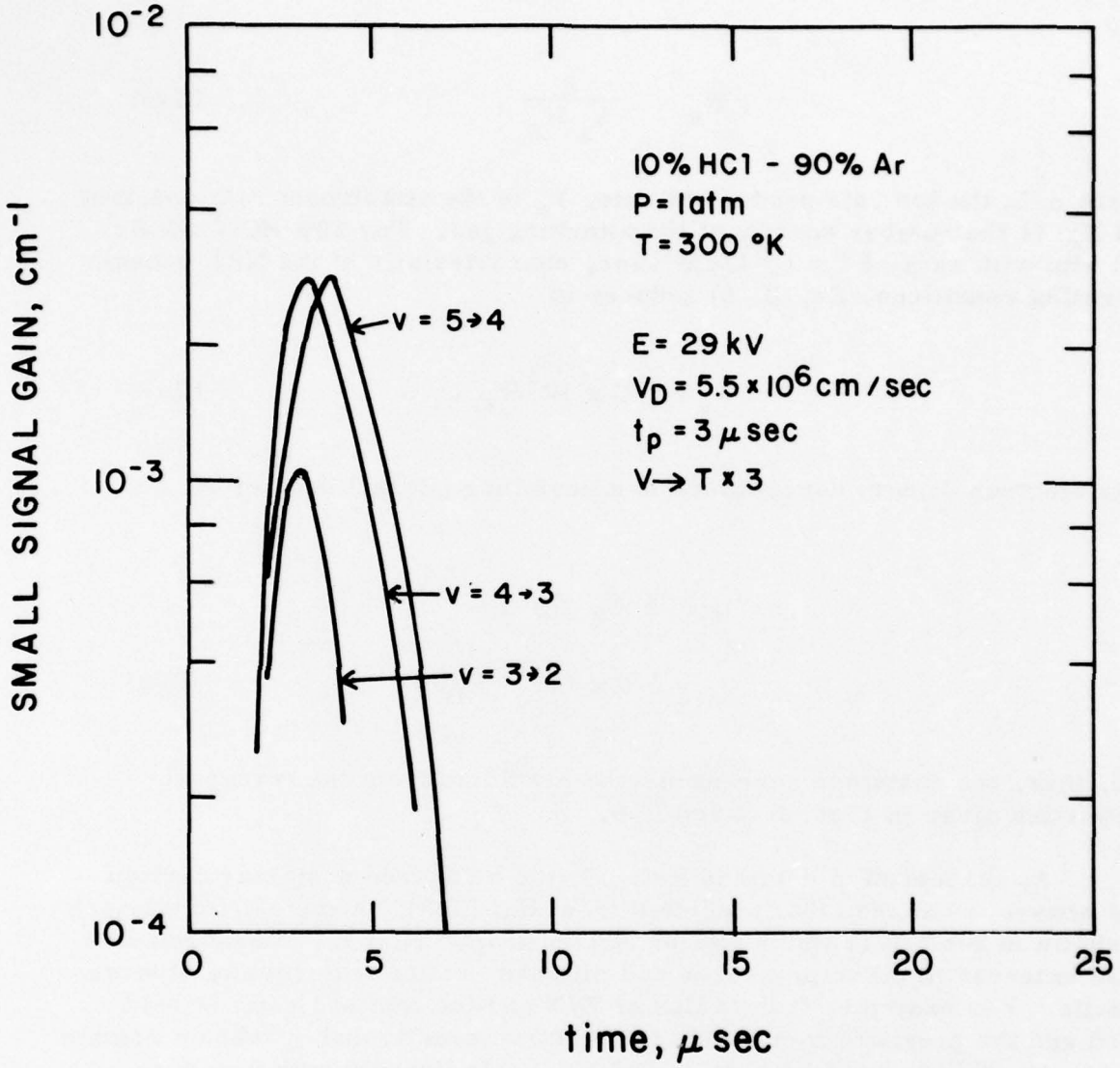

Fig. II-10 Calculation of Small Signal Gain of Several HCl Vibrational Transition as a Function of Time After the Initiation of an E-Beam Sustainer Discharge in a 10% HCl/90% Ar Mixture. The Experimental Conditions are Assumed Identical to those of Fig. II-9 Except that to Simulate the Presence of Atoms Produced in the Discharge, the HCl V→T Rate has been Multiplied by 3.

the observed sustainer currents. These currents are not only lower than theoretically predicted but also behave anomolously with varying E/N, pressure and mixture ratio. As a specific example, in an attachment dominated discharge the local electron density is specified by the relationship

$$N_e = \frac{\alpha}{k_a N_A} , \qquad \text{(II-6)}$$

where α is the ion pair production rate, k_a is the attachment rate constant and N_A is the number density of the attaching gas. For 10% HCl/90% Ar at 1 atm with an α of $3 \times 10^{21}/cm^3$-sec, characteristic of the NRL e-beam operating conditions, Eq. (II-6) reduces to

$$N_e = 1.2 \times 10^3 / k_a . \qquad \text{(II-7)}$$

This electron density corresponds to a sustainer current defined by

$$j_s = e N_e V_D$$

$$= 1.9 \times 10^{-16} V_D / k_a , \qquad \text{(II-8)}$$

and, thus, the sustainer current may be predicted from the transport properties given in Figs. II-4 and II-6.

As discussed in detail in Ref. 69, the measured sustainer current was always lower than that predicted from Eq. (II-8). A typical comparison is shown in Fig. II-11 which was excerpted from Ref. 69. Measurements were extended to other pressures and mixture ratios with equally diverse results. For example, if the value of E/N and the mixture ratio is held fixed and the pressure increased, the electron density and j_s should remain constant. This is because both α and N_A scale linearly with pressure. The experimental observation was that j_s decreased with increasing pressure.

At first it was felt that this discrepancy between theory and experiment could have been a result of additional attachment processes occuring in HCl. For example, apparent attachment effects have been observed near thermal energy in HCl although they are not properly understood

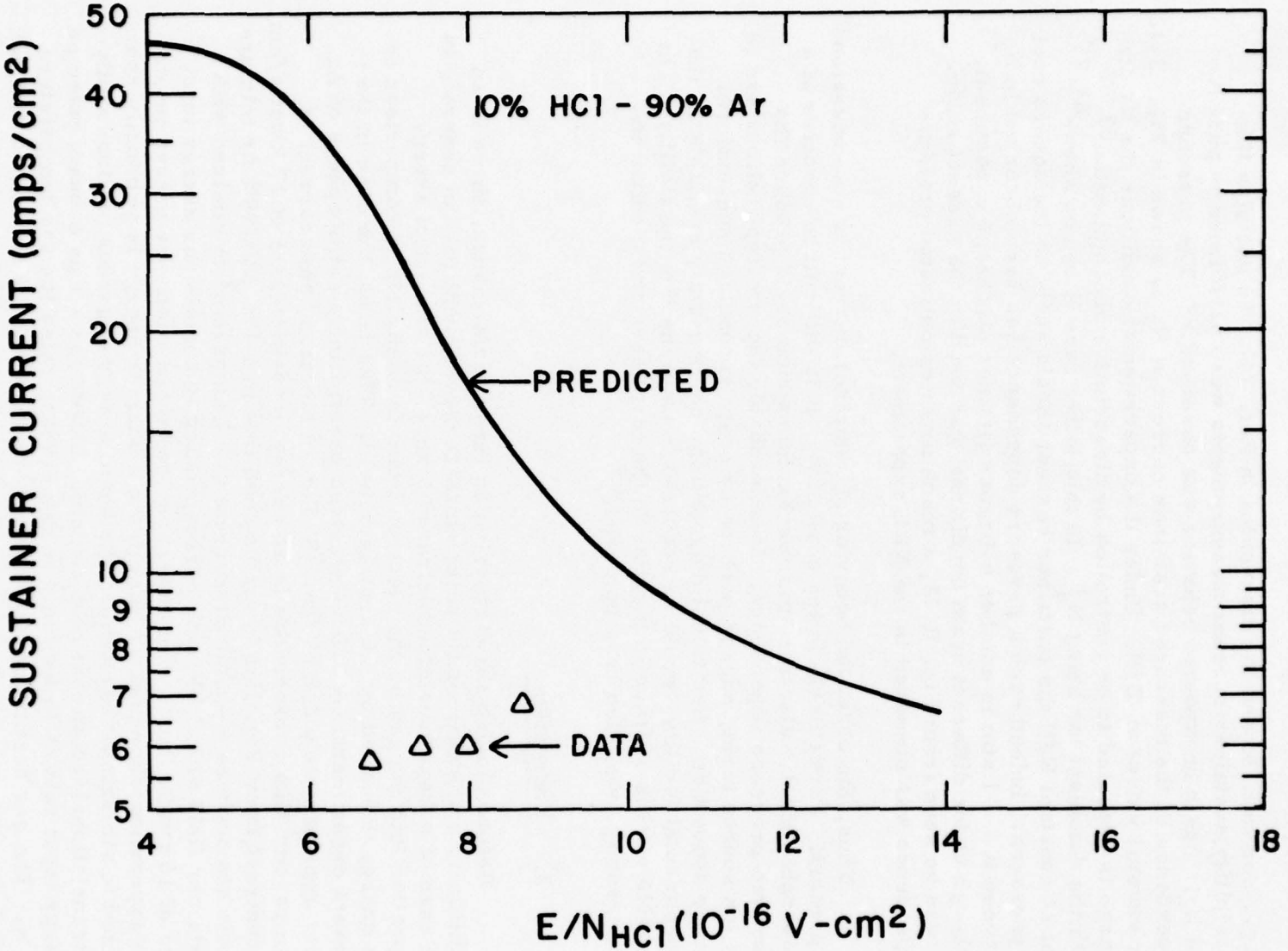

Fig. II-11 Comparison of Predicted and Observed Sustainer Current for an E-Beam Sustainer Discharge in a 10% HCl/90% Ar Mixture at a Total Pressure of 1 Atmosphere.

(e.g., see Ref. 55 and the discussion in Ref. 74). To examine this possibility, sustainer current measurements were performed in pure Ar and N_2. Again unexpected behavior was observed.[69] The pressure dependence of the measured sustainer current in N_2 is shown in Fig. II-12 for several values of E/N. Under the experimental conditions the N_2 discharge is expected to be controlled by dissociative recombination[69,75] with the dominant ion being N_4^+. In this latter case it can be shown[69,75] that at constant E/N the sustainer current should scale as the square root of pressure. Indeed such a pressure dependence has been observed in N_2 between 0.2 - 1 atm in another e-beam sustainer discharge experiment,[75] although under different beam conditions than used in the present study. As can be seen from Fig. II-12, a much more complicated pressure dependence was observed in the NRL experiment.

Thus, the observed behavior of sustainer current is not understood at present. Particularly in the case of N_2, it is difficult to conceive of a reasonable kinetic electron loss mechanism which could produce the observed pressure dependence. Most probably these complications are in the ion source term, caused perhaps by beam spread and non-uniform energy deposition. Additional diagnostics, not presently available on the experimental facility, would be required to examine this possibility. The possible effects of trace impurities in the test gases and medium inhomogeneity must also be considered.[69]

3. Energetics

Before closing the discussion on laser performance, there is an additional, somewhat subtle point which deserves mention. In general, in the case of e-beam sustained infrared lasers, the amount of energy deposited into the gas by the electron beam is negligible in comparison to the energy deposited by the sustainer field. This is not the case in the present experiment. A 300 kV electron penetrating an atmosphere of Ar loses approximately 2.8 kV/cm.[76] For an electron beam current of 6 amps/cm^2 this corresponds to an energy deposition rate of 17 kwatts/cm^3. In contrast, from Fig. II-6 it can be seen that in a 10% HCl/90% Ar mixture at one atmosphere a sustainer current of ~7 amps/cm^2 is attained with a sustainer field of 2.3 kV/cm, corresponding to a sustainer energy input rate of 16 kwatts/cm^3. For this case, beam and sustainer energy inputs are approximately equal. Although the sustainer energy is primarily converted to vibrational excitation, the beam energy degrades predominantly to translational/rotational heat content. Indeed for a 3 μs e-beam pulse an energy input rate of 16 kW/cm^3 is sufficient to raise the gas temperature 80°K. The gas heating caused by electron beam energy deposition was not included in the gain predictions presented in Section II.C.1. The effect of

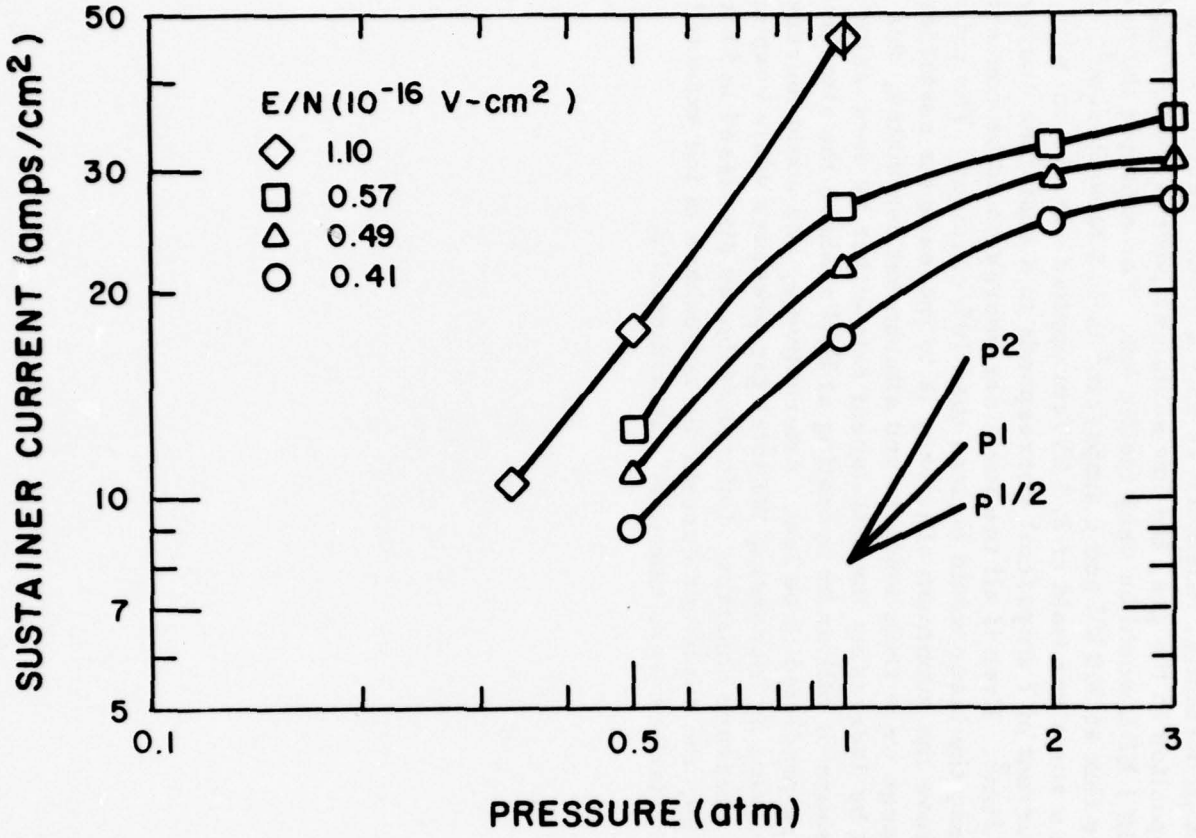

Fig. II-12 Measured Sustainer Currents as a Function of Pressure for Various Values of E/N in Pure N_2. In the lower Right-Hand-Side of the Figure are Lines Indicating the Expected Slope for Various Pressure Dependencies.

the increased gas temperature would be to decrease the small signal gain predictions below the levels shown in Fig. II-10.

More importantly, inasmuch as only a small fraction of the beam power is deposited in the gas, the low sustainer powers would suggest that at best the HCl EDL would be very inefficient. For example the total beam energy flux at 300 kV and 6 amps/cm^2 is 1.8 M watts/cm^2. In comparison a sustainer field of 2.3 kV/cm applied over 10 cm with a sustainer current of 7 amps/cm^2 corresponds to a sustainer energy flux of 0.16 MW/cm^2. Even if all the sustainer energy could be converted to laser photons, the laser would be less than 10% efficient. The primary way to improve the maximum efficiency is to increase the sustainer current. If the discharge were truly uniform and attachment dominated, this could be achieved by decreasing the attachment rate either by decreasing the partial pressure of HCl or by operating at E/N's where the attachment rate constants are predicted to be low. Alternatively, one could increase the sustainer current by increasing the total gas pressure while keeping the HCl partial pressure constant. Unfortunately, as discussed in Section II.C.2 and in Ref. 69, the sustainer current did not behave in the expected manner when such variations were examined experimentally.

D. INFRARED RADIATION STUDIES

At the beginning of the HCl EDL program attempts were made to deduce information about the discharge and vibrational kinetics by monitoring the temporal fluorescence histories of the vibrational/rotational bands of HCl. This study, which was not successful, has been described in Ref. 77 and will only be discussed briefly here.

The first measurements were made in the 3-4μ wavelength region utilizing an indium antimonide detector so positioned as to observe radiation emanating from the full 100 cm active length of the device. Initially, fundamental band fluorescence measurements were performed in discharges of 10% HCl/90% Ar. However, the gas was found to be severely optically thick under such conditions, and the measurements were not useful.

The problem of optical thickness in HCl/Ar mixtures was examined in some detail. It can be shown[78] for an isolated Lorentz broadened spectral line, that the fraction of total emitted radiation which will escape through a radiating/absorbing gas of length L is given by

$$I/I_{\text{optically thin}} = F(x)/x \,, \qquad \text{(II-9)}$$

where

$$x = S\,[HCl]\; L/\pi\,\Delta\nu_L = k_{c.l.}\; L/2 \,, \qquad \text{(II-10)}$$

S is the integrated line strength in $\text{ama}^{-1}\text{-cm}^{-2}$, [HCl] is the concentration of HCl in amagats, $\Delta\nu_L$ is the full Lorentz broadened line width at half height in cm^{-1} and $k_{c.l.}$ is the absorption coefficient at line center. The function F(x) is defined by the relationship

$$F(x) = x e^{-x}\,[J_o(ix) - i J_1(x)] \,, \qquad \text{(II-11)}$$

where the J's are Bessel functions. This expression simplifies somewhat for large values of x, where it can be shown[78] that

$$F(x) \approx (2x/\pi)^{1/2} \,, \qquad \text{(II-12)}$$

and thus that

$$I/I_{\text{optically thin}} \approx \left(\frac{2}{\pi x}\right)^{1/2} \left(\frac{4}{\pi k_{c.l.} L}\right)^{1/2} \qquad \text{(II-13)}$$

Typical values of the R and P branch v = 1→0 line strengths[79] of HCl are listed in Table II-4 along with Argon broadened line widths[80] and the evaluated centerline absorption coefficient. From Eq. (II-10) and Table II-4, it can be seen that for a mixture of 10% HCl/90% Ar at 1 atm and L = 100 cm the quantity x is quite large, and, thus, the approximate expression (II-13) may be used. The fractionally transmitted radiation for these conditions is ~0.04 for significantly populated rotational lines.

The full expression (II-9), has been evaluated as a function of the quantity [HCl] L for a centerline absorption coefficient of 89 cm^{-1}, a value corresponding to the strongest P branch transitions of HCl. The results are shown in Fig. II-13, and it can be seen that conditions corresponding to [HCl] $L < 10^{-1}$ are required to minimize the effects of self absorption. In actuality the predictions shown assume that the chlorine is all isotope 35. Actually the isotope 35 to 37 ratio is 3 to 1, and, thus, in an optically thick environment radiation from HCl^{37} will be enhanced over that from $HCl.^{35}$

Since the experimental facility could not be readily modified to provide fluorescence measurements over a shorter optical path, discharge experiments were performed in .01% - 1% HCl/Ar mixtures. The fluorescence observed in these experiments exhibited a decay rate (upon termination of the e-beam) orders of magnitude more rapid than would be expected for HCl vibrational deactivation. Additional measurements, performed with the emission screened with an HCl gas filter, confirmed that the observed radiation was a result of Ar rather than HCl fluorescence.

Additional measurements, in both pure Ar and Ar/HCl mixtures, were performed over the 3 - 4 μ region using a series of narrow bandpass filters in order to determine the spectral variation of the radiation. It was found that the radiation was strongly peaked at 3.6 and 4.0 μm, wavelengths corresponding to the position of previously observed Ar lines.[81] As a last attempt to monitor HCl fluorescence, a series of measurements were performed at wavelengths of 1.5 - 2.5μm in the region of the HCl first overtone. Again, the observed fluorescence did not exhibit behavior characteristic of HCl. A large number of Ar lines have been reported[82] to occur between 1.5 - 2.5 μm, and these are most probably the source

of the observed radiation. At this point this aspect of the experimental program was abandoned.

It is of some interest to speculate on the origin of the Argon fluorescence. The transitions observed occur between highly excited Ar states which can be excited directly by the electron beam. However, the fluorescence decay was found to occur over times as long as 5 - 10 μsec after termination of the e-beam. This is the same order time scale as for electron-ion recombination for the experimental conditions. The dominant positive ion in the pure Ar and very dilute HCl/Ar mixtures is Ar_2^+ and thus the observed fluorescence may have been a result of the dissociative recombination reaction

$$Ar_2^+ + e \rightarrow Ar^* + Ar \qquad \text{(II-14)}$$

which is known[82] to produce electronically excited Ar. A more detailed investigation would be required in order to confirm this latter possibility.

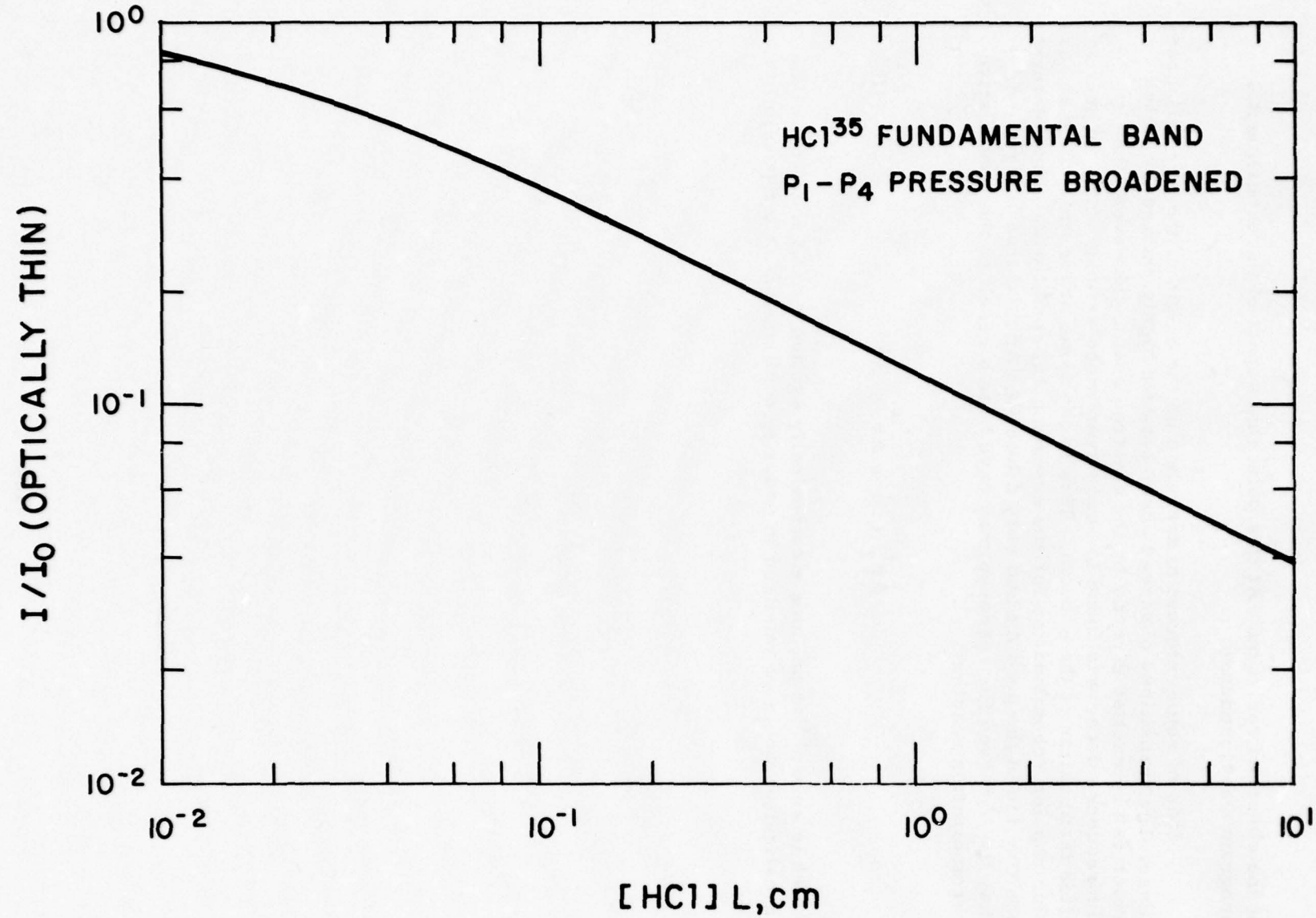

Fig. II-13 Relative Intensity of HCl^{35} Fundamental Vibration/Rotation Band for Various Values of Optical Depth. The Lines are Assumed to be Pressure Broadened.

TABLE II-4

RADIATION PARAMETERS FOR HCl^{35}

	R BRANCH			P BRANCH		
J_l	S	$\Delta\nu_L$	$k_{c.l.}/[HCl]$	S	$\Delta\nu_L$	$k_{c.l.}/[HCl]$
	$Atm^{-1}\text{-}cm^{-2}$	$Atm^{-1}\text{-}cm^{-1}$	cm^{-1}	$Atm^{-1}\text{-}cm^{-2}$	$Atm^{-1}\text{-}cm^{-1}$	cm^{-1}
0	4.9	1.3×10^{-1}	2.4×10^{1}			
1	8.8	8.3×10^{-2}	6.7×10^{1}	4.7	1.3×10^{-1}	2.3×10^{1}
2	10.6	6.9×10^{-2}	9.9×10^{1}	7.8	8.3×10^{-2}	6×10^{1}
3	10.3	5.7×10^{-2}	1.12×10^{2}	8.8	6.9×10^{-2}	8.1×10^{1}
4	8.5	4.8×10^{-2}	1.13×10^{2}	8.0	5.7×10^{-2}	8.9×10^{1}
5	6.	4.0×10^{-2}	9.5×10^{1}	6.2	4.8×10^{-2}	8.2×10^{1}
6	3.7	3.5×10^{-2}	6.7×10^{1}	4.2	4.0×10^{-2}	6.7×10^{1}
7	2.1	2.9×10^{-2}	4.6×10^{1}	2.4	3.5×10^{-2}	4.3×10^{1}
8	1.0	2.5×10^{-2}	2.5×10^{1}	1.3	2.9×10^{-2}	2.8×10^{1}
9	0.5	2×10^{-2}	1.6×10^{1}	0.6	2.5×10^{-2}	1.5×10^{1}

S = Line Strength at $300^{o}K$ for HCl^{35}

$\Delta\nu$ = Full Lorentz width at half height for Ar broadening

$k_{c.l.}/[HCl]$ = Centerline absorption coefficient for Ar broadening; normalized by the HCl mole fraction

E. SUMMARY AND CONCLUSIONS

In summary, the HCl EDL modeling described above has produced several salient but contradictory facts regarding possible system performance. In particular the HCl/Ar discharge predictions suggest that some 80 - 90% of the discharge energy may be channeled into vibrational excitation of the HCl. Unfortunately, however, the subsequent kinetic analysis has demonstrated that atomic species produced in the discharge, primarily by dissociative electron attachment, can severely degrade laser performance through vibration-translation de-activation of the HCl. Since dissociative attachment and vibrational excitation of HCl occur in approximately the same electron energy range, the production of atomic species in the discharge cannot be completely eliminated; however, it can be minimized. A modern study of the transport properties and attachment phenomena occuring in HCl electron swarms would be very useful in determining optimum discharge conditions for laser performance. The use of chemical additives as scavengers for atomic species should also be considered.

An additional feature peculiar to the atmospheric HCl EDL is the projected low efficiency of the device. As discussed in the main text, the unexpected variation of sustainer current as a function of pressure and mixture ratio precluded any specification of the operational parameters required for optimum conversion of electrical energy to vibration. It is possible that the sustainer current observations were device specific. Similar studies performed on a small, low current device, which would allow both absorption free fluorescence measurements and local current density determinations, would be invaluable in specifying the true potential of an HCl EDL.

REFERENCES

1. Carleton, N. P. and Megill, L. R., Phys. Rev. 126, 2089 (1962).

2. Lenander, C. J., "Predictions of Microwave Breakdown in Air from Kinetic Theory Calculations", Aerospace Rpt. TR-0158 (3240-20)-17, June 1968.

3. Englehardt, A. G. and Phelps, A. V., Phys. Rev. 131, 2115 (1963).

4. Kieffer, L. J., "A Compilation of Electron Collision Cross Section Data for Modeling Gas Discharge Lasers", JILA Information Center Report 13, September 30, 1973.

5. Schulz, G. J., Phys. Rev. 135A, 983 (1964).

6. Linder, F. and Schmidt, H. Z., Naturforsch 26A , 1603 (1971).

7. Ramien, H., Z. Physik 70, 353 (1931).

8. Crompton, R. W., Gibson, D. K. and McIntosh, A. I., Australian J. Phys. 22, 715 (1969).

9. Trajmar, S., Truhlar, D. G., Rice, J. K. and Kuppermann, A., J. Chem. Phys. 52, 222 (1968).

10. Ehrhardt, H., Langhans, L., Linder, F. and Taylor, H. S., Phys. Rev. 173, 222 (1968).

11. Gibson, D. K., Australian J. Phys. 23, 683 (1970).

12. Corrigan, S. J. B., J. Chem. Phys. 43, 4381 (1965).

13. Huxley, L. G. H. and Crompton, R. W., "The Diffusion and Drift of Electrons in Gases", John Wiley and Sons, New York, (1974).

14. Frost, L. S. and Phelps, A. V., Phys. Rev. 136A, 1538 (1964).

15. Englehardt, A. G. and Phelps, A. V., Phys. Rev. 133A, 375 (1964).

16. Crompton, R. W., Elford, M. T. and Robertson, A. G., Australian J. Phys. 23, 666 (1976).

17. Kiefer, J. H. and Lutz, R. W., J. Chem. Phys. 44, 658 (1966).

18. Bird, P. F. and Breshears, W. D., Chem. Phys. Lett. 13, 529 (1972).

19. Hopkins, B. M. and Chen, H-L., J. Chem. Phys. 57, 3161 (1972).

20. Kovacs, M. A. and Mach, M. E., Appl. Phys. Lett. 20, 487 (1972).

21. Lukasik, J. and Ducuing, J., J. Chem. Phys. 60, 331 (1974).

22. Lukasik, J. and Ducuing, J., Chem. Phys. Lett. 27, 203 (1974).

23. Breshears, D. and Bird, P. F., J. Chem. Phys. 50, 333 (1969); J. Chem. Phys. 52, 999 (1970).

24. Hopkins, B. M., Chen, H-L., and Sharma, R., J. Chem. Phys. 59, 5758 (1973).

25. Zittel, P. F. and Moore, C. B., J. Chem. Phys. 59, 6636 (1973).

26. Landau, L. and Teller, E., Physik Z. Sowjetunian 10, 34 (1936).

27. Schwartz, R. N., Slawsky, Z. I. and Herzfeld, K., J. Chem. Phys. 20, 1591 (1952).

28. Sharma, R. D. and Brau, C. A., Phys. Rev. Lett. 19, 1273 (1967); J. Chem. Phys., 50, 924 (1969).

29. Hopkins, B. M. and Chen, H-L., "Vibrational Excitation and Relaxation of HCl (v=2) State", J. Chem. Phys. 57, 3817 (1972).

30. Noter, Y., Burak, I., and Szoke, A., "Temperature Dependence of Vibration-to-Vibration Energy Transfer in HCl and HBr", J. Chem. Phys. 59, 970 (1973).

31. Leone, S. R. and Moore, C. B., "V-V Energy Transfer in HCl with Tunable Optical Parametric Oscillator Excitation", Chem. Phys. Lett. 19, 340 (1973).

32. Rosen, D. I., Coughlin, J. and Taylor, R. L., "Investigations of H_2/HCl Advanced Gas Dynamic Laser", Contract DAAH01-76-C-0350, to be published.

33. Bott, J. F. and Cohen, N., J. Chem. Phys. 63, 1518 (1975).

34. Sato, H., "Experimental Investigation on the Transition of Laminar Separated Layer", J. of the Physical Society of Japan, 11, No. 6, pp. 702-709 (1956).

35. Lewis, P., unpublished results.

36. Prandtl, L., "Notes on the Theory of Free Turbulence", Z. Angew. Math. Mech., Bd. 22, No. 5, pp. 241 - 243 (1942).

37. Shapiro, A. H., Compressible Fluid Flow, The Ronald Press Co., New Yor, Vol. I (1953).

38. "NRML Laser, Phase I", Final Technical Report, ARC No. 47-5629, Contract No. DAAH01-74-C-0611, Atlantic Research Corporation, Alexandria, VA. 22314, February 1975.

39. "Advanced H_2-HCl Gas Dynamic Laser, Phase II", Final Technical Report, ARC No. 47-5655, Contract DAAH01-75-C-0789, Atlantic Research Corporation, Alexandria, VA. 22314, January 1976.

40. Teare, J. D., Taylor, R. L. and von Rosenberg, C. W., Jr., Nature 225, 240 (1970).

41. Taran, J. P. E., Charpenel, M. and Borghi, R., "Investigation of a Mixing CO_2 GDL", AIAA Paper, No. 73-622 (1973).

42. Schlichting, H., "Über das ebene Windschattenproblem", Ing.-Arch., Bd. 1, p. 567 (1930).

43. Clauser, F. H., The Turbulent Boundary Layer, Vol. IV of Advances in Applied Mechanics, H. L. Dryden and Th. von Kármán, eds., Academic Press Inc., pp. 1-51 (1956).

44. Schetz, J. A., "Free Turbulent Mixing in a Coflowing Stream", NASA SP-321, Free Turbulent Shear Flow Conf. Vol. I, pp. 259-275 (1972).

45. Chevray, R. and Kovasznay, L. S., "Turbulence Measurement in the Wake of a Thin Flat Plate", AIAA J. Vol. 7, No. 8, p. 1461 (1969).

46. McCarthy, J. F., Jr. and Kubota, T., "A Study of Wakes Behind a Circular Cylinder at M = 5.7", AIAA J. Vol. 2, No. 4, pp. 629-636 (1964).

47. Behrens, W., "The Far Wake Behind Cylinders at Hypersonic Speeds: Part I: Flowfield", AIAA J. Vol. 5, No. 12, pp. 2135-2141 (1967).

48. Demetriades, A., "Turbulent Mean-Flow Measurements in a Two-Dimensional Supersonic Wake", The Phy. of Fluids, Vol. 12, No. 1, pp. 24-32 (1969).

49. Hirschfelder, J. O., Curtiss, C. F. and Bird, R. B., Molecular Theory of Gases and Liquids, Wiley, New York (1954).

50. Frost, L. S. and Phelps, A. V., Phys. Rev. 129, 1621 (1962).

51. Bailey, V. A. and Duncanson, W.E., Phil. Mag., 10, 145 (1930).

52. Healey, R. H. and Reed, J. W., "The Behaviour of Slow Electrons in Gases", Amalgamated Wireless, Ltd., Sydney, 1941.

53. Gilardini, A., "Low Energy Electron Collisions in Gases", Ch. 3, John Wiley and Sons, New York, 1972.

54. Shirley, J. A., Bronfin, B.R., Nighan, W. L. and Churchill, T. L., "E-Beam HCl Laser - Semi-Annual Technical Report - No. 1", United Technologies Research Center Report L911340-3, November 1972.

55. Christophorou, L. G., Compton, R. N. and Dickson, H. W., J. Chem. Phys. 48, 1944 (1968).

56. Itikawa, W. and Takayanagi, K., J. Phys. Soc. of Japan 26, 1254 (1969).

57. Compton, R. N., Huebner, R. H., Reinhardt, P. W. and Christophorou, L. G., J. Chem. Phys. 48, 901 (1968).

58. Rohr, K. and Linder, F., J. Phys. B.: Atom. Molec. Phys. 8, L200 (1975).

59. Rohr, K., Private communication, July 1975.

60. Ziesel, J. P., Nenner, I. and Schulz, G. J., J. Chem. Phys. 63, 1943 (1975).

61. Schulz, G. J., Private communication, June 1975.

62. Center, R. E. and Chen, J. Chem. Phys. 61, 3785 (1974).

63. Mayan, J. T., Yos, J. M. and Fante, R. L., "Re-entry Antenna Test Program Final Report. Appendix 1, Antenna Breakdown Model", Avco Government Products Group, Systems Division, Report AVSD-0060-74-RR, April 1974.

64. Brüche, E., Ann. Phys. (Leipzig) 82, 25 (1927).

65. Buchel'nikova, I. S., Sov. Phys. JETP 35, 783 (1959).

66. Azria, R., Roussier, L. Paineau, R. and Trone, M., Rev. Phys. Appl. 9, 469 (1974).

67. Burrow, P. D., J. Phys. B.: Atom. Molec. Phys. 7, L385 (1974).

68. Compton, K. T. and Van Voorhs, C. C., Phys. Rev. 26, 436 (1925).

69. Hart, G. et al, "E-Beam Sustainer Pumped HCl Laser", DARPA-NRL Laser Program Semiannual Technical Report, to be published, 1976.

70. Lias, S. G., unpublished results.

71. Good, A., Chem. Rev. 75, 561 (1975).

72. Arnoldi, D. and Wolfrum, J., Chem. Phys. Lett. 24, 234 (1974).

73. MacDonald, R. G., Moore, C. B., Smith, I. W. M. and Wodarczyk, F. J., J. Chem. Phys. 62, 2934 (1975).

74. Caledonia, C. E., Chem. Rev. 75, 333 (1975).

75. Douglas-Hamilton, D. H., J. Chem. Phys. 58, 4820 (1973).

76. Berger, M. J. and Seltzer, S. M., "Tables of Energy Losses and Ranges of Electrons and Positrons", NASA SP-3012, 1964.

77. DARPA-NRL Laser Program Semiannual Technical Report, 1 January 1975 - 30 June 1975, NRL Memorandum Report 3217, February 1976, pp. 21-35.

78. Penner, S. S., "Quantitative Molecular Spectroscopy and Gas Emissivities", Addison-Wesley, Reading, MA. 1959.

79. Toth, R. A., Hunt, R. H. and Plyler, E. K., J. Molec. Spectrosc. 35, 110 (1970).

80. Babrov, H., Ameer, G. and Benesch, W., J. Chem. Phys. 33, 145 (1960).

81. Taylor, R. L. and Caledonia, G. E., JQSRT 9, 657 (1969).

82. Wiese, W. L., Smith, M. W. and Miles, B. M., "Atomic Transition Probabilities, Vol. II Sodium Through Calcium", NSRDS-NBS 22, U. S. Government Printing Office, 1969.

83. Frommhold, L. and Biondi, M. A., Phys. Rev. 185, 244 (1969).

APPENDIX A

Electron Impact Rotational Excitation of H_2/D_2

Homonuclear molecules having non-zero nuclear spin may have both even and odd rotational levels corresponding to either symmetric or antisymmetric alignments of nuclear spin respectively, depending on the ground electronic state configuration of the molecule. Since transitions between symmetric and anti-symmetric alignments are strongly forbidden, the total concentration of odd and of even states remains constant independent of temperature and is dependent only upon the alignment degeneracies, i.e. statistical weights. The state, i.e., odd or even, which has the higher statistical weight is termed the ortho modification, while the state with lower weight is termed the para modification.

In the case of H_2, which has nuclear spin 1/2, the statistical weight of odd states is 3 and that of even states is 1. Thus, at all temperatures 75% of the H_2 molecules will be in odd rotational levels and 25% in even. The situation is reversed in D_2, which has nuclear spin 1. For this latter situation, even states have statistical weight 6 and odd states 3. Thus 66.7% of the D_2 molecules will be in even rotational levels and 33.3% in odd. The resulting predicted rotational populations of the lower levels of H_2 and D_2 are shown vs temperature in Figs. A-1 and A-2. The rotational constants used for these calculations were taken from Herzberg.[1] As can be seen, at low temperatures, ~ 100°K, only the J = 0 and 1 states have significant populations, although some 18% of the D_2 molecules are in the J = 2 state. However, higher rotational levels begin to play a more important role with increasing temperature. Indeed, by 300°K 4 or 5 rotational levels have populations $\geq$ 10%. As can be seen from Fig. A-2, the temperature variation is particularly pronounced in the case of D_2; at a temperature of 300°K J = 2 is the most populated state and the populations of J = 3 and 4 are within a factor of two of those for J = 0 and 1.

Based on these significant population variations it might be expected that the amount of discharge energy absorbed by rotation and also the transport properties of H_2/D_2 discharges would vary with temperature, since each rotational state has a different onset energy and excitation cross section. Crompton[2] et al, performed a careful study of the transport properties of normal and parahydrogen at 77°K and normal hydrogen at

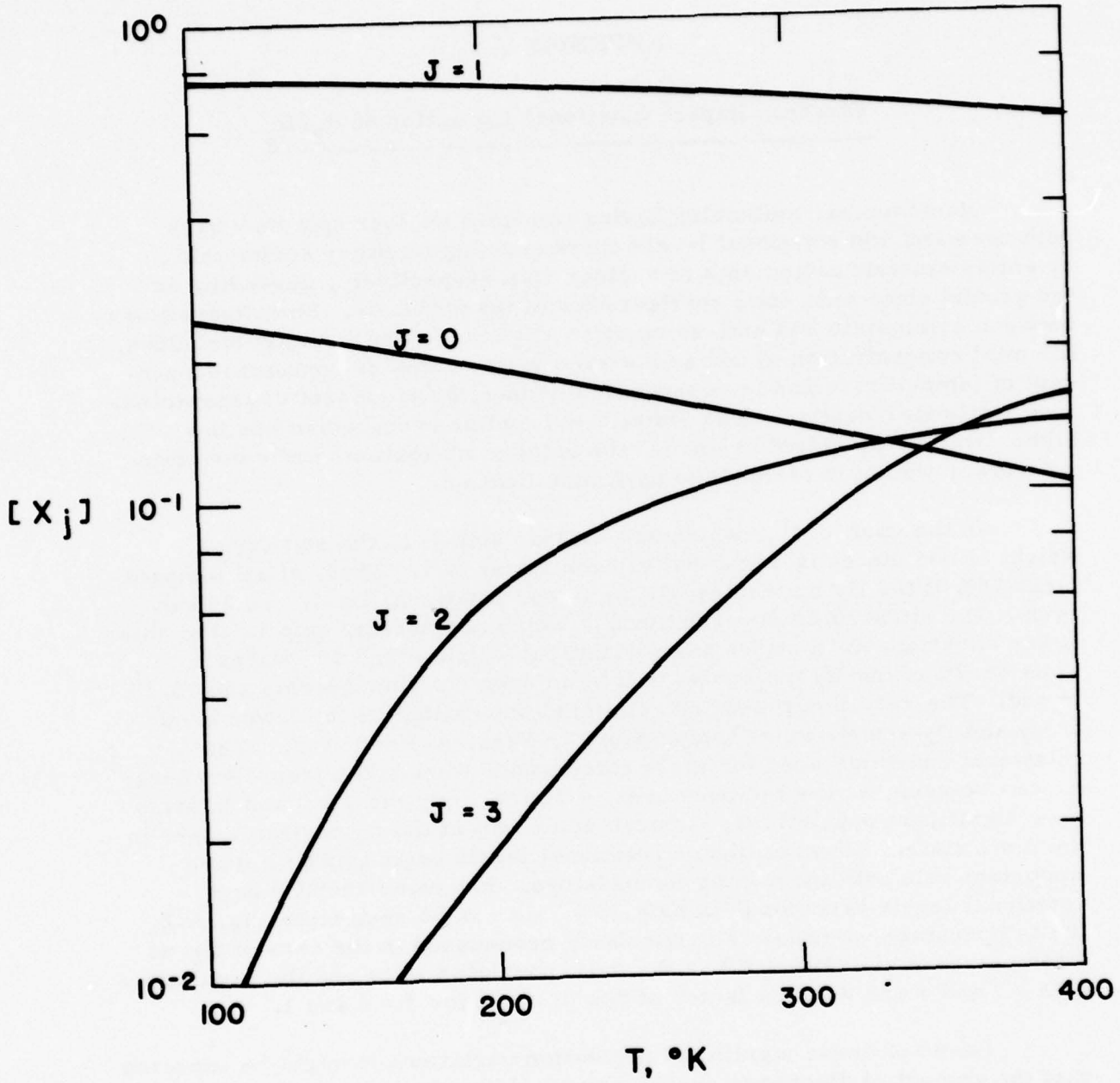

Fig. A-1 Relative Rotational Populations for H_2 as a Function of Temperature.

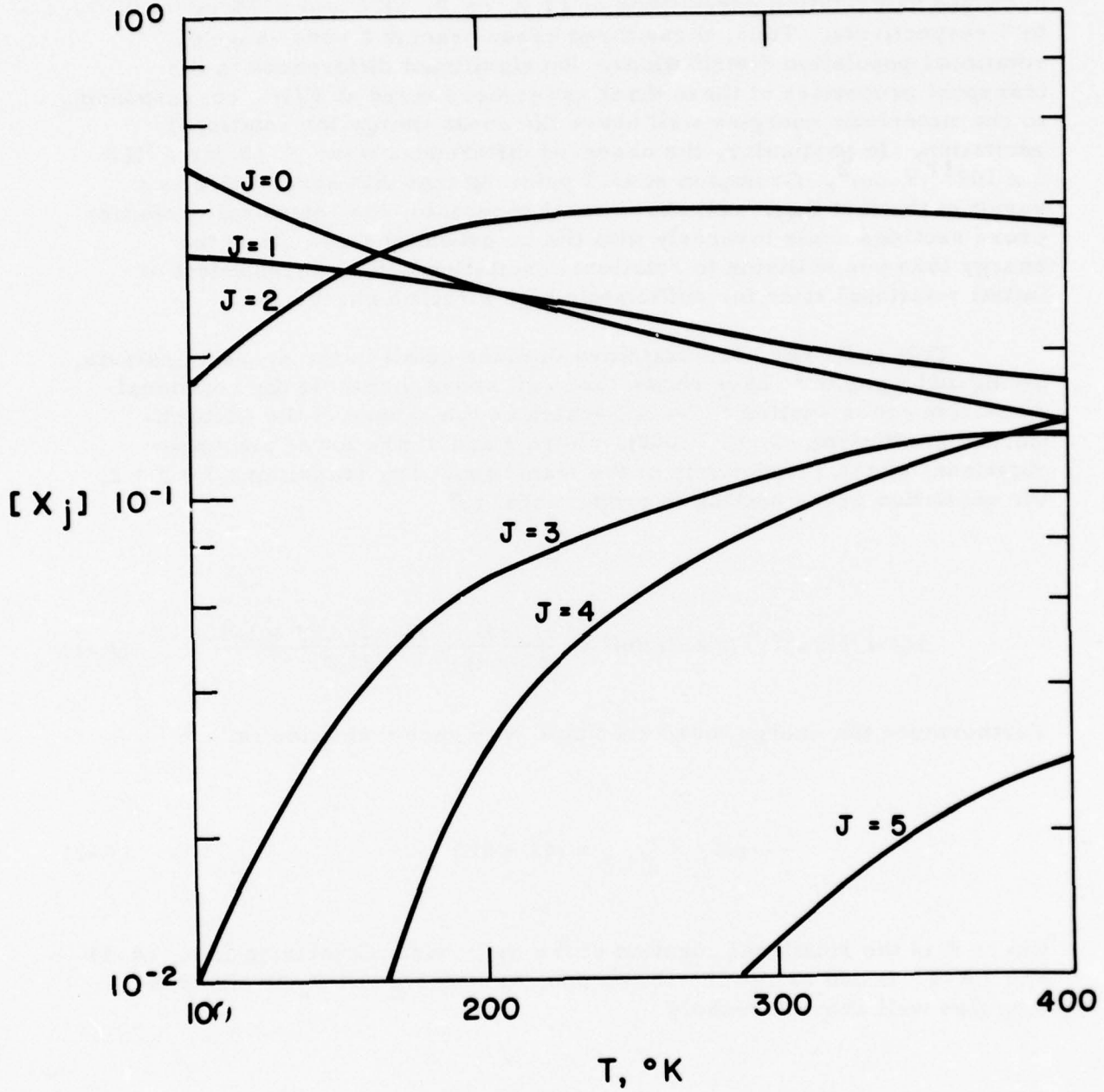

Fig. A-2 Relative Rotational Populations for D_2 as a Function of Temperature.

300°K. At 77°K parahydrogen is almost completely in the J = 0 state, whereas normal hydrogen is populated 75% in J = 1. At 300°K, normal hydrogen has rotation populations of 13.2, 66.2, 11.6 and 8.7% in J = 0 to 3 respectively. Thus, these three cases bracket a wide range of rotational population distributions. No significant differences in the transport properties of these three cases were noted at E/N's corresponding to characteristic energies well above the onset energy for rotational excitation. In particular, the observed differences were $\lesssim$ 1% for E/N $\gtrsim$ 5×10^{-17} V-cm^2. Crompton et al,[2] point out that this observation is a result of the fact that, well above onset threshold, the rotational excitation cross sections scale inversely with the threshold energy. Thus the energy loss per collision to rotational excitation will be independent of initial rotational state for sufficiently high electron energies.

This point has been examined in more detail in the present analysis. Chang and Temkin[3] have shown that well above threshold the rotational excitation cross section $\sigma(J \rightarrow J')$ scales as the square of the Clebsch-Gordon coefficient, $C(J2J':000)$, where J and J' are lower and upper rotational states, respectively, of the transition. For transitions $J \rightarrow J + 2$, the excitation cross section is proportional to[4]

$$\sigma(J \rightarrow J') \propto C^2(J2J':000) = \frac{3!\,(2J)!}{(2J+4)!}\,\frac{(J+2)!\,(J+2)!}{J!\,J!} \qquad \text{(A-1)}$$

Furthermore the energy loss associated with each transition is

$$\Delta E_{J \rightarrow J+2} = (4J + 6)B \ , \qquad \text{(A-2)}$$

where B is the rotational constant of the molecule. Combining Eqs. (A-1) and (A-2) it can be readily shown that for both H_2 and D_2 at electron energies well above threshold

$$\frac{\sigma(J \rightarrow J+2)\,\Delta E_{J \rightarrow J+2}}{\sigma(0 \rightarrow 2)\,\Delta E_{0 \rightarrow 2}} = \frac{(J+1)(J+2)}{2(2J+1)} \qquad \text{(A-3)}$$

Expression (A-3) can be readily shown to have the values 1.0, 1.0, 1.2, 1.43 and 1.67 for J = 0 - 4 respectively.

The conclusion is that, at temperatures where only the J = 0 and 1 populations are significantly populated, the degree of rotational excitation will be independent of the relative populations of the J = 0 and 1 states for discharge parameters corresponding to characteristic energies well above threshold. This observation was borne out by detailed discharge predictions as discussed in the main text. This behavior may not hold true when states with $J \geq 2$ are significantly populated, as in the case of D_2 at T = 300°K. In this limit however, the effect of collisions of the second kind, i.e. $J \rightarrow J - 2$, must also be considered.

At present, one must rely on theory for the specification of the rotational excitation cross sections for $J \geq 2$. For purposes of completeness a set of quasi-analytical cross sections have been developed for use in specifying the rotational excitation of states J = 0 - 3 in H_2 and J = 0 - 4 in D_2. These results are shown in Figs. A-3 and 4. The solid portions of the cross sections shown are as determined from the theoretical predictions of Lane and Geltman[5] and Henry and Lane.[6, 7] The dashed portions represent empirical extrapolations of this theoretical work which were developed in the present analysis. If it were desired to examine the effect of rotational temperature on rotational excitation in more detail, such cross sections, modified slightly to improve the agreement between theory and experiment, could be used in conjunction with the Boltzmann computer code. Such an effort was not warranted under the present program.

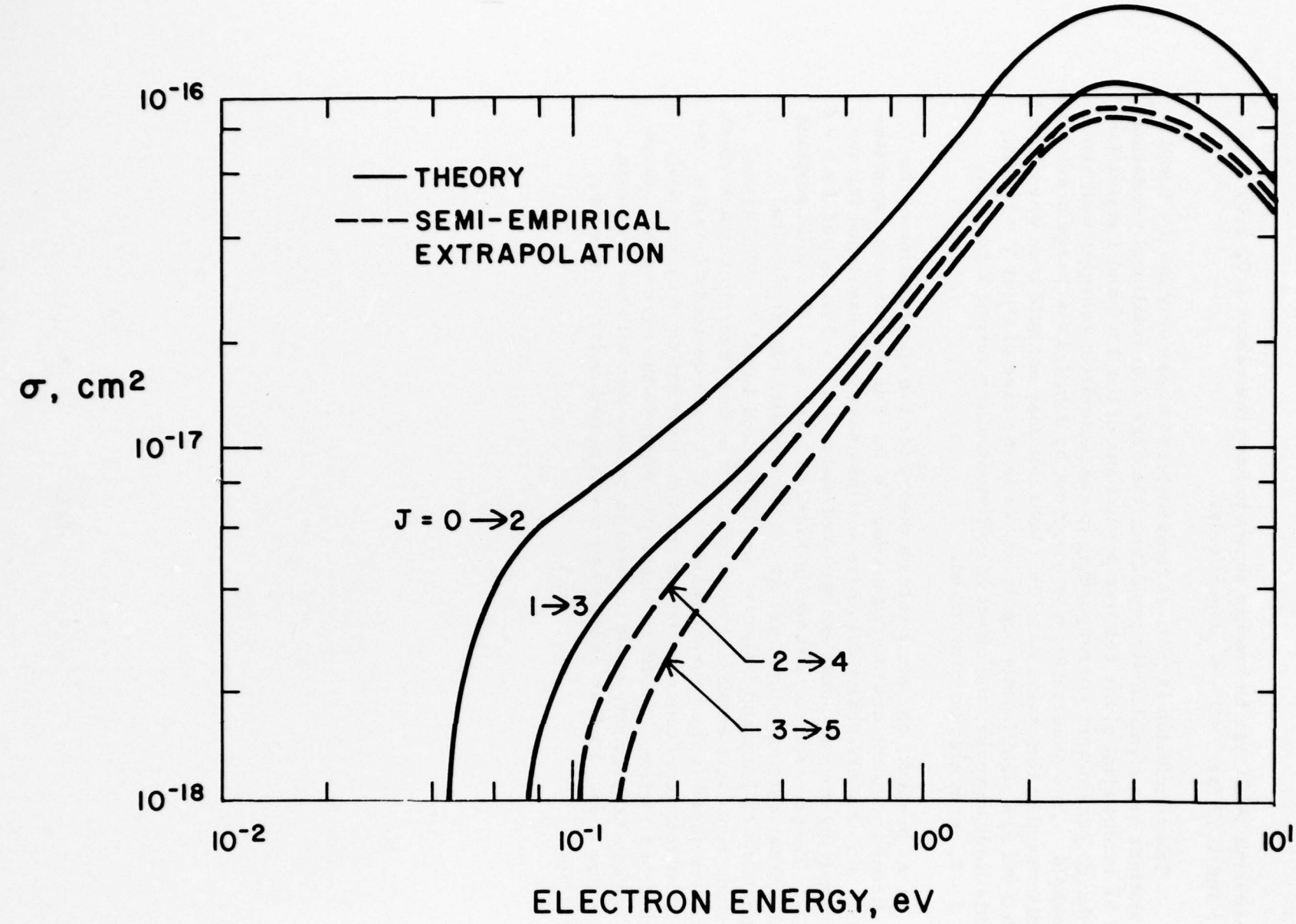

Fig. A-3 Electron Excitation Cross Sections for Rotational Transitions of H_2 as a Function of Electron Energy.

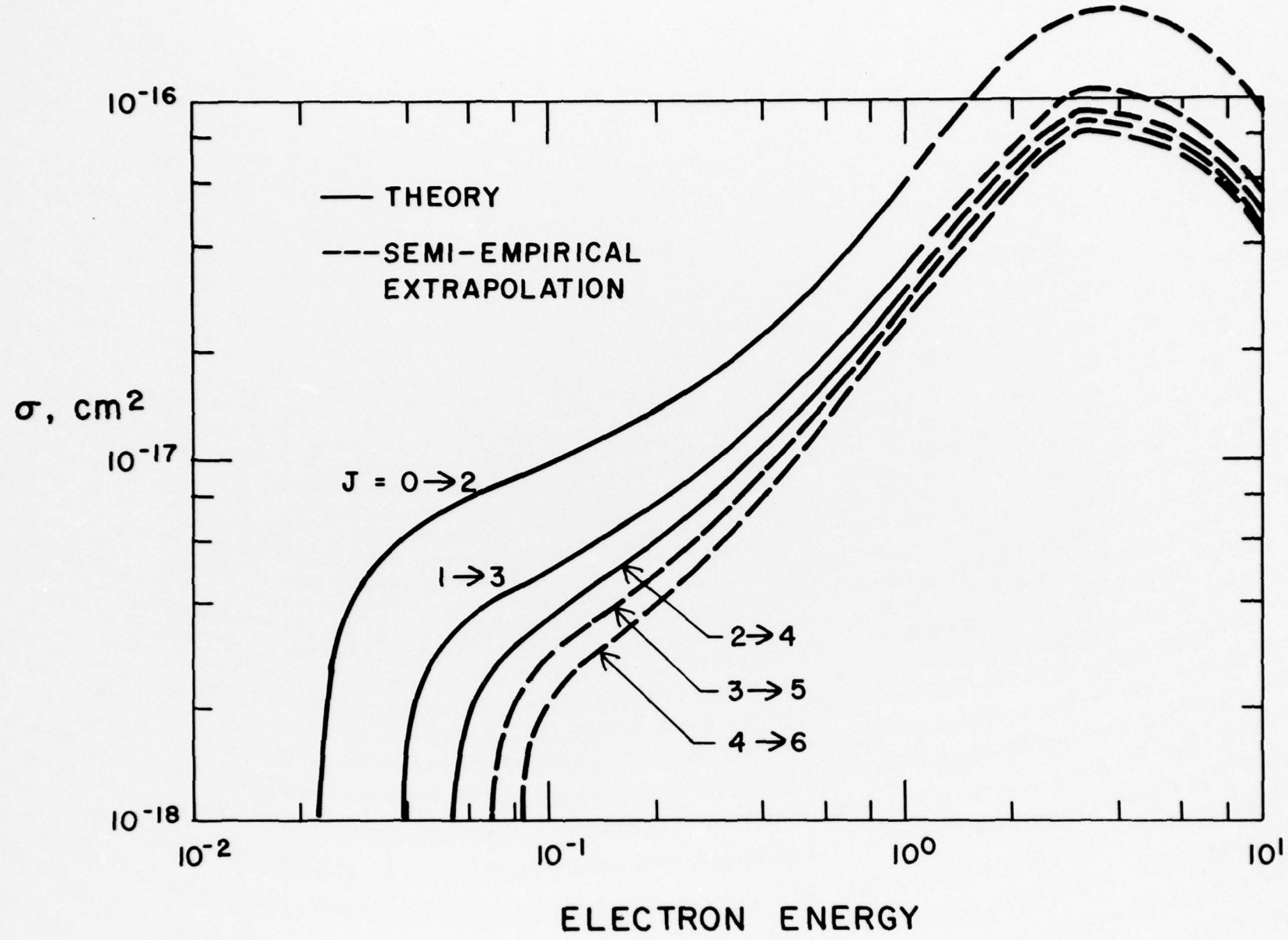

Fig. A-4 Electron Excitation Cross Sections for Rotational Transitions of D_2 as a Function of Electron Energy.

APPENDIX B

Rotational Excitation of HCl

For most molecules a large number of rotational levels can be populated at room temperature. Because of this, when modeling rotational excitation by electrons one must consider the effect of collisions of the second kind, i.e. electron-molecule collisions in which the rotational state of the molecule is decreased rather than increased. This topic has been discussed by Hake and Phelps[8] in some detail. For polar molecules the cross section for rotational excitation is given by[9]

$$\sigma_{J,\,J+1}(\epsilon) = \frac{(J+1)\,\mathrm{Ry}\,\sigma_r}{(2J+1)\,\epsilon}\ln\left(\frac{\left[\epsilon^{1/2} + (\epsilon - \epsilon_J)^{1/2}\right]}{\left[\epsilon^{1/2} - (\epsilon - \epsilon_J)^{1/2}\right]}\right) \qquad \text{(B-1)}$$

where J is the rotational level of the molecule, ϵ is the electron energy, Ry is the Rydberg, $\sigma_r = 8\pi\mu^2 a_o^2/3$, μ is the electric dipole moment in units of ea_o, a_o is the Bohr radius and ϵ_J is the energy lost by the electron in the collision, $2(J+1)B_o$, where B_o is the rotational constant for the molecule. The cross section for rotational de-excitation may be determined from Eq. (B-1) by the use of detailed balancing and is given by

$$\sigma_{J+1,\,J}(\epsilon) = \frac{(J+1)\,\mathrm{Ry}\,\sigma_r}{(2J+3)\,\epsilon}\ln\left(\frac{\left[(\epsilon + \epsilon_J)^{1/2} + \epsilon^{1/2}\right]}{\left[(\epsilon + \epsilon_J)^{1/2} - \epsilon^{1/2}\right]}\right) \qquad \text{(B-2)}$$

where ϵ_J is now energy gained by the electron in the collision.

To properly account for rotational excitation the cross sections (B-1) and (B-2) should be included for each rotational level J which is populated at the rotational temperature of interest. In practice this is quite unwieldy and effective single level approximations have been developed.[8,10] The resulting effective cross section is given by[8]

$$\sigma_{01} = \sigma_2 \frac{Ry}{\epsilon} \ln \left[\frac{\epsilon^{1/2} + (\epsilon - 2B')^{1/2}}{\epsilon^{1/2} - (\epsilon - 2B')^{1/2}} \right] , \qquad (B-3)$$

where

$$\sigma_2 = \frac{B_o}{B'} \sigma_r \left[1 - \exp(-2B'/kT) \right]^{-1} \qquad (B-4)$$

and B' is an effective rotational constant equal to $(B_o kT)^{1/2}$. Shkarofsky et al[10] have shown that the average energy lost in a rotational collision including the effects of rotational de-excitation is

$$\frac{\overline{\Delta\epsilon}}{\epsilon} = \frac{(\Delta E)^2}{kT\epsilon} , \qquad (B-5)$$

where ΔE is $2JB'$. With the definition of B' given above relationship (B-5) reduces to

$$\Delta\epsilon = 2 B_o \qquad (B-6)$$

Relationships (B-3) - (B-6) were used in the present analysis in the manner prescribed by Shkarofsky et al.[10] which is slightly different than that developed by Hake and Phelps.[8] Both analyses assume that $2B' \ll kT$ and that the characteristic energy of the discharge is much higher than the threshold for rotational excitation. In the case of HCl, which has an electric dipole moment of 1.08×10^{-18} esu-cm and a rotational constant of 1.3×10^{-3} eV, the quantity $2B'$ evaluated at 300°K has a value of 1.2×10^{-2} eV, and, thus, the above approximations are only marginally valid.

Finally, the computer code used in the analysis as developed by Yos and co-workers[11] had assumed that the logarithmic factor in Eq. (B-3) could be treated as a constant. The present program was modified to include the correct functional form of the cross section. It was noted however, that the discharge predictions performed at the lowest values of E/N considered, did not accurately satisfy energy conservation, i. e. the balance between energy transferred to electrons from the electric field and energy transferred from the electrons to the gas molecules. It is suspected that this inaccuracy results from numerical difficulties in integrating the rotational excitation cross section over the electron velocity

distribution at low values of ϵ_K. Inasmuch as the predictions at low values of E/N were not of interest for laser applications this matter was not pursued further.

APPENDIX C

A Note on Vibrational Excitation of HCL By Electron Impact*

One of the present authors recently co-authored a paper describing an experimental determination of the rate constant for electron impact vibrational excitation (EIVE) of HCl.[12] In this experiment an electron beam sustained discharge was used to excite gas mixtures of HCl-CO-N_2-Ar and the EIVE rate constant of HCl relative to that for CO was determined via infrared fluorescence measurements. This note describes a re-analysis of this experimental data which tends to reduce the uncertainty in the previously published rate constants.

It was shown earlier[12] that, with the E-beam sustainer on, the time evoluation of vibrationally excited HCl could be approximately represented by the relationship

$$[HCl^*] = [HCl^*]_{s.s.} [1 - \exp(-t/\tau)] \qquad (C-1)$$

where $[HCl^*]_{s.s.}$ is a quantity proportional to the EIVE rate constant for HCl and τ is the time constant for collisional quenching of HCl.* It was further shown that upon termination of the sustainer pulse, at time $t = \tau_d$, the decay of HCl^* could be described by the relationship

$$[HCl^*] = [HCl^*]_{\infty} - ([HCl^*]_{t=\tau_D} - [HCl^*]_{\infty}) \exp[(\tau_D - t)/\tau] \qquad (C-2)$$

---

* Authored by G. E. Caledonia of PSI and R. E. Center, Mathematical Sciences Northwest, Inc., Bellevue, Wash. 98009 and published in J. Chem. Phys. 64, 4237 (1976).

where $[HCl^*]_\infty$ is a residual level of HCl excitation resulting from the vibration-vibration exchange reaction with N_2, and, is linearly proportional to the EIVE rate constant for N_2.

Relative measurements of the fluorescence histories of both HCl and CO were performed in this experiment for a range of mixture ratios and discharge parameter E/N. It was shown that the EIVE rate constant for HCl could be determined relative to that for CO through use of the parameter τ (see Eq. 13 of Ref. 12) which could be deduced directly from the HCl fluorescence measurements. Unfortunately, it was found that the observed rise time of the HCl emission was always shorter than the decay time, in some instances by as much as a factor of two. Although the measured decay time was more in accord with kinetic estimates for τ, both measurements were used to provide upper and lower bounds for the rate constant.

It has since been realized that the apparent difference in the rise and decay times of HCl fluorescence arose from an error in the data analysis. In the evaluation of the risetime it was assumed that $[HCl^*]_{t=\tau_D}$ was equal to $[HCl^*]_{s.s.}$. This was not the case. Indeed for the range of parameters considered $[HCl^*]_{t=\tau_D}$ varied from 50 to 90 percent of $[HCl^*]_{s.s.}$. The effects of this error were that the reduced fluorescence data appeared to be quasi-exponential and that the deduced risetime was always less than the actual value of τ. On a proper evaluation of the data employing a detailed kinetic analysis, it was found that τ_{rise} was indeed equal to τ_{decay}. Thus the fluorescence data may be consistently explained by the lower value of the rate constants shown in Fig. 3 of Ref. 12.

Furthermore, it has been found that the EIVE rate constant may also be determined from the data without reference to the CO fluorescence. It may be shown that the ratio of the EIVE rate constant for HCl relative to that for N_2 can be determined from the measured ratio of $[HCl^*]_{t=\tau_d}$ to $[HCl^*]_\infty$ (see Eqs. 11 and 14 of Ref. 12). The rate constants deduced in this manner were typically 20% higher than those deduced from comparison with the CO fluorescence measurements. This additional comparison provides a good consistency check on the experiment.

The quantity measured in this experiment is the EIVE rate constant for HCl vs. the characteristic energy of the discharge. This measured rate constant is thus a function of the specific non-Maxwellian electric energy distribution peculiar to the experimental range of E/N and mixture ratio. Indeed the rate constants shown are not necessarily representative of those

for other gas mixtures under discharge conditions corresponding to the same characteristic energy. Such information can only be determined from the energy dependent EIVE cross section for HCl which cannot be deduced from the present data.

There have been two recent measurements[13, 14] of the EIVE cross section for HCl. In the first of these[13] the energy dependence of the cross section was measured in the energy range of 0 - 10 eV. This was a relative measurement and was normalized at an electron energy of 10 eV to an absolute measurement of the total scattering cross section for HCl taken by Bruche.[15] The peak cross section observed was 1.3×10^{-15} cm^2 ± 50% where the error bars represent the experimental uncertainty but do not include the uncertainty in Bruche's cross section.

The EIVE cross section for HCl was also studied by Ziesel et al[14] in the onset region. These measurements, taken between 0.36 - 0.5 eV, were consistent with the observations of Rohr and Linder; however, once again the measurements were relative, in this instance normalized to the dissociative attachment cross section for HCl. The peak cross section was estimated to be in the range of 2×10^{-16} - 2×10^{-15} cm^2 depending upon the choice of the dissociative attachment cross section.[14]

Thus there is still a significant uncertainty in the magnitude of the EIVE cross section for HCl. Discharge predictions have been performed for the experimental conditions of Ref. 12, using the relative HCl cross section determined by Rohr and Linder[13] in order to ascertain what magnitude cross section would be consistent with the experimental rate constants. It was found that a peak cross section of 0.8×10^{-15} cm^2 provided good agreement with the measured rate constants. This value is within the error bars of the other measurements[13, 14] and thus it would appear that the peak cross section for EIVE of HCl is approximately 1×10^{-15} cm^2.

There is one last point to be made concerning the results presented in Ref. 12. In that work it was found that approximately 20% of the observed HCl fluorescance arose from transitions higher than $v = 1 \rightarrow 0$ and it was suggested that this emission resulted from direct electron excitation into the second or higher vibrational levels.[12] Since that time detailed anharmonic oscillator kinetic calculations, including all relevant inter-mode and intra-mode vibration-vibration reactions for HCl and N_2,[16] have been performed for typical experimental discharge and mixture conditions. These calculations demonstrate that approximately 10% of the vibrationally excited HCl could reside in states higher than $v = 1$ even if there were no direct electron excitation of these states. This result is solely due to vibration-vibration exchange collisions occurring over the 60μ sec duration of the discharge. Thus no information concerning EIVE to vibrational levels greater than $v = 1$ can be deduced from the data.

APPENDIX
REFERENCES

1. Herzberg, G., "Molecular Spectra and Molecular Structure I, Spectra of Diatomic Molecules", D. Van Nostrand Co., New York, 1950.

2. Crompton, R. W., Gibson, D. K. and Robertson, A. G., Phys. Rev. A 2, 1387 (1970).

3. Chang, E. S. and Temkin, A., Phys. Rev. Lett. 23, 399 (1969).

4. Messiah, A., "Quantum Mechanics, Vol. II", P. 1059, North Holland Publishing Co., Amsterdam, 1966.

5. Lane, N. F. and Geltman, S., Phys. Rev. 160, 53 (1967).

6. Henry, R. J. W. and Lane, N. F., Phys. Rev. 183, 221 (1969).

7. Henry, R. J. W. and Lane, N. F., Phys. Rev. A 4, 410 (1971).

8. Hake, Jr., R. D. and A. V. Phelps, Phys. Rev. 158, 70 (1967).

9. Takayanagi, K., J. Phys. Soc. Japan 21, 507 (1966).

10. Shkarofsky, I. P., Johnston, T. W. and Bachynski, M. P., "The Particle Kinetics of Plasmas", Ch. 3, Addison-Wesley Publishing Company, Reading, Massachusetts, 1966.

11. Mayan, J. T., Yos, J. M. and Fante, R. L., "Re-entry Antenna Test Program Final Report, Appendix 1, Antenna Breakdown Model", AVCO Government Products Group, Systems Division, report AVSD-0060-74-RR, April 1974.

12. Center, R. E. and Chen, H. L., J. Chem. Phys. 61, 3785 (1974).

13. Rohr, K. and Linder, F., J. Phys. B. Atom. Molec. Phys. 8, L200 (1975).

14. Ziesel, J. P., Nenner, I. and Schulz, G. J., J. Chem. Phys. 63, 1943 (1975).

15. Brüche, E., Ann. Phys. Lpz 82, 25 (1927).

16. Taylor, R. L. and Lewis, P. F., unpublished results.

DISTRIBUTION LIST
FOR
FINAL REPORT

Contract No. N00014-75-C-0035

RECIPIENT	CYS
Director Naval Research Laboratory 4555 Overlook Avenue, S.W. Washington, D.C. 20375 Attn: Dr. J. Stregack, Code 5540	1
Commander, Defense Contract Administration Services Region Code S2202A 666 Summer Street Boston, MA 02210	1
Director, U. S. Naval Research Laboratory Washington, D.C. 20375 Attn: Code 2629	6
Attn: Code 2627	6
Defense Documentation Center Bldg. 5 Cameron Station Alexandria, VA 22314	12

RECIPIENT	CYS
Avco Everett Research Lab. 2385 Revere Beach Pkwy. Everett, MA 02159 ATTN: J. Daugherty	1
Bell Aerospace Co. Box 1 Buffalo, N. Y. 14240 ATTN: Dr. W. Solomon	1
Calspan Corporation 4455 Genesee Street P. O. Box 235 Buffalo, N.Y. 14221 ATTN: J. Rich	1
Defense Advanced Research Projects Agency 1200 Wilson Boulevard Arlington, VA 22209 ATTN: P. Clark	1
Rocketdyne Division Rockwell International 6633 Canoga Avenue Canoga Park, CA 91304 ATTN: J. Hon	1
TRW Inc. 1 Space Park Redondo Beach, CA 90278 ATTN: J. Miller	1
UTRC 400 Main Street E. Hartford, Conn. 06108 ATTN: J. Shirley	1

UNCLASSIFIED

SECURITY CLASSIFICATION OF THIS PAGE (When Data Entered)

REPORT DOCUMENTATION PAGE	READ INSTRUCTIONS BEFORE COMPLETING FORM
1. REPORT NUMBER	2. GOVT ACCESSION NO. DN 480-222 / 3. RECIPIENT'S CATALOG NUMBER
4. TITLE (and Subtitle) ANALYTIC MODELING OF ELECTRICALLY EXCITED D_2/HCl AND HCl LASER EXPERIMENTS.	5. TYPE OF REPORT & PERIOD COVERED FINAL REPORT - 8/1/74 - 5/31/76
	6. PERFORMING ORG. REPORT NUMBER PSI-TR-58
7. AUTHOR(s) R. Taylor, G. Caledonia, P. Lewis, P. Wu, J. D. Teare and J. Cronin	8. CONTRACT OR GRANT NUMBER(s) N0014-75-C-0035
9. PERFORMING ORGANIZATION NAME AND ADDRESS Physical Sciences Inc. 30 Commerce Way Woburn, MA 01801	10. PROGRAM ELEMENT, PROJECT, TASK AREA & WORK UNIT NUMBERS 63754N SAA 76
11. CONTROLLING OFFICE NAME AND ADDRESS Office of Naval Research Department of the Navy Arlington, Virginia 22217	12. REPORT DATE July 1976 / 13. NUMBER OF PAGES 145
14. MONITORING AGENCY NAME & ADDRESS(if different from Controlling Office) U. S. Naval Research Laboratory Washington, D.C. 20375	15. SECURITY CLASS. (of this report) UNCLASSIFIED / 15a. DECLASSIFICATION/DOWNGRADING SCHEDULE
16. DISTRIBUTION STATEMENT (of this Report) (9) Final rept. 1 Aug 74 - 31 May 76, (12) 146 p.	
17. DISTRIBUTION STATEMENT (of the abstract entered in Block 20, if different from Report)	
18. SUPPLEMENTARY NOTES	
19. KEY WORDS (Continue on reverse side if necessary and identify by block number) Laser; Modeling; Electric Discharge; D_2/HCl; HCl	

20. ABSTRACT (Continue on reverse side if necessary and identify by block number)

An analytic capability has been developed to model two types of laser experiments: (i) a D_2/HCl EDL and (ii) an e-beam sustainer discharge HCl laser.

For the former device, a discharge in D_2/inert gas mixtures provides excitation of the vibrational mode of D_2. This gas is then

DD FORM 1 JAN 73 1473 EDITION OF 1 NOV 65 IS OBSOLETE

UNCLASSIFIED

SECURITY CLASSIFICATION OF THIS PAGE (When Data Entered)

391 105 LB

supersonically expanded and HCl injected. The gases mix and flow into a cavity where vibrational energy transfer pumps the HCl. Complete modeling of this sequence of steps has been achieved. The relevant electron impact rate constants for D_2 (and H_2) as well as the vibrational energy transfer rate constants for the D_2/HCl molecular system were selected from available data and theory. Comparison of the results of this model with data from the NRL EDL experiment were in qualitative agreement, although more definitive comparison was precluded by experimental difficulties. A conceptual design of a next generation experiment was performed and indicates the requirement for an e-beam sustainer discharge operating at about one atmosphere plenum pressure. Under these conditions laser demonstration of a D_2/HCl EDL is predicted to be feasible.

In the second experiment, HCl/inert gas mixtures are directly excited by a pulsed, high current e-beam sustainer discharge. The discharge conditions were modeled by developing a set of electron impact cross sections for HCl by a critical review of existing data. The results of model calculations indicate that for the conditions of the NRL experiment, sufficient atoms may be generated in the discharge to prevent attainment of high gain. Definitive modeling of the atom generation is not possible at present due to lack of kinetic information. A significant range of experimental variation could not be achieved due to device limitations. Additional, controlled experiments are suggested to assess the critical technical questions concerning an HCl discharge laser.